UNIVERSITY OF MINNESOTA

CENTER FOR TRANSPORTATION STUDIES

INTELLIGENT TRANSPORTATION SYSTEMS INSTITUTE

Development of a Novel Tilt-Controlled Narrow Commuter Vehicle

Final Report

Prepared by:
J. Gohl, R. Rajamani, P. Starr, L. Alexander

Department of Mechanical Engineering
University of Minnesota

CTS 06-05

Technical Report Documentation Page

1. Report No.	2.	3. Recipients Accession No.
CTS 06-05		

4. Title and Subtitle	5. Report Date
Development of a Novel-Tilt Controlled Narrow Commuter Vehicle	May 2006
	6.

7. Author(s)	8. Performing Organization Report No.
J. Gohl, R. Rajamani, P. Starr, L. Alexander	

9. Performing Organization Name and Address	10. Project/Task/Work Unit No.
Department of Mechanical Engineering University of Minnesota 111 Church St SE Minneapolis, MN 55455	CTS Project Number 2001030
	11. Contract (C) or Grant (G) No.

12. Sponsoring Organization Name and Address	13. Type of Report and Period Covered
Intelligent Transportation Systems Institute Center for Transportation Studies University of Minnesota 511 Washington Avenue SE, Suite 200 Minneapolis, MN 55455	Final Report
	14. Sponsoring Agency Code

15. Supplementary Notes

http://www.cts.umn.edu/pdf/CTS-06-05.pdf

16. Abstract (Limit: 200 words)

Traffic congestion is growing in urban areas of every size and is expected to double by 2010. A relatively unexplored but very promising solution to the problem of congestion is the adoption of narrow vehicles for commuter travel. Narrow vehicles like motorcycles can promote significantly improved highway utilization by the use of half-width lanes. However, in order for the general public to adopt this form of personal transportation, narrow vehicles should perceptibly provide the same ease of use and the same level of safety as passenger sedans.

The research team in this project has developed a new concept vehicle that is relatively tall compared to its track width so as to provide a travel height that is comparable to that of other vehicles on the highway. To help the driver balance a relatively tall, narrow vehicle, it incorporates an electronic tilt control system that ensures tilt stability. The tilt control system balances the vehicle and improves ease of use, especially on curves where the vehicle must lean into the curve to ensure tilt stability.

In this report the design and implementation of a control system that ensures the tilt stability of the prototype narrow vehicle is presented. The control system is based on the use of steer-by-wire technology and is called Steering Tilt Control (STC). The report includes significant details on the design of the prototype narrow vehicle constructed by the research team, on dynamic modeling for narrow tilting vehicles and also includes experimental results on the performance of the control system on the prototype narrow vehicle.

17. Document Analysis/Descriptors	18.Availability Statement
Narrow commuter vehicle, narrow tilting vehicle, tilt control, rollover control, rollover prevention, covered motorcycle	No restrictions. Document available from: National Technical Information Services, Springfield, Virginia 22161

19. Security Class (this report)	20. Security Class (this page)	21. No. of Pages	22. Price
Classified	Classified	189	

Development of a Novel Tilt-Controlled Narrow Commuter Vehicle

Final Report

Prepared by:
J. Gohl
R. Rajamani
P. Starr
L. Alexander

Department of Mechanical Engineering
University of Minnesota

May 2006

Intelligent Transportation Systems Institute
Center for Transportation Studies
University of Minnesota

CTS 06-05

Development of a Novel Tilt-Controlled Narrow Commuter Vehicle

Final Report

J. Gohl, R. Rajamani, P. Starr and L. Alexander

Department of Mechanical Engineering

University of Minnesota

Executive Summary

Traffic congestion is growing in urban areas of every size and is expected to double by 2010. A relatively unexplored but very promising solution to the problem of congestion is the adoption of narrow vehicles for commuter travel. Narrow vehicles like motorcycles can promote significantly improved highway utilization by the use of half-width lanes. However, in order for the general public to adopt this form of personal transportation, narrow vehicles should perceptibly provide the same ease of use and the same level of safety as passenger sedans.

The research team in this project has developed a new concept vehicle that is relatively tall compared to its track width so as to provide a travel height that is comparable to that of other vehicles on the highway. To help the driver balance a relatively tall, narrow vehicle, it incorporates an electronic tilt control system that ensures tilt stability. The tilt control system balances the vehicle and improves ease of use, especially on curves where the vehicle must lean into the curve to ensure tilt stability.

In this report the design and implementation of a control system that ensures the tilt stability of the prototype narrow vehicle is presented. The control system is based on the use of steer-by-wire technology and is called Steering Tilt Control (STC). The STC system uses steer-by-wire operation in which the front wheel steering angle is used to control tilt while at the same time perceptibly allowing the driver to use the steering angle for purposes of lateral control. A novel innovative algorithm is presented for STC that satisfies both the driver handling requirements and the tilt stability requirements.

The report includes significant detail on the design of the prototype narrow vehicle constructed by the research team. Significant details on dynamic modeling for narrow tilting vehicles are presented. The report also includes experimental results on the performance of the control system on the prototype narrow vehicle. Comparisons are made between the simulated system and the experimental vehicle. This illustrates the limitations encountered in the simulations but also shows

similarities that validate the model. Also, experimental results show that the vehicle is stabilized very well by the controller within the limitations of our prototype hardware.

Future work on the narrow vehicle should include the development of a direct tilt control system in the vehicle suspension so as to enable good control at low vehicle speeds.

Table of Contents

Page

Page

List of Figures

List of Tables

Narrow Tilting Vehicle: Modeling and Control

Chapter I. Introduction

With increased traffic congestion on today's roads comes increased interest in new solutions. Many solutions rely on increasing person per vehicle statistics by the use of mass transit or carpooling. This is done, in the case of mass transit, by using larger vehicles to accommodate more riders per vehicle. In the case of carpooling, the existing vehicles' person per vehicle number is increased to be closer to its capacity. The goal of this is to increase the flow rate of a particular traffic artery. A converse approach to increase the flow rate would be not to make the vehicles larger but to make the vehicles smaller. In this way, although the person per vehicle number might only be one but the capacity of the smaller vehicle might only be one or two. In this way, the average person per vehicle number would be over 50% of a vehicle's capacity. The benefit to overall traffic flow then, comes from fitting more vehicles on a lane and so increasing the flow rate.

It's true that there will be many issues to address before wide scale implementation of such a system could be started. Questions like, what will be the expected increase in flow rate? How will the smaller vehicles interact or even conflict with larger vehicles also using the roads? Along with these questions are human factors issues. Will there be significant changes to driving habits? What will be the perception of smaller vehicles? Certainly there are questions of safety. For instance, what happens in a crash? Also, there are technical questions to ask. How fast can a smaller vehicle accelerate and travel? What is the most efficient propulsion? Finally, there is a question of stability. Will the vehicle tip over and what can be done to prevent it? This is the problem of concern in this paper.

Narrow vehicles that do not lean are unstable when they corner too hard. A simple statics calculation can illustrate this fact. Imagine looking at the front of a vehicle as it accelerates toward

the right as in Figure 1.1. This figure shows the equipollent moment and force action on the center of gravity of the vehicle leaning at an angle θ.

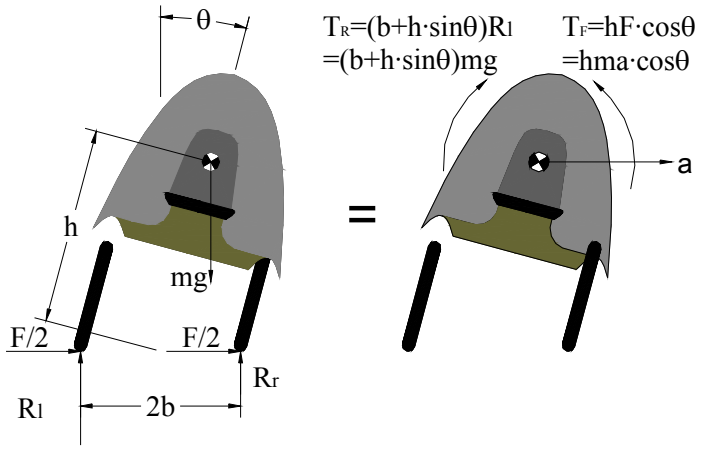

Figure 1.1 Tipping Statics Diagram

Label the height of the center of gravity as h, and the wheelbase width as $2b$. Then as the vehicle accelerates to the right in a turn, due to increasing F, R_r approaches zero while R_l approaches mg. At this limit $F = ma$ so that $T_F = hF\cos\theta = hma\cos\theta$ and $T_R = (b + h\sin\theta)mg$. T_R refers to the moment due to the normal reactions and T_F refers to the moment due to the lateral forces. Stability is maintained if $T_F < T_R$ this implies stability for $a < g\frac{b+h\sin\theta}{h\cos\theta}$. By introducing tilt we increase the limit on a. In the next section we will use the nonlinear model to derive a relation between the lateral acceleration, a , the vehicle's yaw rate and velocity at steady state. As expected, this will also be related to the lean and steady state steer angle.

From this discussion, a solution to the tipping problem for a narrow vehicle, it seems, is to lean while cornering. It turns out that motorcycles have already addressed this issue. Since they are the limiting case for narrow vehicles, they must lean while cornering. One of the difficulties of wide spread implementation for relieving traffic in this way is that it takes practice to ride a motorcycle well, see (29:pp. 68) and (22). In the absence of experience, they can be dangerous. The following

statement was taken from a brochure issued by the National Highway Traffic Safety Administration (42):

"...The causes of many motorcycle crashes can be attributed to:

- lack of basic riding skills
- failure to appreciate the inherent operating characteristics
- failure to appreciate the limitations of the motorcycle
- failure to use special precautions while riding
- failure to use defensive driving techniques
- lack of specific braking and cornering skills
- failure to follow speed limit"

Now this is not a paper on the dangers of motorcycles but these issues do illustrate the point that experience and skill is necessary to drive one safely. Also, if wide scale implementation is to occur for narrow/leaning commuter vehicles, they had better be easy to drive.

There is a fundamental difference between driving a non-leaning vehicle versus a free leaning vehicle. The second issue stated above regarding the "inherent operating characteristics", is primarily due to counter-steer. A motorcycle requires counter steer to change directions. To maneuver a non-leaning vehicle, however, simply requires the steering wheel be turned in the desired direction of travel. This creates problems when switching from one type of vehicle to another, especially when a fast maneuver is necessary in an emergency situation. The project objective was to design a controller that would make driving a narrow tilting vehicle as easy for anyone to do without any motorcycle riding experience. We explored possible controllers and analyzed their usefulness both in stabilizing the vehicle and in interacting with the driver.

Other groups have also studied vehicles of this type. The "F 300 Life-Jet" shown in Figures 1.2 and 1.3 is a three wheeled tilting concept vehicle built by Mercedes-Benz. General Motors was also involved in some research with leaning vehicles. The "Lean Machine" shown in Fgure 1.4 is a concept vehicle built by GM. These photos were obtained from the websites listed in references (43) and

(44), respectively.

Figure 1.2 F 300 Life-Jet front cornering view

Figure 1.3 F 300 Life-Jet side view

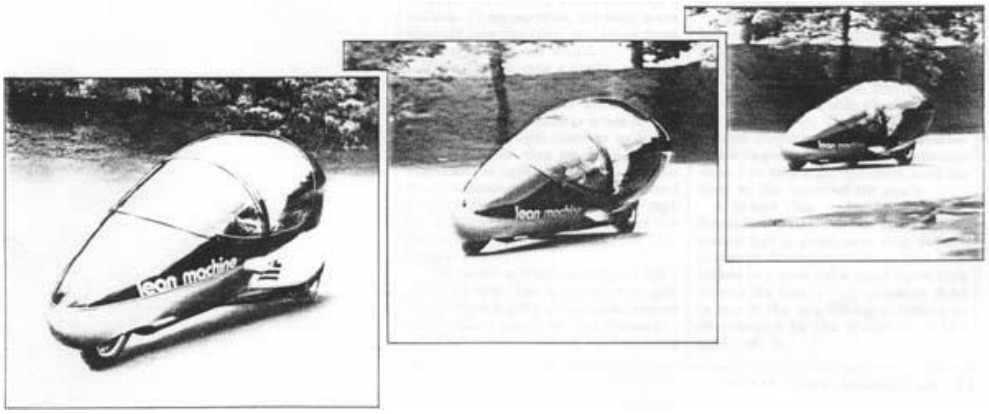

Figure 1.4 The GM Lean Machine

The design of leaning vehicles is a challenge that goes beyond a simple research project. Even respected car companies see the possible benefits of this type of vehicle.

A narrow tilting vehicle (NTV) has some similarities to the classic control problem of the inverted pendulum. In the classic inverted pendulum problem, the system dynamics have two real valued poles with equal magnitude but opposite sign. One pole is stable while the other is unstable. The magnitude of these poles is determined by the mass, height of the center of gravity, acceleration of gravity and the moment of inertia. In the NTV, we still have approximately these poles along with poles due to the lateral dynamics. The tilting poles are shifted slightly due to coupling between the tilting and lateral modes. With the inverted pendulum, active control must be applied to stabilize the tilting. This also occurs with an NTV. On a motorcycle, the rider performs this function in conjunction with controlling the lateral motion. To control the tilting automatically on an NTV, as we would like to do, there are two distinct methods. The two methods are Direct Tilt Control (DTC) and Steering Tilt Control (STC), see (2).

Direct tilt control uses an actuator to apply a leaning torque directly to the leaning dynamics of the vehicle. This allows the controller to position the vehicle at any desired angle. There are two important issues to address with the DTC method. The first is determining the desired lean angle

of the vehicle. In some way, the driver's actions must determine the required lean angle for a desired maneuver. Interpreting these intentions is not a trivial task and requires thoughtful consideration. The second issue is reducing the torque that an actuator needs to exert. Even though a vehicle in a perfectly coordinated turn is at an equilibrium position (and hence only requires small torque for small deviations), getting to that point can require large peaks in the applied torque.

The other method, the one studied in this paper, is STC. The control input that balances the vehicle is the lateral force between the road and the wheels. This is the same lateral force that controls the lateral modes of the vehicle. In our case we modeled this force with slip angles of the wheels such that the control input to the system plant is the front wheel angle. Because the input depends on the steering, this method is called "Steering Tilt Control", (2). Since the control input influences both modes, we need to account for this when designing the tilt controller. We need to be aware that one mode can destabilize the other. This type of control is the same method used by bicycle and motorcycle riders to balance the vehicle. This active control is most apparent at slow speeds and becomes less so at higher speeds when the gyroscopic moments are greater. This is especially true on motorcycles where the wheels can have significant mass. An interesting phenomenon already hinted at that arises in this system is counter-steering. Experienced motorcycle riders are often familiar with this such that a negative steering input must be given to attain the proper lean angle prior to entering a steady state turn. This behavior can be demonstrated from the dynamic model and is part of the reason that it takes practice to proficiently ride a motorcycle. This is fundamentally different from driving a non-leaning automobile.

Many of the research projects we found relating to tilting vehicles used either DTC or driver controlled STC. The F 300 Life-Jet for instance seems to use DTC with an hydraulic actuator. Most of the details of the F 300 Life-Jet, however, are proprietary. Other leaning vehicle projects include, but are not limited to, the GM Lean Machine, which uses a driver controlled DTC, and the Millennium Tracer, (45), which uses driver controlled STC. The website listed in reference (44) is a

good source for further information on the subject. The lack of experimental results on automatic STC is the void this research aims to fill.

Ultimately, a combination of both DTC and STC would be needed for a useful vehicle. DTC is needed to keep the vehicle upright at slow speeds and when the vehicle is stopped. This will be shown from the vehicle model in the next section. STC, conversely, is a good control method at higher speeds. This paper represents a starting point to implementing STC on a vehicle.

Chapter II. Dynamic Model

We started the process of designing a controller by deriving a model for the system. The derivation of this model is described in appendix C. Some of the highlights of this are shown here.

2.1 Nonlinear Model

The nonlinear equations are derived as equations 311, 315, and 316. By neglecting the terms $\breve{D}_5^x$, $\breve{D}_4^y$, and $\breve{D}_5^z$ we get the nonlinear dynamic model listed here as equations 1 to 3.

$$\begin{aligned} & \ddot{\psi}\left(\left(\cos\theta\right)I^{zz}+\left(\tan\theta\right)\left(\sin\theta\right)I^{yy}\right) \\ & \dot{\theta} \qquad\qquad\qquad\qquad = \dot{2} \\ & \dot{\psi}\left(\sin\theta\right)\left(I^{zz}-I^{yy}\right) \\ & +\left(2F_f l_f - F_r l_r\right)\left(\left(\tan\theta\right)\left(\sin\theta\right)+\left(\cos\theta\right)\right) \end{aligned} \tag{1}$$

$$\ddot{\theta} = \frac{1}{J}\left(mgh\left(\sin\theta\right)-h^2 m\left(\cos\theta\sin\theta\right)\dot{\theta}^2\right) + \frac{1}{J}\left(\dot{\psi}^2\left(\cos\theta\sin\theta\right)\left(I^{yy}-I^{zz}\right)-h\left(2F_f+F_r\right)\left(\cos\theta\right)\right) \tag{2}$$

$$\begin{aligned} \ddot{y} = & -v\dot{\psi}-\frac{1}{J}gh^2 m\cos\theta\sin\theta+h\dot{\theta}^2\left(\left(\sin\theta\right)+\frac{1}{J}h^2 m\cos^2\theta\sin\theta\right) \\ & +h\dot{\psi}^2\left(\sin\theta+\frac{1}{J}\left(\cos^2\theta\sin\theta\right)\left(I^{zz}-I^{yy}\right)\right) \\ & +\left(2F_f+F_r\right)\left(\frac{1}{J}h^2\cos^2\theta+\frac{1}{m}\right) \end{aligned} \tag{3}$$

The first step in analyzing any nonlinear dynamic equations is usually to search for any equilibrium solutions. To start this process, let us make the following variable substitutions:

$$\mathbf{x} = \begin{bmatrix} x_1 & x_2 & x_3 & x_4 & x_5 & x_6 \end{bmatrix}^{\mathbf{T}} \tag{4}$$

$$x_1 = y,\ x_2 = \dot{y},\ x_3 = \psi,\ x_4 = \dot{\psi},\ x_5 = \theta,\ x_6 = \dot{\theta} \tag{5}$$

Using these definitions with equations 1 - 3, we get the first order model equations 6 - 12.

$$\dot{x}_1 = f_1(\mathbf{x}) = x_2 \tag{6}$$

$$\begin{aligned}\dot{x}_2 = f_2(\mathbf{x}) &= -v\dot{\psi} - \frac{1}{J}gh^2 m\cos\theta\sin\theta \\ &+h\dot{\theta}^2\left((\sin\theta) + \frac{1}{J}h^2 m\cos^2\theta\sin\theta\right) \\ &+h\dot{\psi}^2\left(\sin\theta + \frac{1}{J}\left(\cos^2\theta\sin\theta\right)\left(I^{z^2} - I^{y^2}\right)\right) \\ &+(2F_f + F_r)\left(\frac{1}{J}h^2\cos^2\theta + \frac{1}{m}\right)\end{aligned} \tag{7}$$

$$\dot{x}_3 = f_3(\mathbf{x}) = x_4 \tag{8}$$

$$\dot{x}_4 = f_4(\mathbf{x}) = \tag{9}$$

$$\left(2\dot{\theta}\dot{\psi}(\sin\theta)\left(I^{zz} - I^{yy}\right) + (2F_f l_f - F_r l_r)((\tan\theta)(\sin\theta) + (\cos\theta))\right) / \tag{10}$$

$$\left((\cos\theta)I^{zz} + (\tan\theta)(\sin\theta)I^{yy}\right)$$

$$\dot{x}_5 = f_5(\mathbf{x}) = x_6 \tag{11}$$

$$\begin{aligned}\dot{x}_6 = f_6(\mathbf{x}) &= \frac{1}{J}\left(mgh(\sin\theta) - h^2 m(\cos\theta\sin\theta)\dot{\theta}^2\right) \\ &+\frac{1}{J}\left(\dot{\psi}^2(\cos\theta\sin\theta)\left(I^{yy} - I^{zz}\right) - h(2F_f + F_r)(\cos\theta)\right)\end{aligned} \tag{12}$$

2.2 Equilibrium Solution

Now, an equilibrium solution, $\mathbf{x}_{ss}$, must satisfy $\dot{\mathbf{x}} = \mathbf{0}$. The trivial solution is of course one possibility but the more interesting one comes from neglecting equation 8. In this case we get, from equations 6 and 11, $x_2 = \dot{y} = 0$ and $x_6 = \dot{\theta} = 0$. To start, we solve the steady state solution of

equation 7 for $2F_f + F_r$. Doing so, we get:

$$\begin{aligned}
& (2F_f + F_r) \\
= & \left(v\dot{\psi}_{ss} + \frac{1}{J} g h^2 m \cos\theta_{ss} \sin\theta_{ss} \right) \frac{1}{\left(\frac{1}{J} h^2 \cos^2\theta_{ss} + \frac{1}{m}\right)} && (13) \\
& - \left(h\dot{\psi}_{ss}^2 \left(\sin\theta_{ss} + \frac{1}{J} \left(\cos^2\theta_{ss} \sin\theta_{ss}\right) \left(I^{z^2} - I^{y^2} \right) \right) \right) \frac{1}{\left(\frac{1}{J} h^2 \cos^2\theta_{ss} + \frac{1}{m}\right)} && (14)
\end{aligned}$$

This expression is then used in the steady state solution to equation 12, $f_6(\mathbf{x}) = 0$. Upon simplification, we get:

$$\left(I^{yy} - I^{zz} + mh^2\right) \dot{\psi}_{ss}^2 \sin\theta_{ss} \cos\theta_{ss} - mhv \left(\cos\theta_{ss}\right) \dot{\psi}_{ss} + mgh \sin\theta_{ss} = 0 \tag{15}$$

This becomes:

$$\frac{1}{mgh} \left(I^{yy} - I^{zz} + mh^2\right) \left(\sin\theta_{ss}\right) \dot{\psi}_{ss}^2 - \frac{v}{g} \dot{\psi}_{ss} + \tan\theta_{ss} = 0 \tag{16}$$

Which is a quadratic expression relating θ_{ss} and v to $\dot{\psi}_{ss}$. Assuming that $I^{yy} \simeq I^{zz}$, the solutions to this equation will have the form:

$$\begin{aligned}
\dot{\psi}_{ss} &= \frac{1}{2h \sin\theta_{ss}} \left[v + \sqrt{v^2 - 4gh \sin\theta_{ss} \tan\theta_{ss}} \right] && (17) \\
\dot{\psi}_{ss} &= \frac{1}{2h \sin\theta_{ss}} \left[v - \sqrt{v^2 - 4gh \sin\theta_{ss} \tan\theta_{ss}} \right] && (18)
\end{aligned}$$

Observe that the limit of equation 17 as $\theta_{ss} \to 0$ does not exist. This is obvious by the computing the limits of the numerator and denominator separately.

$$\begin{aligned}
\lim_{\theta_{ss} \to 0} \left[v + \sqrt{v^2 - 4gh \sin\theta_{ss} \tan\theta_{ss}} \right] &= 2v && (19) \\
\lim_{\theta_{ss} \to 0} 2h \sin\theta_{ss} &= 0 && (20)
\end{aligned}$$

The limit of the other solution, equation 18, as $\theta_{ss} \to 0$ on the other hand is indeterminate but can be shown to exist using L'Hopital's rule (41:pp. 79).

$$\lim_{\theta_{ss}\to 0}\left[v - \sqrt{v^2 - 4gh\sin\theta_{ss}\tan\theta_{ss}}\right] = 0 \tag{21}$$

$$\lim_{\theta_{ss}\to 0} 2h\sin\theta_{ss} = 0 \tag{22}$$

Therefore, L'Hopital's rule applies.

$$\lim_{\theta_{ss}\to 0}\frac{d}{d\theta_{ss}}\left[v - \sqrt{v^2 - 4gh\sin\theta_{ss}\tan\theta_{ss}}\right] = 0 \tag{23}$$

$$\lim_{\theta_{ss}\to 0}\frac{d}{d\theta_{ss}}\left(2h\sin\theta_{ss}\right) = 2h \tag{24}$$

Using this result:

$$\lim_{\theta_{ss}\to 0}\dot{\psi}_{ss} = 0 \tag{25}$$

Now, for the solution given by equation 18 to be real we must have:

$$v^2 - 4gh\sin\theta_{ss}\tan\theta_{ss} \geq 0 \tag{26}$$

Or:

$$v \geq \sqrt{4gh\sin\theta_{ss}\tan\theta_{ss}} \tag{27}$$

A typical value of θ_{ss} might be 30° in which case with our value of h given in appendix B we get the following limit on v:

$$v \geq 1.68\frac{\mathrm{m}}{\mathrm{s}} \tag{28}$$

This is a lower limit on the velocity for an equilibrium solution to exist beyond 30° of lean. A plot of equation 18 is shown in Figure 2.1.

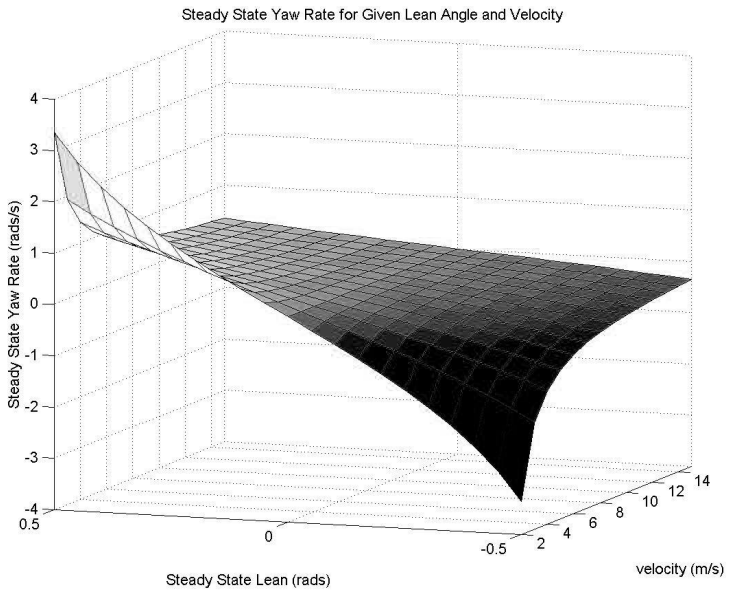

Figure 2.1 Steady state yaw rate for vehicle based on equation 18

Now, the equilibrium solution to equation 9 is found:

$$\begin{aligned} f_4(\mathbf{x}) &= 0 = \\ &(2F_f l_f - F_r l_r)\left((\tan\theta_{ss})(\sin\theta_{ss}) + (\cos\theta_{ss})\right) \end{aligned} \tag{29}$$

With the definitions of F_f and F_r given by equations 327 and 328, we get the following expression:

$$\dot{\psi}_{ss} - \left(\frac{l_r\lambda_r - 2l_f\lambda_f}{C_r l_r^2 - 2C_f l_f^2}\theta_{ss} - 2C_f\frac{l_f}{C_r l_r^2 - 2C_f l_f^2}\delta_{ss}\right)v = 0 \tag{30}$$

Equation 30 along with equation 18 and $x_2 = \dot{y} = 0$ and $x_6 = \dot{\theta} = 0$ represents the steady state solution with one degree of freedom. Throughout this project, we considered this solution

parameterized by θ_{ss}. Thus, $\mathbf{x}_{ss}$ for the state space representation 339 becomes:

$$\mathbf{x}_{ss} = \begin{bmatrix} 0 & \dot{\psi}_{ss} & \theta_{ss} & 0 \end{bmatrix}^{\mathbf{T}} \tag{31}$$

Equation 30 will yield the standard kinematic steady state expressions $\delta_{ss} = \frac{l}{R}$ and $\dot{\psi}_{ss} = \frac{v}{R}$ under certain vehicle configurations. First when there is no leaning, $\theta_{ss} = 0$, equation 30 becomes:

$$\dot{\psi}_{ss} = -2C_f \frac{l_f}{C_r l_r^2 - 2C_f l_f^2} \delta_{ss} v \tag{32}$$

Next, when there are an equal number of wheels on both the front and back all with the same slip angle gains, $C_f = C_r$, equation 32 becomes:

$$\dot{\psi}_{ss} = -\frac{l_f}{l_r^2 - l_f^2} \delta_{ss} v = -\frac{l_f}{(l_r + l_f)(l_r - l_f)} \delta_{ss} v = -\frac{l_f}{l \cdot (l_r - l_f)} \delta_{ss} v \tag{33}$$

Now, let us look at a projection of a two wheeled vehicle configuration in the ground plane.

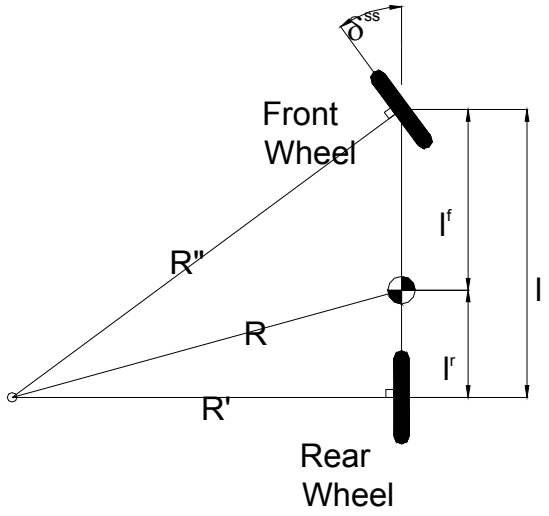

Figure 2.2 Two wheeled ground plane projection

From this diagram, figure 6, we get:

$$\tan \delta_{ss} = \frac{l}{R'} \tag{34}$$

Which approximates to:

$$\tan \delta_{ss} \simeq \delta_{ss} \simeq \frac{l}{R'} \tag{35}$$

when δ_{ss} is small. Also, as $l_f \to l$, $R \to R'$ and so we get:

$$\delta_{ss} = \frac{l}{R} \tag{36}$$

Using this approximation equation 33 becomes:

$$\dot{\psi}_{ss} = -\frac{l_f}{l \cdot (l_r - l_f)} \delta_{ss} v \simeq \frac{1}{l} \delta_{ss} v \simeq \frac{v}{R} = v C_v \tag{37}$$

This expression can be used to re-write equation 18 as:

$$C_v = \frac{1}{2vh \sin \theta_{ss}} \left[v - \sqrt{v^2 - 4gh \sin \theta_{ss} \tan \theta_{ss}} \right] \tag{38}$$

This substitution was made because the curvature is easier to interpret than the yaw rate since it is simply the inverse of R which is an easy quantity to visualize. A plot of this solution for the range of velocities and lean angles typical for a leaning vehicle is shown in Figure 2.3.

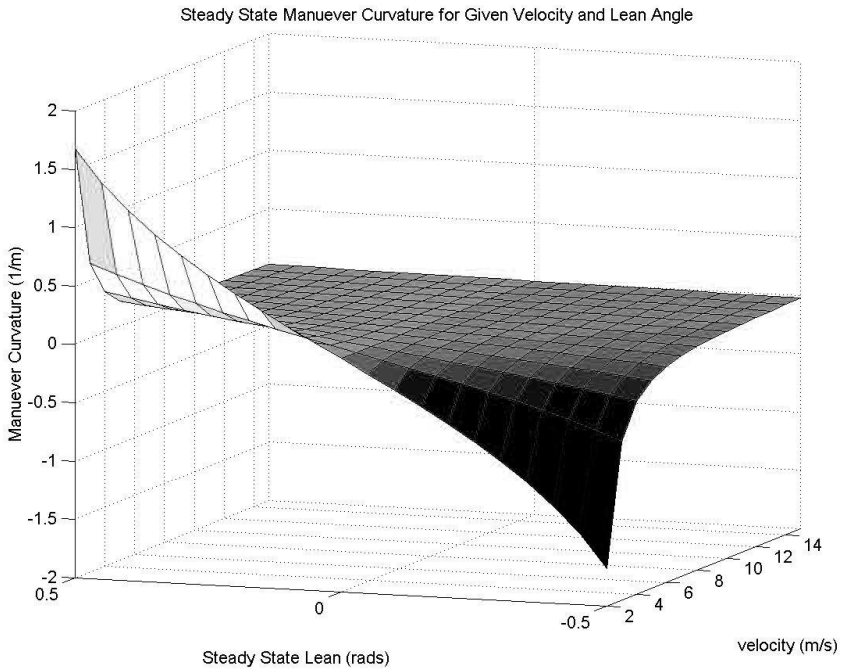

Figure 2.3 Steady state manuever curvature based on equation 38

Thus, the maneuver curvature is a way of parameterizing the equilibrium solution or desired steady state motion of the vehicle. The last step of this section is to make an approximation to this solution by assuming the second order term of equation 16 is negligible. This occurs when $\dot{\psi}_{ss}$ and θ_{ss} are small. Making this approximation, equation 16 becomes:

$$-\frac{v}{g}\dot{\psi}_{ss} + \tan\theta_{ss} = 0 \tag{39}$$

This simplifies to the typical relation between θ_{ss} and $\dot{\psi}_{ss}$:

$$\dot{\psi}_{ss} = \frac{g}{v}\tan\theta_{ss} \tag{40}$$

$$C_v = \frac{g}{v^2}\tan\theta_{ss} \tag{41}$$

If equation 40 is linearized about $\theta_{ss} = 0$, we get:

$$\dot{\psi}_{ss} = \frac{g}{v}\theta_{ss} \tag{42}$$

This shows the approximate linear nature between θ_{ss} and $\dot{\psi}_{ss}$ via the coefficient $\frac{g}{v}$. Also, as v increases, the slope of this expression approaches zero. The difference between equations 38 and 41 is a way of showing the error imposed by using equation 41 instead of equation 38. This is shown in Figure 2.4.

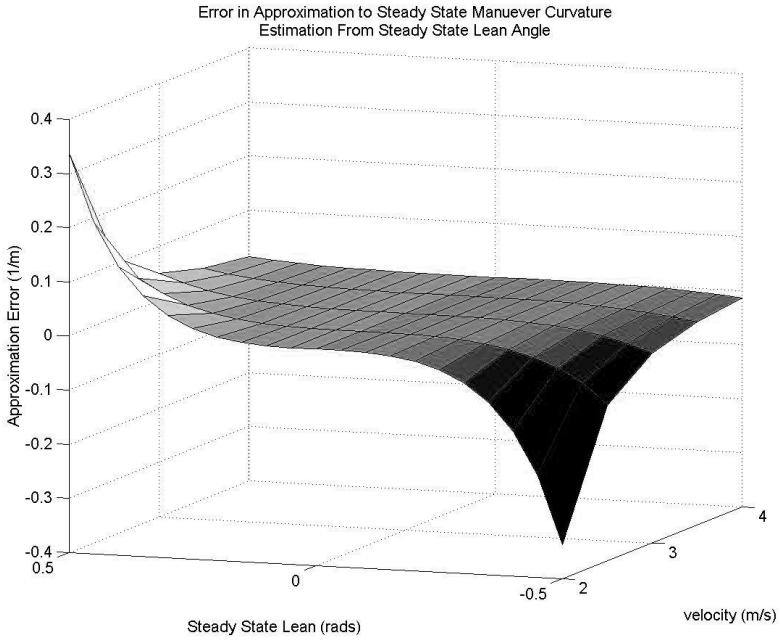

Figure 2.4 Curvature estimation error by using equation 41

We see that except for large lean angles at slow speeds, this approximation results in reasonable estimates of the maneuver curvature.

2.3 Linearized Model

The final linearized equations are found by evaluating the Jacobian of the system of equations 6 - 12 at the steady state solution. This linearized set of equations is parameterized by θ_{ss} (and $\dot{\psi}_{ss}$ which is itself parameterized by θ_{ss} from equation 30).

$$\dot{\mathbf{x}} = \mathbf{A}\mathbf{x} + \mathbf{B}\delta \tag{43}$$

Where:

$$\mathbf{A} = \left[\frac{\partial \mathbf{f}}{\partial \mathbf{x}}\right]_{\mathbf{x}=\mathbf{x}_{ss}} = \begin{bmatrix} 0 & 1 & 0 & 0 & 0 & 0 \\ 0 & A_{2,2} & 0 & A_{2,4} & A_{2,5} & A_{2,6} \\ 0 & 0 & 0 & 1 & 0 & 0 \\ 0 & A_{4,2} & 0 & A_{4,4} & A_{4,5} & A_{4,6} \\ 0 & 0 & 0 & 0 & 0 & 1 \\ 0 & A_{6,2} & 0 & A_{6,4} & A_{6,5} & A_{6,6} \end{bmatrix} \tag{44}$$

$$\mathbf{B} = \left[\frac{\partial \mathbf{f}}{\partial \delta}\right]_{\delta=\delta_{ss}} \tag{45}$$

$$= \begin{bmatrix} 0 & B_2 & 0 & B_4 & 0 & B_6 \end{bmatrix}^{\mathbf{T}} \tag{46}$$

With the following expressions for the entries of the second row:

$$A_{2,2} = \left[\frac{\partial}{\partial \dot{y}} f_2\right]_{\mathbf{x}=\mathbf{x}_{ss}} = -\frac{1}{v}\left(\frac{h^2}{J}\cos^2\theta_{ss} + \frac{1}{m}\right)(2C_f + C_r) \tag{47}$$

$$A_{2,4} = \left[\frac{\partial}{\partial \dot{\psi}} f_2\right]_{\mathbf{x}=\mathbf{x}_{ss}} = -v + 2\left(\frac{I^{zz} - I^{yy}}{J}\cos^2\theta_{ss} + 1\right) h\left(\sin\theta_{ss}\right)\dot{\psi}_{ss} \tag{48}$$

$$-\frac{2C_f l_f - C_r l_r}{Jv} h^2 \cos^2\theta_{ss} - \frac{2C_f l_f - C_r l_r}{vm} \tag{49}$$

$$A_{2,5} = \left[\frac{\partial}{\partial\theta} f_2\right]_{\mathbf{x}=\mathbf{x}_{ss}} = \left(\frac{-2\left(\cos\theta_{ss}\sin\theta_{ss}\right)\theta_{ss} + \cos^2\theta_{ss}}{J} h^2 + \frac{1}{m}\right)\left(2\lambda_f + \lambda_r\right) \tag{50}$$

$$+h\left(\frac{3I^{zz} - 3I^{yy}}{J}\cos^3\theta_{ss} + \left(1 + \frac{-2I^{zz} + 2I^{yy}}{J}\right)\cos\theta_{ss}\right)\dot{\psi}_{ss}^2 \tag{51}$$

$$+2h^2\frac{2C_f l_f - C_r l_r}{vJ}\left(\cos\theta_{ss}\right)\left(\sin\theta_{ss}\right)\dot{\psi}_{ss} \tag{52}$$

$$-4h^2\left(\cos\theta_{ss}\sin\theta_{ss}\right)\frac{C_f}{J}\delta \tag{53}$$

$$+\frac{1 - 2\cos^2\theta_{ss}}{J} mgh^2 \tag{54}$$

$$A_{2,6} = \left[\frac{\partial}{\partial\dot{\theta}} f_2\right]_{\mathbf{x}=\mathbf{x}_{ss}} = 0 \tag{55}$$

For the forth row:

$$A_{4,2} = \left[\frac{\partial}{\partial\dot{y}} f_4\right]_{\mathbf{x}=\mathbf{x}_{ss}} = -\frac{2C_f l_f - C_r l_r}{v\left(\left(I^{zz} - I^{yy}\right)\cos^2\theta_{ss} + I^{yy}\right)} \tag{56}$$

$$A_{4,4} = \left[\frac{\partial}{\partial\dot{\psi}} f_4\right]_{\mathbf{x}=\mathbf{x}_{ss}} = -\frac{2C_f l_f^2 + C_r l_r^2}{v\left(\left(I^{zz} - I^{yy}\right)\cos^2\theta_{ss} + I^{yy}\right)} \tag{57}$$

$$A_{4,5} = \left[\frac{\partial}{\partial\theta} f_4\right]_{\mathbf{x}=\mathbf{x}_{ss}} = 4\left(I^{zz} - I^{yy}\right)\frac{\cos\theta_{ss}}{\breve{E}}\left(\sin\theta_{ss}\right) C_f l_f \delta \tag{58}$$

$$+\left(I^{zz} - I^{yy}\right)\left(\frac{\cos^2\theta_{ss} + 2\theta_{ss}\left(\cos\theta_{ss}\sin\theta_{ss}\right) + I^{yy}}{\breve{E}}\right)\left(2l_f\lambda_f - l_r\lambda_r\right) \tag{59}$$

$$-2\left(2l_f^2 C_f + l_r^2 C_r\right)\left(\frac{\left(I^{zz} - I^{yy}\right)\left(\cos\theta_{ss}\sin\theta_{ss}\right)}{v\breve{E}}\right)\dot{\psi} \tag{60}$$

With:

$$\breve{E} = \left(-2I^{zz}I^{yy} + \left(I^{zz}\right)^2 + \left(I^{yy}\right)^2\right)\cos^4\theta_{ss} + \left(-2\left(I^{yy}\right)^2 + 2I^{zz}I^{yy}\right)\cos^2\theta_{ss} + \left(I^{yy}\right)^2 \tag{61}$$

$$A_{4,6} = \left[\frac{\partial}{\partial\dot{\theta}} f_4\right]_{\mathbf{x}=\mathbf{x}_{ss}} = 2\left(\cos\theta_{ss}\right)\dot{\psi}_{ss}\left(\sin\theta_{ss}\right)\frac{I^{zz} - I^{yy}}{\left(I^{zz} - I^{yy}\right)\cos^2\theta_{ss} + I^{yy}} \tag{62}$$

For the sixth row:

$$A_{6,2} = \left[\frac{\partial}{\partial\dot{y}} f_6\right]_{\mathbf{x}=\mathbf{x}_{ss}} = \frac{1}{J} h\frac{2C_f + C_r}{v}\cos\theta_{ss} \tag{63}$$

$$A_{6,4} = \left[\frac{\partial}{\partial \dot{\psi}} f_6\right]_{\mathbf{x}=\mathbf{x}_{ss}} = -\left(2\frac{I^{zz}-I^{yy}}{J}\dot{\psi}_{ss}\sin\theta_{ss} + \frac{-2l_fC_f+l_rC_r}{Jv}h\right)\cos\theta_{ss} \tag{64}$$

$$\begin{aligned} A_{6,5} &= \left[\frac{\partial}{\partial \theta} f_6\right]_{\mathbf{x}=\mathbf{x}_{ss}} = \left(\frac{I^{yy}-I^{zz}}{J}\right)\left(2\cos^2\theta_{ss}-1\right)\dot{\psi}_{ss}^2 && (65)\\ &+\left(\frac{-2l_fC_f+l_rC_r}{Jv}\right)h\left(\sin\theta_{ss}\right)\dot{\psi}_{ss} && (66)\\ &+h\left(\frac{\left(\sin\theta_{ss}\right)\theta_{ss}-\cos\theta_{ss}}{J}\right)\left(2\lambda_f+\lambda_r\right) && (67)\\ &+2h\left(\sin\theta_{ss}\right)\frac{C_f}{J}\delta && (68)\\ &+mgh\frac{\cos\theta_{ss}}{J} && (69)\end{aligned}$$

$$A_{6,6} = \left[\frac{\partial}{\partial \dot{\theta}} f_6\right]_{\mathbf{x}=\mathbf{x}_{ss}} = 0 \tag{70}$$

For the input we have:

$$\begin{aligned} B_2 &= \left[\frac{\partial}{\partial \delta} f_2\right]_{\delta=\delta_{ss}} = 2\left(\frac{1}{J}h^2\cos^2\theta_{ss}+\frac{1}{m}\right)C_f && (71)\\ B_4 &= \left[\frac{\partial}{\partial \delta} f_4\right]_{\delta=\delta_{ss}} = 2l_f\frac{C_f}{\left(I^{zz}-I^{yy}\right)\cos^2\theta_{ss}+I^{yy}} && (72)\\ B_6 &= \left[\frac{\partial}{\partial \delta} f_6\right]_{\delta=\delta_{ss}} = -\frac{2}{J}h\left(\cos\theta_{ss}\right)C_f && (73)\end{aligned}$$

Thus, the system matrices will depend upon the desired steady state maneuver curvature which was developed in the previous section. When this system is linearized about the upright position, we

get for **A**:

$$\begin{bmatrix} 0 & 1 & 0 & 0 & 0 & 0 \\ 0 & -\frac{1}{mv}\alpha\left(2C_f + C_r\right) & 0 & -\left(v + \frac{\alpha}{mv}\left(2C_f l_f - C_r l_r\right)\right) & \frac{\alpha}{m}\left(2\lambda_f + \lambda_r\right) - \frac{mh^2}{J}g & 0 \\ 0 & 0 & 0 & 1 & 0 & 0 \\ 0 & \frac{C_r l_r - 2C_f l_f}{vI^{zz}} & 0 & -\frac{2C_f l_f^2 + C_r l_r^2}{vI^{zz}} & \frac{1}{I^{zz}}\left(2l_f\lambda_f - l_r\lambda_r\right) & 0 \\ 0 & 0 & 0 & 0 & 0 & 1 \\ 0 & h\frac{2C_f + C_r}{Jv} & 0 & h\frac{2l_f C_f - l_r C_r}{Jv} & \frac{mgh}{J} - \frac{h}{J}\left(2\lambda_f + \lambda_r\right) & 0 \end{bmatrix} \tag{74}$$

Where $\alpha = \left(\frac{mh^2}{J} + 1\right)$. For **B** we get:

$$\begin{bmatrix} 0 & 2\frac{\alpha}{m}C_f & 0 & 2l_f\frac{C_f}{I^{zz}} & 0 & -\frac{2}{J}hC_f \end{bmatrix}^{\mathbf{T}} \tag{75}$$

Equations 332 - 334 represent these equations linearized about the upright, $\theta_{ss} = 0$, position. Using the parameter values given in B with a nominal velocity of $v = 5.0\frac{\mathrm{m}}{\mathrm{s}}$, we get nominal values of system.

$$\begin{aligned} \dot{\mathbf{x}} &= \mathbf{A}\mathbf{x} + \mathbf{B}\delta = \begin{bmatrix} 0 & 1 & 0 & 0 & 0 & 0 \\ 0 & -34.67 & 0 & -5.63 & 52.29 & 0 \\ 0 & 0 & 0 & 1 & 0 & 0 \\ 0 & -0.76 & 0 & -24.00 & -5.0 & 0 \\ 0 & 0 & 0 & 0 & 0 & 1 \\ 0 & 34.67 & 0 & 0.63 & -42.48 & 0 \end{bmatrix}\mathbf{x} + \begin{bmatrix} 0 \\ 97.22 \\ 0 \\ 80.50 \\ 0 \\ -97.22 \end{bmatrix}\delta \\ \mathbf{y} &= \mathbf{C}\mathbf{x} = \begin{bmatrix} 0 & 0 & 0 & 1 & 0 & 0 \\ 0 & 0 & 0 & 0 & 1 & 0 \\ 0 & 0 & 0 & 0 & 0 & 1 \end{bmatrix}\mathbf{x} \end{aligned} \tag{76}$$

The input to these equations is δ. We need to be aware that this is the angle the front wheels make about the $\mathbf{k}_5$ axis (see appendix A) and not necessarily the steering wheel angle. The steering wheel angle is a separate quantity that represents the driver's lateral direction intention. We need to be explicit about this since we will see in the next section that how we interpret this will determine the way in which we can define our controller.

We now list $\mathbf{A}$ and $\mathbf{B}$ partitioned into modes.

$$\mathbf{A} = \begin{bmatrix} \mathbf{A}_{11} & \mathbf{A}_{12} \\ \mathbf{A}_{21} & \mathbf{A}_{22} \end{bmatrix}, \ \mathbf{B} = \begin{bmatrix} \mathbf{B}_1 \\ \mathbf{B}_2 \end{bmatrix}, \ \mathbf{x} = \begin{bmatrix} \mathbf{x}_{lat} \\ \mathbf{x}_{tilt} \end{bmatrix} \tag{77}$$

$$\frac{d}{dt} \begin{bmatrix} \mathbf{x}_{lat} \\ \mathbf{x}_{tilt} \end{bmatrix} = \begin{bmatrix} \mathbf{A}_{11} & \mathbf{A}_{12} \\ \mathbf{A}_{21} & \mathbf{A}_{22} \end{bmatrix} \begin{bmatrix} \mathbf{x}_{lat} \\ \mathbf{x}_{tilt} \end{bmatrix} + \begin{bmatrix} \mathbf{B}_1 \\ \mathbf{B}_2 \end{bmatrix} \delta \tag{78}$$

The size of the $\mathbf{A}_{11}$, $\mathbf{A}_{12}$, and $\mathbf{A}_{21}$ matrices depends on how we treat the global position states y and ψ. If the concern is about lateral control, these states are included. In this case:

$$\begin{array}{lll} \mathbf{A}_{11} \in \mathbb{R}^{4\times 4} & \mathbf{A}_{12} \in \mathbb{R}^{4\times 2} & \mathbf{B}_1 \in \mathbb{R}^4 \\ \mathbf{A}_{21} \in \mathbb{R}^{2\times 4} & \mathbf{A}_{22} \in \mathbb{R}^{2\times 2} & \mathbf{B}_2 \in \mathbb{R}^2 \end{array} \tag{79}$$

When we are not concerned with the lateral control and so neglect these states, we remove the first and third rows and columns of matrix $\mathbf{A}$ and rows of matrix $\mathbf{B}$ in equations 74 and 75 respectively. These are shown in the appendix C as equations 339 and 340. The partitioned matrices change in size accordingly.

By partitioning this way, the submatrix $\mathbf{A}_{11}$ represents the dynamics for a non-tilting vehicle. It is also obvious by the forms of $\mathbf{A}_{12}$ and $\mathbf{A}_{21}$ that there is significant coupling between the two modes as expected. Clearly the vehicle tilting depends on the lateral motion and vice versa since

Non leaning	**Leaning**	**Leaning**	**Leaning**
Vehicle, $\mathbf{A}_{11}$	**Vehicle,** $\mathbf{A} \in \mathbb{R}^{6\times6}$	**Vehicle,** $\tilde{\mathbf{A}} \in \mathbb{R}^{6\times6}$	**Vehicle,** $\mathbf{A} \in \mathbb{R}^{4\times4}$
0	0	0	−23.3
0	0	0	−33.6
−23.6	−23.3	−22.7	−4.4
−35.1	−33.6	−34.1	2.7
	−4.4	−4.7	
	2.7	2.8	

Table 2.1 Plant eigenvalues

these two submatrices are not zero. It is now useful to list the eigenvalues for $\mathbf{A}$ and $\mathbf{A}_{11}$ to better understand the dynamics of the vehicle.

We see that the non-leaning vehicle, a vehicle where the tilt angle is held at zero, has two stable poles along with two poles at the origin. These poles at the origin are associated with the global lateral motion of the vehicle. For the leaning vehicle, there are two extra first order poles. These are the poles that arise due to the inverted pendulum nature of the vehicle. In a classical inverted pendulum, these poles would be of equal magnitude along the real axis, symmetric about the imaginary. In the leaning vehicle however, the lateral dynamics shift these slightly so they are not of equal magnitude. It is the pole at 2.7 that we must control to make the vehicle stable. The last thing to notice in this table is the small difference between the eigenvalues of $\mathbf{A}$ and $\tilde{\mathbf{A}}$. This will be significant in the controls section 3.1.2.

From the model of the system, for example equation 76, and the eigenvalues as listed in Table 2.1 we see that there is an unstable pole associated with the tilting. We have already shown in the introduction that tilting will be necessary as the width of the vehicle decreases beyond a certain limit to prevent tipping of the vehicle. In a typical tilting vehicle like a motorcycle or bicycle the driver provides the input δ, the front wheel angle, of the vehicle. The driver uses δ to do the lateral control of the vehicle and to stabilize the unstable tilting mode shown in table 1. This dual control mode is part of the difficulty in learning to ride a motorcycle or bicycle and why a control system would be useful. This was the main design criteria of the project, to design a tilting controller to stabilize the unstable pole of the model and so make the vehicle laterally controllable for the driver without any need to account for the leaning. In our model, δ is the input to equation 76 and influences the leaning through the term B_6. Since $B_6 < 0$, a positive steering angle will cause a negative acceleration of the lean angle. The lateral modes are just the opposite. This is what causes the phenomenon of counter-steering.

Block diagrams can provide useful insights to a dynamical system. A block diagram of a rider and motorcycle system is shown in Figure 3.1.

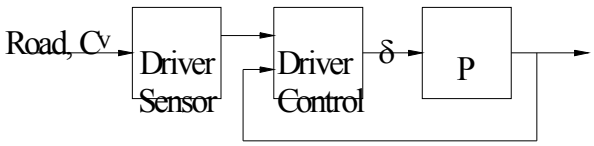

Figure 3.1 Block diagram of a motorcyle/driver system, (18:pp. 14)

References (18), (17), and (14) offer additional details to a driver's lateral control loop.

Another type of control that we originally considered studying was Direct Tilt Control (DTC) (3). In this type of control scheme, a moment is applied between the wheel suspension chassis and

the vehicle frame or body. This type of controller requires at least three wheels in order to apply this moment. Since two wheeled vehicles like motorcycles and bicycles have their wheels in line, this type of control is not suitable. From a controls point of view, it is easier to implement DTC since there is an additional system input and the tilting can in general be done independently of the lateral control performed by the driver. Figure 3.2 shows a block diagram of what this type of system might resemble.

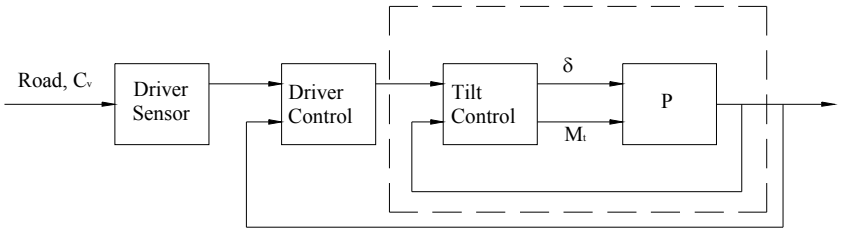

Figure 3.2 DTC block diagram

In this type of system, there are two inputs that feed into the plant. It is possible that the front wheel angle, δ, simply passes through the tilt controller unaffected making the design much simpler.

The DTC was in contrast to the Steering Tilt Control (STC) (3) we implemented on our vehicle.

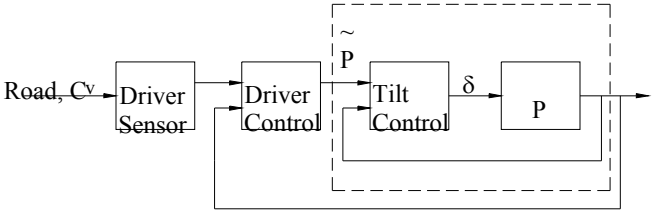

Figure 3.3 STC block diagram

In this case, the only input to the plant is the front wheel's angle. This is used to stabilize the tilting and laterally control the vehicle. The next few sections, elaborate on some of the steering-tilt-controllers we explored. One of the first controllers we explored could have been considered a steering assist type system.

3.1 Lateral Based Control

We initially spent a fair amount of time trying to design the control system with the assumption that the controller we implemented needed to stabilize both the lateral motion and the tilting motion of the vehicle. This presents a few difficulties. In order to analyze this situation, we need a method of measuring lateral tracking. To do this, we made the coordinate transformation of the system model as outlined in appendix C.6. The system equations are given by equations 350 - 352. As a state space model, these become:

$$\tilde{\mathbf{x}} = \begin{bmatrix} e_1 & \dot{e}_1 & e_2 & \dot{e}_2 & e_3 & \dot{e}_3 \end{bmatrix}^{\mathbf{T}} \tag{80}$$

$$= \begin{bmatrix} \tilde{\mathbf{x}}_{lat} & \tilde{\mathbf{x}}_{tilt} \end{bmatrix}^{\mathbf{T}} \tag{81}$$

$$\tilde{\mathbf{x}}_{lat} = \begin{bmatrix} e_1 & \dot{e}_1 & e_2 & \dot{e}_2 \end{bmatrix}^{\mathbf{T}} \tag{82}$$

$$\tilde{\mathbf{x}}_{tilt} = \begin{bmatrix} e_3 & \dot{e}_3 \end{bmatrix}^{\mathbf{T}} \tag{83}$$

$$\begin{aligned} \dot{\tilde{\mathbf{x}}} &= \tilde{\mathbf{A}}\tilde{\mathbf{x}} + \tilde{\mathbf{B}}\delta + \mathbf{F}(C_v) \\ &= \begin{bmatrix} \tilde{\mathbf{A}}_{11} & \tilde{\mathbf{A}}_{12} \\ \tilde{\mathbf{A}}_{21} & \tilde{\mathbf{A}}_{22} \end{bmatrix} \begin{bmatrix} \tilde{\mathbf{x}}_{lat} \\ \tilde{\mathbf{x}}_{tilt} \end{bmatrix} + \begin{bmatrix} \tilde{\mathbf{B}}_1 \\ \tilde{\mathbf{B}}_2 \end{bmatrix} \delta + \mathbf{F}(C_v) \end{aligned} \tag{84}$$

The last term is due to the desired states of the vehicle as discussed below. With the parameter values for our vehicle the matrices become:

$$\tilde{\mathbf{A}}_{11} = \begin{bmatrix} 0 & 1 & 0 & 0 \\ 0 & -34.667 & 173.3 & -5.63 \\ 0 & 0 & 0 & 1 \\ 0 & -0.756 & 3.78 & -23.998 \end{bmatrix} \tag{85}$$

$$\tilde{\mathbf{A}}_{12} = \begin{bmatrix} 0 & 0 \\ 52.286 & 0 \\ 0 & 0 \\ -5.0 & 0 \end{bmatrix} \tag{86}$$

$$\tilde{\mathbf{A}}_{21} = \begin{bmatrix} 0 & 0 & 0 & 0 \\ 0 & 34.667 & -173.3 & 0.63 \end{bmatrix} \tag{87}$$

$$\tilde{\mathbf{A}}_{22} = \begin{bmatrix} 0 & 1 \\ -42.476 & 0 \end{bmatrix} \tag{88}$$

$$\tilde{\mathbf{B}}_1 = \begin{bmatrix} 0 & 97.222 & 0 & 80.5 \end{bmatrix}^{\mathbf{T}} \tag{89}$$

$$\tilde{\mathbf{B}}_2 = \begin{bmatrix} 0 & -97.222 \end{bmatrix}^{\mathbf{T}} \tag{90}$$

The output equation for this system depends on the lateral or tilt controller. For the driver performing lateral control, we assumed access to all the lateral mode states, e_1, $\dot{e}_1$, e_2, and $\dot{e}_2$. Since our objective was to remove the driver from the tilting control loop, we assumed the lateral controller, the driver, did not have access to the tilting states, e_3 and $\dot{e}_3$. As such, the output for

the lateral control took the form:

$$\mathbf{y} = \begin{bmatrix} \mathbf{I} & \mathbf{0} \end{bmatrix} \begin{bmatrix} \tilde{\mathbf{x}}_{lat} \\ \\ \tilde{\mathbf{x}}_{tilt} \end{bmatrix} \tag{91}$$

The significant feature of this transformation is the inclusion of the desired parameters as shown in equations 350 - 352. At steady state, the desired values must match the steady state values derived in the section 2.2. In such a case, the lateral control of the vehicle error coordinates $e_1, e_2 \to 0$. This will also cause $e_3 \to 0$ because $\dot{\psi}_{ss}$ and θ_{ss} are the steady state solutions to the system equations.

3.1.1 Steering Assist, Independent Driver and Tilting Controller. One of the first controllers we tried was a steering assist type controller. In this case, the output from a tilt controller was superimposed on the driver's output. The front wheel angle was then based on the sum of these two signals, see Figure 3.4.

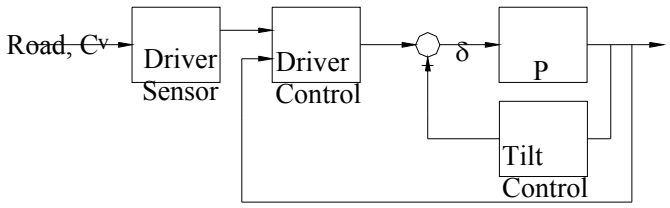

Figure 3.4 Unstable tilt control configuration

With this configuration, if the tilt controller is designed independently from the lateral control, we cannot guarantee stability. Recall, the lateral control is performed by the driver as he or she is maneuvering the vehicle in some desired way. The question was, could we design a tilt controller to form the signal δ_{tilt} based solely on the tilting states and guarantee stability of the tilting mode? The answer is no. In this case, the front wheel angle input of the vehicle is of the form $\delta = \delta_{lat} + \delta_{tilt}$. The problem is the coupling between modes. The non-zero form of system matrices $\tilde{\mathbf{A}}_{12}$ and $\tilde{\mathbf{A}}_{21}$ make the independent design impossible. This can be demonstrated in a simple example. Consider

a hypothetical case of the driver performing state feedback of the lateral states. Assume that the driver behaves in such a way that the steering output is $\delta_{lat} = -\mathbf{k}_{lat}\tilde{\mathbf{x}}_{lat} + \delta_{ff}$. δ_{ff}, in this case, is used to drive the error in on of the lateral modes to zero. In this case, $\mathbf{k}_{lat}$ makes the following equation stable.

$$\dot{\tilde{\mathbf{x}}}_{lat} = \left(\tilde{\mathbf{A}}_{11} - \tilde{\mathbf{B}}_1\mathbf{k}_{lat}\right)\tilde{\mathbf{x}}_{lat} \tag{92}$$

If the tilt controller is designed in the same manner such that, $\delta_{tilt} = -\mathbf{k}_{tilt}\tilde{\mathbf{x}}_{tilt}$ we get for the tilting mode:

$$\dot{\tilde{\mathbf{x}}}_{tilt} = \left(\tilde{\mathbf{A}}_{22} - \tilde{\mathbf{B}}_2\mathbf{k}_{tilt}\right)\tilde{\mathbf{x}}_{tilt} \tag{93}$$

The problem is that the off diagonal terms, $\tilde{\mathbf{A}}_{12}$ and $\tilde{\mathbf{A}}_{21}$ were neglected. In forming the total closed loop, we get:

$$\delta = -\begin{bmatrix}\mathbf{k}_{lat} & \mathbf{k}_{tilt}\end{bmatrix}\begin{bmatrix}\tilde{\mathbf{x}}_{lat} \\ \tilde{\mathbf{x}}_{tilt}\end{bmatrix} \tag{94}$$

$$\dot{\tilde{\mathbf{x}}} = \begin{bmatrix}\tilde{\mathbf{A}}_{11} & \tilde{\mathbf{A}}_{12} \\ \tilde{\mathbf{A}}_{21} & \tilde{\mathbf{A}}_{22}\end{bmatrix}\begin{bmatrix}\tilde{\mathbf{x}}_{lat} \\ \tilde{\mathbf{x}}_{tilt}\end{bmatrix} - \begin{bmatrix}\tilde{\mathbf{B}}_1 \\ \tilde{\mathbf{B}}_2\end{bmatrix}\begin{bmatrix}\mathbf{k}_{lat} & \mathbf{k}_{tilt}\end{bmatrix}\begin{bmatrix}\tilde{\mathbf{x}}_{lat} \\ \tilde{\mathbf{x}}_{tilt}\end{bmatrix} \tag{95}$$

$$= \left(\begin{bmatrix}\tilde{\mathbf{A}}_{11} & \tilde{\mathbf{A}}_{12} \\ \tilde{\mathbf{A}}_{21} & \tilde{\mathbf{A}}_{22}\end{bmatrix} - \begin{bmatrix}\tilde{\mathbf{B}}_1 \\ \tilde{\mathbf{B}}_2\end{bmatrix}\begin{bmatrix}\mathbf{k}_{lat} & \mathbf{k}_{tilt}\end{bmatrix}\right)\begin{bmatrix}\tilde{\mathbf{x}}_{lat} \\ \tilde{\mathbf{x}}_{tilt}\end{bmatrix} \tag{96}$$

$$= \left(\begin{bmatrix}\tilde{\mathbf{A}}_{11} & \tilde{\mathbf{A}}_{12} \\ \tilde{\mathbf{A}}_{21} & \tilde{\mathbf{A}}_{22}\end{bmatrix} - \begin{bmatrix}\tilde{\mathbf{B}}_1\mathbf{k}_{lat} & \tilde{\mathbf{B}}_1\mathbf{k}_{tilt} \\ \tilde{\mathbf{B}}_2\mathbf{k}_{lat} & \tilde{\mathbf{B}}_2\mathbf{k}_{tilt}\end{bmatrix}\right)\begin{bmatrix}\tilde{\mathbf{x}}_{lat} \\ \tilde{\mathbf{x}}_{tilt}\end{bmatrix} \tag{97}$$

$$= \begin{bmatrix}\tilde{\mathbf{A}}_{11} - \tilde{\mathbf{B}}_1\mathbf{k}_{lat} & \tilde{\mathbf{A}}_{12} - \tilde{\mathbf{B}}_1\mathbf{k}_{tilt} \\ \tilde{\mathbf{A}}_{21} - \tilde{\mathbf{B}}_2\mathbf{k}_{lat} & \tilde{\mathbf{A}}_{22} - \tilde{\mathbf{B}}_2\mathbf{k}_{tilt}\end{bmatrix}\begin{bmatrix}\tilde{\mathbf{x}}_{lat} \\ \tilde{\mathbf{x}}_{tilt}\end{bmatrix} \tag{98}$$

Now, we see that the diagonal terms were chosen to be stable however the off diagonal terms were not considered in the design. As an example consider the case with the parameter values for our

$\tilde{\mathbf{A}}_{11} - \tilde{\mathbf{B}}_1\mathbf{k}_{lat}$	$\tilde{\mathbf{A}}_{22} - \tilde{\mathbf{B}}_2\mathbf{k}_{tilt}$
-130.8	-10.1
-9.5	-96.3
-4.9	
-22.3	

Table 3.1 Control loop eigenvalues

Closed Loop
-239.6
$-12.8 \pm 6.9j$
-9.5
-1.3
2.1

Table 3.2 Closed loop eigenvalues

vehicle and the assumed and chosen forms of $\mathbf{k}_{lat}$ and $\mathbf{k}_{tilt}$ respectively.

$$\mathbf{k}_{lat} = \begin{bmatrix} 10.00 & 0.66 & 7.85 & 0.55 \end{bmatrix} \tag{99}$$

$$\mathbf{k}_{tilt} = \begin{bmatrix} -9.57 & -1.09 \end{bmatrix} \tag{100}$$

Then, $\tilde{\mathbf{A}}_{11} - \tilde{\mathbf{B}}_1\mathbf{k}_{lat}$ and $\tilde{\mathbf{A}}_{22} - \tilde{\mathbf{B}}_2\mathbf{k}_{tilt}$ are stable with the eigenvalues shown in Table 3.1. The total closed loop equation 98, however, is unstable. These eigenvalues are shown in Table 3.2.

It is possible that the driver might adjust to this since he or she is not limited to using only state feedback however this would not meet the design criteria for our tilt controller. Recall we desired a vehicle that anyone could get in and control without requiring any extra learning as is required with motorcycle. The problem with this method is that the lateral and the tilt controllers oppose each other because each one needs to control the input in opposite directions to achieve its control objective. The next controller we experimented with tried to take this into account.

3.1.2 Steer-by-Wire, Lateral State Observer (LSO). This controller was a steer-by-wire method, (14). The tilt control block, shown in figure 12, estimated the lateral and tilt states, as represented by equation 84, to form the front wheel angle δ. From the dynamics of the vehicle we

see that the lateral modes are coupled with the tilt modes. This can be seen in the form of matrix $\tilde{\mathbf{A}}$. Since $\tilde{\mathbf{A}}_{12}$ is nonzero, the tilt modes influence the lateral modes, and since $\tilde{\mathbf{A}}_{21}$ is nonzero, the lateral modes influence the tilt. Without a well defined objective, it might seem that any controller designed for this system needs to control both modes. The problem is that for this project we are not trying to design an autonomous vehicle that somehow has access to the drivers intentions. There are two aspects of this. First, with matrix $\mathbf{A}$, the system matrix for the global states, we see that the first and third columns are zeros. This means that the global position variables y, and ψ do not affect how the state of the vehicle changes except through the lateral controller. Secondly, from the form of $\mathbf{C}$, we see that we cannot even directly observe these states. Even the laterally transformed error state space is not fully state observable since:

$$rank\left[\mathbf{C^T} \quad \left(\mathbf{C\tilde{A}}\right)^{\mathbf{T}} \quad \left(\mathbf{C\tilde{A}}^2\right)^{\mathbf{T}} \quad \left(\mathbf{C\tilde{A}}^3\right)^{\mathbf{T}} \quad \left(\mathbf{C\tilde{A}}^4\right)^{\mathbf{T}} \quad \left(\mathbf{C\tilde{A}}^5\right)^{\mathbf{T}}\right]^{\mathbf{T}} \tag{101}$$

$$= \quad rank\left(obsv\left(\tilde{\mathbf{A}}, \mathbf{C}\right)\right) = 4 \tag{102}$$

Where $\mathbf{C} = \begin{bmatrix} 0 & 0 & 0 & 1 & 1 & 1 \end{bmatrix}$. We realized that a possible solution to this was to assume that the driver was performing some form of stable lateral control. When this was occurring, the lateral modes were theoretically observable through the rest of the states of the system. If we could assume some form for the lateral controller like state feedback of the lateral states, then the driver indirectly acts as a state observer. The trick then would be to design a stable state observer and controller that stabilized the system. We did try some initial design based on this method. As I will explain, there were a few problems. First I will show the design.

We start out in a manner similar to the last section. The input from the user is again considered a steering angle and is summed with the tilt controller output to form the front wheels'

angle, $\delta = \delta_{lat} + \delta_{tilt}$. If $\delta_{lat} = -\mathbf{k}_{lat}\tilde{\mathbf{x}}_{lat} + \delta_{ff}$ we get:

$$\dot{\tilde{\mathbf{x}}} = \begin{bmatrix} \tilde{\mathbf{A}}_{11} & \tilde{\mathbf{A}}_{12} \\ \tilde{\mathbf{A}}_{21} & \tilde{\mathbf{A}}_{22} \end{bmatrix} \begin{bmatrix} \tilde{\mathbf{x}}_{lat} \\ \tilde{\mathbf{x}}_{tilt} \end{bmatrix} + \begin{bmatrix} \tilde{\mathbf{B}}_1 \\ \tilde{\mathbf{B}}_2 \end{bmatrix} \delta_{lat} + \begin{bmatrix} \tilde{\mathbf{B}}_1 \\ \tilde{\mathbf{B}}_2 \end{bmatrix} \delta_{tilt} + \mathbf{F}(C_v) \tag{103}$$

$$= \begin{bmatrix} \tilde{\mathbf{A}}_{11} & \tilde{\mathbf{A}}_{12} \\ \tilde{\mathbf{A}}_{21} & \tilde{\mathbf{A}}_{22} \end{bmatrix} \begin{bmatrix} \tilde{\mathbf{x}}_{lat} \\ \tilde{\mathbf{x}}_{tilt} \end{bmatrix} - \begin{bmatrix} \tilde{\mathbf{B}}_1 \\ \tilde{\mathbf{B}}_2 \end{bmatrix} \begin{bmatrix} \mathbf{k}_{lat} & 0 \end{bmatrix} \begin{bmatrix} \tilde{\mathbf{x}}_{lat} \\ \tilde{\mathbf{x}}_{tilt} \end{bmatrix} \tag{104}$$

$$+ \begin{bmatrix} \tilde{\mathbf{B}}_1 \\ \tilde{\mathbf{B}}_2 \end{bmatrix} \delta_{tilt} + \begin{bmatrix} \tilde{\mathbf{B}}_1 \\ \tilde{\mathbf{B}}_2 \end{bmatrix} \delta_{ff} + \mathbf{F}(C_v) \tag{105}$$

$$\dot{\tilde{\mathbf{x}}} = \begin{bmatrix} \tilde{\mathbf{A}}_{11} - \tilde{\mathbf{B}}_1\mathbf{k}_{lat} & \tilde{\mathbf{A}}_{12} \\ \tilde{\mathbf{A}}_{21} - \tilde{\mathbf{B}}_2\mathbf{k}_{lat} & \tilde{\mathbf{A}}_{22} \end{bmatrix} \begin{bmatrix} \tilde{\mathbf{x}}_{lat} \\ \tilde{\mathbf{x}}_{tilt} \end{bmatrix} + \begin{bmatrix} \tilde{\mathbf{B}}_1 \\ \tilde{\mathbf{B}}_2 \end{bmatrix} (\delta_{tilt} + \delta_{ff}) + \mathbf{F}(C_v) \tag{106}$$

$$= \tilde{\mathbf{A}}_{fb\_lat}\tilde{\mathbf{x}} + \tilde{\mathbf{B}}\delta_{tilt} + \tilde{\mathbf{B}}\delta_{ff} + \mathbf{F}(C_v) \tag{107}$$

$$\mathbf{y} = \mathbf{C}\tilde{\mathbf{x}} \tag{108}$$

The term δ_{ff} comes from the steady state solution to the system equations. Recall from section 2.2 that the front wheel has a non-zero steady state value for a non-zero steady state lean. Now, if $\mathbf{C} = \begin{bmatrix} 0 & 0 & 0 & 0 & 1 & 0 \end{bmatrix}$, then $rank\left(obsv\left(\tilde{\mathbf{A}}_{fb\_lat}, \mathbf{C}\right)\right) = 6$ and the driver has made the rest of the states observable. This form of $\mathbf{C}$ was chosen because the lean angle of our vehicle was readily available from the absolute encoder although any of the states could have been used. Define the observer dynamics, with $\hat{\delta}_{lat} = -\begin{bmatrix} \mathbf{k}_{lat} & 0 \end{bmatrix} \tilde{\mathbf{z}} = -\mathbf{K}_{lat}\tilde{\mathbf{z}}$ and $\hat{\mathbf{y}} = \mathbf{C}\tilde{\mathbf{z}}$, as:

$$\dot{\tilde{\mathbf{z}}} = \tilde{\mathbf{A}}\tilde{\mathbf{z}} + \tilde{\mathbf{B}}\hat{\delta}_{lat} + \tilde{\mathbf{B}}\delta_{tilt} - \mathbf{E}\hat{\mathbf{y}} + \mathbf{E}\mathbf{y} + \mathbf{F}(C_v)$$

$$= \tilde{\mathbf{A}}\tilde{\mathbf{z}} - \tilde{\mathbf{B}}\mathbf{K}_{lat}\tilde{\mathbf{z}} + \tilde{\mathbf{B}}\delta_{tilt} - \mathbf{E}\mathbf{C}\tilde{\mathbf{z}} + \mathbf{E}\mathbf{y} + \mathbf{F}(C_v) \tag{109}$$

Now, define δ_{tilt} as, $\delta_{tilt} = -\mathbf{K}\tilde{\mathbf{z}}$. Then we need $\mathbf{E}$ chosen to make $\tilde{\mathbf{A}}_{fb\_lat} - \mathbf{EC}$ stable and $\mathbf{K}$ chosen to make $\tilde{\mathbf{A}}_{fb\_lat} - \tilde{\mathbf{B}}\mathbf{K}$ stable. This must be done with an assumed form of $\mathbf{k}_{lat}$. Using $\mathbf{k}_{lat}$ as shown in equation 99 and the "lqr" command in Matlab we get:

$$\mathbf{K} = \begin{bmatrix} -20.0 & -6.5 & -21.9 & 0.5 & -22.0 & -6.7 \end{bmatrix} \tag{110}$$

$$\mathbf{E} = \begin{bmatrix} 9.0 & -24.2 & 0.9 & -100.3 & 37.3 & 194.1 \end{bmatrix}^{\mathbf{T}} \tag{111}$$

The last 2 terms of equation 109, depend on the driver's intended trajectory. This means that as the vehicle approaches the intended trajectory, $\tilde{\mathbf{x}} \rightarrow \mathbf{0}$ (see section C.6), $\delta_{lat} \rightarrow \delta_{ff}$ and if the observer was chosen correctly, $-\mathbf{K}_{lat}\tilde{\mathbf{z}} = \hat{\delta}_{lat} \rightarrow \delta_{ff}$. Thus the driver's steering output is an indication of the intended trajectory and we can use the equations of section 2.2 to find C_v and $\mathbf{y}$ which are needed for the observer. The problem is that during transient parts of the maneuver, these are not strictly correct and the observer will yield poor results. The overall system equations are thus:

$$\dot{\tilde{\mathbf{x}}} = \tilde{\mathbf{A}}\tilde{\mathbf{x}} + \tilde{\mathbf{B}}\delta_{tilt} + \tilde{\mathbf{B}}\delta_{lat} + \mathbf{F}(C_v) \tag{112}$$

$$\begin{aligned} \dot{\tilde{\mathbf{z}}} &= \tilde{\mathbf{A}}\tilde{\mathbf{z}} - \tilde{\mathbf{B}}\mathbf{K}_{lat}\tilde{\mathbf{z}} - \mathbf{EC}\tilde{\mathbf{z}} + \tilde{\mathbf{B}}\delta_{tilt} + \mathbf{Ey} + \mathbf{F}(C_v) \\ &= \hat{\mathbf{A}}\tilde{\mathbf{z}} + \tilde{\mathbf{B}}\delta_{tilt} + \mathbf{Ey} + \mathbf{F}(C_v) \end{aligned} \tag{113}$$

Neglecting the term $\mathbf{F}(C_v)$ which does not affect stability, we can use equation 113 and the control law, $\delta_{tilt} = -\mathbf{K}\tilde{\mathbf{z}}$, to find the form of the tilt controller in figure 3.4.

$$\begin{aligned} \frac{\delta_{tilt}(s)}{\mathbf{y}(s)} &= \\ C(s) &= -\left[1 + \mathbf{K}\left(sI - \hat{\mathbf{A}}\right)^{-1}\tilde{\mathbf{B}}\right]^{-1}\mathbf{K}\left(sI - \hat{\mathbf{A}}\right)^{-1}\mathbf{E} \end{aligned} \tag{114}$$

The augmented state equation becomes:

$$\begin{bmatrix} \dot{\tilde{\mathbf{x}}} \\ \dot{\tilde{\mathbf{z}}} \end{bmatrix} = \begin{bmatrix} \tilde{\mathbf{A}} & \mathbf{0} \\ \mathbf{EC} & \tilde{\mathbf{A}} - \tilde{\mathbf{B}}\mathbf{K}_{lat} - \mathbf{EC} \end{bmatrix} \begin{bmatrix} \tilde{\mathbf{x}} \\ \tilde{\mathbf{z}} \end{bmatrix} + \begin{bmatrix} \tilde{\mathbf{B}} \\ \tilde{\mathbf{B}} \end{bmatrix} \delta_{tilt} + \begin{bmatrix} \tilde{\mathbf{B}} \\ \mathbf{0} \end{bmatrix} \delta_{lat} + \begin{bmatrix} \mathbf{F}(C_v) \\ \mathbf{F}(C_v) \end{bmatrix} \tag{115}$$

$$= \begin{bmatrix} \tilde{\mathbf{A}} & -\tilde{\mathbf{B}}\mathbf{K} \\ \mathbf{EC} & \tilde{\mathbf{A}} - \mathbf{EC} - \tilde{\mathbf{B}}\mathbf{K}_{lat} - \tilde{\mathbf{B}}\mathbf{K} \end{bmatrix} \begin{bmatrix} \tilde{\mathbf{x}} \\ \tilde{\mathbf{z}} \end{bmatrix} + \begin{bmatrix} \tilde{\mathbf{B}} \\ \mathbf{0} \end{bmatrix} \delta_{lat} + \begin{bmatrix} \mathbf{F}(C_v) \\ \mathbf{F}(C_v) \end{bmatrix} \tag{116}$$

The closed loop becomes:

$$\begin{bmatrix} \dot{\tilde{\mathbf{x}}} \\ \dot{\tilde{\mathbf{z}}} \end{bmatrix} = \begin{bmatrix} \tilde{\mathbf{A}} - \tilde{\mathbf{B}}\mathbf{K}_{lat} & -\tilde{\mathbf{B}}\mathbf{K} \\ \mathbf{EC} & \tilde{\mathbf{A}} - \tilde{\mathbf{B}}\mathbf{K}_{lat} - \mathbf{EC} - \tilde{\mathbf{B}}\mathbf{K} \end{bmatrix} \begin{bmatrix} \tilde{\mathbf{x}} \\ \tilde{\mathbf{z}} \end{bmatrix} + \begin{bmatrix} \tilde{\mathbf{B}} \\ \mathbf{0} \end{bmatrix} \delta_{ff} + \begin{bmatrix} \mathbf{F}(C_v) \\ \mathbf{F}(C_v) \end{bmatrix} \tag{117}$$

$$= \tilde{\mathbf{A}}_{tot} \begin{bmatrix} \tilde{\mathbf{x}} \\ \tilde{\mathbf{z}} \end{bmatrix} + \begin{bmatrix} \tilde{\mathbf{B}} \\ \mathbf{0} \end{bmatrix} \delta_{ff} + \begin{bmatrix} \mathbf{F}(C_v) \\ \mathbf{F}(C_v) \end{bmatrix} \tag{118}$$

-187.0	-130.6	$-28.1 \pm 5.0j$	-19.7
$-7.9 \pm 5.8j$	$-7.7 \pm 1.1j$	-3.5	-2.2
-1.7			

Table 3.3 Total closed loop eigenvalues

We can see that this system is stable by row and column manipulations of $\tilde{\mathbf{A}}_{tot}$ from which we get:

$$\begin{bmatrix} \tilde{\mathbf{A}} - \tilde{\mathbf{B}}\mathbf{K}_{lat} & -\tilde{\mathbf{B}}\mathbf{K} \\ \mathbf{EC} & \tilde{\mathbf{A}} - \tilde{\mathbf{B}}\mathbf{K}_{lat} - \mathbf{EC} - \tilde{\mathbf{B}}\mathbf{K} \end{bmatrix} \tag{119}$$

$$\rightarrow \begin{bmatrix} \tilde{\mathbf{A}} - \tilde{\mathbf{B}}\mathbf{K}_{lat} - \tilde{\mathbf{B}}\mathbf{K} & -\tilde{\mathbf{B}}\mathbf{K} \\ \tilde{\mathbf{A}} - \tilde{\mathbf{B}}\mathbf{K}_{lat} - \tilde{\mathbf{B}}\mathbf{K} & \tilde{\mathbf{A}} - \tilde{\mathbf{B}}\mathbf{K}_{lat} - \mathbf{EC} - \tilde{\mathbf{B}}\mathbf{K} \end{bmatrix} \tag{120}$$

$$\rightarrow \begin{bmatrix} \tilde{\mathbf{A}} - \tilde{\mathbf{B}}\mathbf{K}_{lat} - \tilde{\mathbf{B}}\mathbf{K} & -\tilde{\mathbf{B}}\mathbf{K} \\ \mathbf{0} & \tilde{\mathbf{A}} - \tilde{\mathbf{B}}\mathbf{K}_{lat} - \mathbf{EC} \end{bmatrix} \tag{121}$$

$$\rightarrow \begin{bmatrix} \tilde{\mathbf{A}}_{fb\_lat} - \tilde{\mathbf{B}}\mathbf{K} & -\tilde{\mathbf{B}}\mathbf{K} \\ \mathbf{0} & \tilde{\mathbf{A}}_{fb\_lat} - \mathbf{EC} \end{bmatrix} \tag{122}$$

From this, we see that the closed loop poles are stable. The eigenvalues of the system matrix, $\tilde{\mathbf{A}}_{tot}$ with our parameter values are shown in Table 3.3.

There are two problems with this system. The first is that we have actually destabilized the lateral modes of the system. If we look at the closed loop poles of equation 114 or the eigenvalues of the system matrix in equation 116, we find two poles in the right half plane. Recall that in table 1, the non leaning vehicle had two poles at the origin and two stable first order poles. With this tilt controller however, the system to be stabilized by the driver still had two poles at the origin along with 8 stable poles from the high order tilt controller and two unstable poles. The interesting thing is that the driver could perform the same type of control to stabilize this vehicle laterally as the non-leaning vehicle. Remember the form of δ_{lat} was $\delta_{lat} = -\mathbf{k}_{lat}\tilde{}\mathbf{x}_{lat} + \delta_{ff}$.

The second problem is that there is a robustness issue with this controller. When we analyze the system from the point of view of implementation, we need to replace the system matrix $\tilde{\mathbf{A}}$ with $\mathbf{A}$. This is because the matrix $\tilde{\mathbf{A}}$ was used to simulate the driver's response. In a real vehicle, we do not have access to the output e_3 but to θ. When this is done, we see that the system matrix given by equation 116 is no longer stabilized by the lateral controller δ_{lat} even though the eigenvalues did not change significantly, see Table 2.1.

3.2 Steer-by-Wire, Desired Lean Angle (DLA)

In the previous two controllers, the driver output a quantity that we interpreted as a steer angle. We have seen the difficulty in translating this into a usable quantity for the tilt controller. In the first section, the lateral and the tilt controllers conflicted with one another and so destabilized the system. In the second section, the tilt controller attempted to take the lateral control into account so that the two separate controllers would not conflict. The problem with that controller was that it was not robust as was shown. The tilt controller that we actually implemented on our experimental vehicle and had moderate success with was another steer-by-wire approach. In that scheme, the output from the user was interpreted as the desired vehicle motion parameter, C_v. The output from the driver did not need to be the front wheel angle, δ as it was considered in the other control schemes we analyzed. Whatever sensor measured the drivers intentions, steering wheel, joy-stick, etc., we could interpret it as C_v since both quantities were simply scalars. The tilt controller then caused the vehicle to track this desired motion. Figure 11 showed the block diagram of this type of system. The control law that we implemented was a modified version of an STC control law suggested in (3) - (5):

$$\delta = k_p \left(\theta_{des} - \theta\right) - k_d \dot{\theta} \tag{123}$$

Where the desired tilt rate term was dropped to avoid "set-point kick". With respect to equation 339 this becomes:

$$\begin{aligned} \delta &= -\begin{bmatrix} 0 & 0 & k_p & k_d \end{bmatrix} \mathbf{x} + k_p \theta_{des} && (124) \\ &= -\begin{bmatrix} 0 & \mathbf{K} \end{bmatrix} \begin{bmatrix} \mathbf{x}_{lat} \\ \mathbf{x}_{tilt} \end{bmatrix} + k_p \theta_{des} && (125) \end{aligned}$$

Where θ_{des} is solved from equation 41 when we are given C_v as the driver's input. We could have used equation 38 but as seen in figure 8 the approximation should be adequately close for small lean angles and typical running speeds. Substituting equation 125 into equation 78 we get:

$$\begin{aligned} \dot{\mathbf{x}} &= \begin{bmatrix} \mathbf{A}_{11} & \mathbf{A}_{12} \\ \mathbf{A}_{21} & \mathbf{A}_{22} \end{bmatrix} \begin{bmatrix} \mathbf{x}_{lat} \\ \mathbf{x}_{tilt} \end{bmatrix} - \begin{bmatrix} \mathbf{B}_1 \\ \mathbf{B}_2 \end{bmatrix} \begin{bmatrix} 0 & \mathbf{K} \end{bmatrix} \begin{bmatrix} \mathbf{x}_{lat} \\ \mathbf{x}_{tilt} \end{bmatrix} + \begin{bmatrix} \mathbf{B}_1 \\ \mathbf{B}_2 \end{bmatrix} k_p \theta_{des} \\ &= \left(\begin{bmatrix} \mathbf{A}_{11} & \mathbf{A}_{12} \\ \mathbf{A}_{21} & \mathbf{A}_{22} \end{bmatrix} - \begin{bmatrix} \mathbf{0} & \mathbf{B}_1\mathbf{K} \\ \mathbf{0} & \mathbf{B}_2\mathbf{K} \end{bmatrix} \right) \begin{bmatrix} \mathbf{x}_{lat} \\ \mathbf{x}_{tilt} \end{bmatrix} + \begin{bmatrix} \mathbf{B}_1 \\ \mathbf{B}_2 \end{bmatrix} k_p \theta_{des} && (126) \\ &= \begin{bmatrix} \mathbf{A}_{11} & \mathbf{A}_{12} - \mathbf{B}_1\mathbf{K} \\ \mathbf{A}_{21} & \mathbf{A}_{22} - \mathbf{B}_2\mathbf{K} \end{bmatrix} \begin{bmatrix} \mathbf{x}_{lat} \\ \mathbf{x}_{tilt} \end{bmatrix} + \begin{bmatrix} \mathbf{B}_1 \\ \mathbf{B}_2 \end{bmatrix} k_p \theta_{des} = \mathbf{A}_{tilt}\mathbf{x} + \mathbf{B}_{tilt}\theta_{des} && (127) \end{aligned}$$

The output equation corresponding to equation 127 is:

$$y = \mathbf{C}_{tilt}\mathbf{x} = \begin{bmatrix} 0 & 0 & 1 & 0 \end{bmatrix} \mathbf{x} = \theta \tag{128}$$

The open loop transfer function $P(s) = \frac{\theta(s)}{\delta(s)}$ of figure 11 is calculated from:

$$\begin{aligned} P(s) &= \frac{\theta(s)}{\delta(s)} = \mathbf{C}(s\mathbf{I} - \mathbf{A})^{-1}\mathbf{B} \\ &= -\frac{97s^2 + 2282s + 13585}{s^4 + 59s^3 + 870s^2 + 682s - 9184} && (129) \end{aligned}$$

The form of the inner loop block, $\tilde{P}(s)$, for the control law defined as 123 is shown in Figure 3.5.

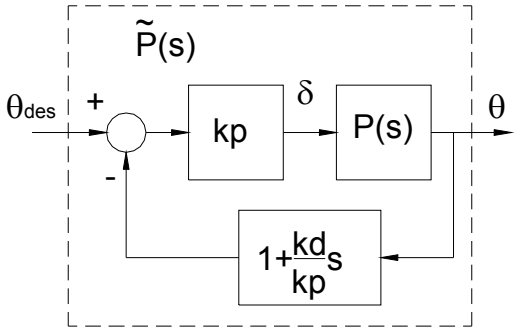

Figure 3.5 Inner loop block diagram

Let the following functions be defined as:

$$G(s) = k_p P(s) \tag{130}$$

$$H(s) = \frac{k_d}{k_p} s + 1 \tag{131}$$

We can calculate the closed loop transfer function $\frac{\theta(s)}{\theta_{des}(s)}$. This gives us a way of analyzing the robustness and performance properties of the so defined controller. The transfer function is calculated as:

$$\frac{\theta(s)}{\theta_{des}(s)} = \mathbf{C}_{tilt} \left(s\mathbf{I} - \mathbf{A}_{tilt}\right)^{-1} \mathbf{B}_{tilt} = \frac{G(s)}{1 + G(s)H(s)} \tag{132}$$

We designed **K** using Matlab's "lqr" command with **A** and **B** given by equations 339 and 340 respectively with the penalty matrices:

$$\mathbf{Q} = \begin{bmatrix} 1 & 0 & 0 & 0 \\ 0 & 1 & 0 & 0 \\ 0 & 0 & 1 & 0 \\ 0 & 0 & 0 & 0.01 \end{bmatrix}, \ \mathbf{R} = 1 \tag{133}$$

With these values, we get:

$$k_p = -3.89, \ k_d = -1.16 \tag{134}$$

$$\frac{\theta(s)}{\theta_{des}(s)} = \frac{378s^2 + 8872s + 52809}{s^4 + 171s^3 + 3892s^2 + 25294s + 43625} \tag{135}$$

$$= \frac{G(s)}{1 + G(s)H(s)} \tag{136}$$

The steady state value of $\theta(s)$ for a step in $\theta_{des}(s)$ is:

$$\theta_{ss} = \frac{52809}{43625} = 1.21 \tag{137}$$

Since $G(s)H(s)$ has 1 pole in the right half plane (see table 1) then by the Nyquist stability criterion, we need 1 counterclockwise encirclement of the -1 point in the Nyquist diagram. Figure 3.6 shows this for k_p and k_d given by 134 as the solid line and when $k_p = -3.89$ and $k_d = 0$ as the dash-dot line. The dotted line is the unit circle.

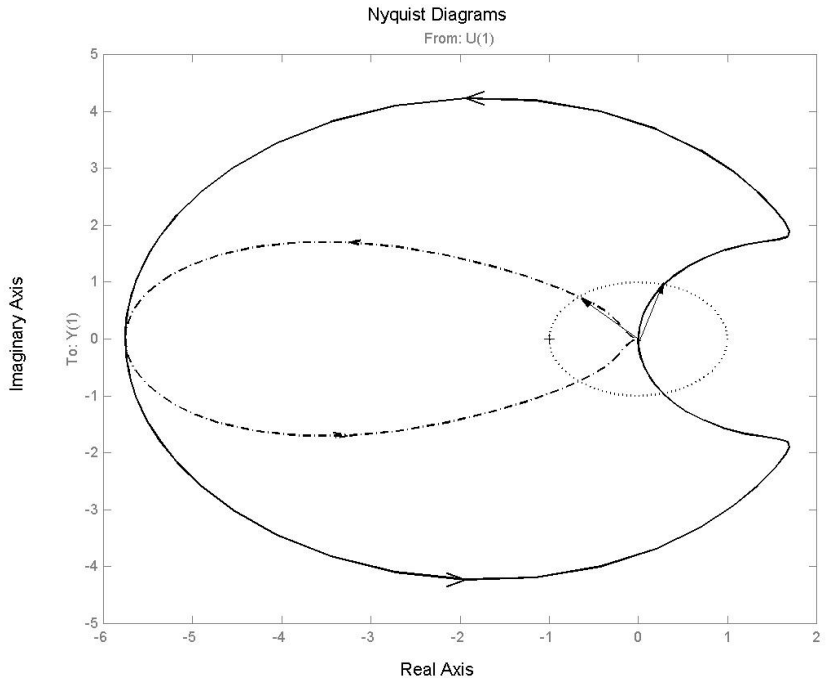

Figure 3.6 Nyquist plot of $G(s)H(s)$.

The Nyquist diagram also gives us the relative stability of the closed loop system. We see that the gain margin under both control systems is 20dB. The phase margin on the other hand is shown as the intersection of the Nyquist plot with the unit circle. This is indicated as an arrow for each system. For the system with no derivative term, the phase margin is about 42°. The phase margin for the other system is much greater, about 107°. This shows that the system should be robustly stable.

The bode plot of the closed loop system without the derivative term is shown in Figure 3.7.

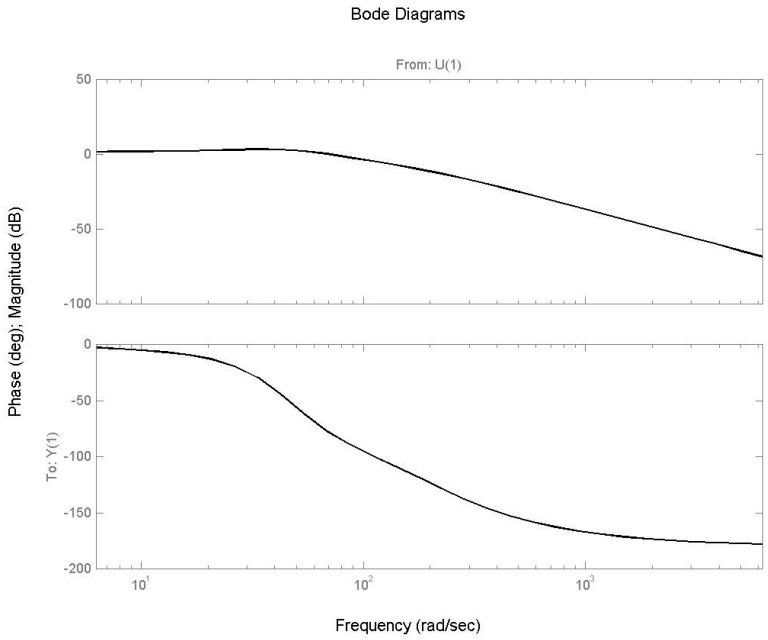

Figure 3.7 Closed loop bode diagram without derivative control term

The bandwidth, the frequencies of $\theta_{des}(s)$ that are tracked by the system, can be estimated from this diagram. The DC gain is about 1.66dB so the bandwidth is calculated as 12.7rad/s for -1.34dB. The frequency response with the derivative term is shown in Figure 3.8.

Leaning Vehicle Eigenvalues, $\mathbf{A}_{tilt} \in \mathbb{R}^{4\times4}$
-145.8
-16.0
-6.8
-2.7

Table 3.4 Leaning vehicle closed inner loop eigenvalues with PD controller

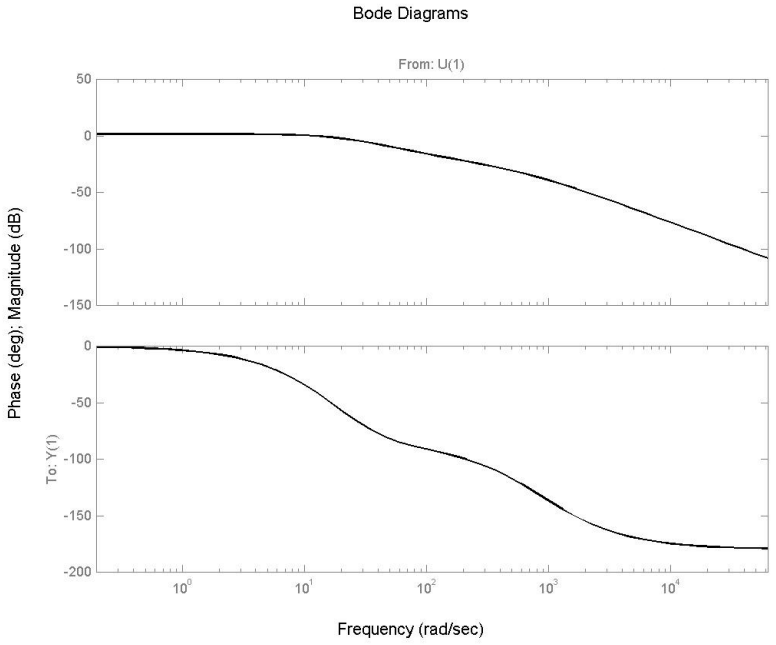

Figure 3.8 Closed loop bode diagram with derivative control term

For the system with the derivative term, we see an expected decrease in the bandwidth which was the price for increasing the robustness. The DC gain is still about 1.66dB so the bandwidth is calculated as 2.6rad/s for -1.34dB. It is this limited bandwidth that limits the lateral control.

Lastly, the eigenvalues of $\mathbf{A}_{tilt}$ of equation 127 for the controller with the derivative term are given in Table 3.4. From this, we see confirmation that we have made the vehicle stable to the input θ_{des}.

Chapter IV. Simulations

Having designed a few control systems, our next step was to implement them in simulation. We did this with two different methods. The first was to use Matlab/Simulink. The problem in doing this was that we also needed to simulate the driver's actions. Since human intention simulation could be a whole research project in itself, we did not spend too much time with that but chose simple state feed back of the lateral modes. As a verification that the lateral modes could be stabilized from the steer-by-wire controller's desired lean angle, we implemented this controller on a crude simulator in a Visual Basic program that took a real time input from the user as the driver's output.

4.1 Matlab/Simulink

4.1.1 Lateral Implications. In order to simulate this system, we needed to use equations 350 - 352 so that a driver model was included. This required deriving an expression for $\mathbf{F}(C_v)$ of equation 84.

$$\mathbf{F}(C_v) = \mathbf{F}_1\dot{\psi}_{des} + \mathbf{F}_2\ddot{\psi}_{des} + \mathbf{F}_3\theta_{des} + \mathbf{F}_4\ddot{\theta}_{des} \tag{138}$$

$$\mathbf{F}_1 = \begin{bmatrix} 0 \\ \left(\frac{\alpha}{mv}\left(C_r l_r - 2C_f l_f\right) - v\right) \\ 0 \\ -\frac{1}{vI^{zz}}\left(2C_f l_f^2 + C_r l_r^2\right) \\ 0 \\ \frac{h}{vI^{xx}}\left(2C_f l_f - C_r l_r\right) \end{bmatrix} \tag{139}$$

$$\mathbf{F}_2 = \begin{bmatrix} 0 & 0 & 0 & -1 & 0 & 0 \end{bmatrix}^{\mathbf{T}} \tag{140}$$

$$\mathbf{F}_3 = \begin{bmatrix} 0 \\ -\left(\frac{\alpha}{m}\left(2\lambda_f + \lambda_r\right) - g\left(1-\alpha\right)\right) \\ 0 \\ \frac{1}{I^{zz}}\left(l_r\lambda_r - 2l_f\lambda_f\right) \\ 0 \\ \frac{h}{I^{xx}}\left(mg + 2\lambda_f + \lambda_r\right) \end{bmatrix} \tag{141}$$

$$\mathbf{F}_4 = \begin{bmatrix} 0 & 0 & 0 & 0 & 0 & -1 \end{bmatrix}^{\mathbf{T}} \tag{142}$$

Using the simplified expressions of $\dot{\psi}_{ss}$ and θ_{ss}, equations 37 and 41 respectively, we get:

$$\dot{\psi}_{ss} = vC_v \equiv \dot{\psi}_{des} \tag{143}$$

$$\theta_{ss} = \arctan\frac{v^2 C_v}{g} \equiv \theta_{des} \tag{144}$$

Now, for a vehicle that is initially travelling on a straight road, we have $C_v \equiv 0$. When the vehicle enters a turn, $C_v \equiv \frac{1}{R}$. Thus, C_v goes through a step input. The question is, what is the value of $\ddot{\psi}_{des}$ and $\ddot{\theta}_{des}$. For the definitions given by equations 143 and 144, we get:

$$\ddot{\psi}_{des} = \frac{d\dot{\psi}_{des}}{dC_v}\dot{C}_v = v\dot{C}_v \tag{145}$$

$$\dot{\theta}_{des} = \frac{d\theta_{des}}{dC_v}\dot{C}_v \tag{146}$$

$$\ddot{\theta}_{des} = \frac{d\theta_{des}}{dC_v}\ddot{C}_v + \frac{d}{dt}\left[\frac{d\theta_{des}}{dC_v}\right]\dot{C}_v \tag{147}$$

$$\frac{d}{dt}\left[\frac{d\theta_{des}}{dC_v}\right] = \frac{d}{dC_v}\left[\frac{d\theta_{des}}{dC_v}\right]\dot{C}_v = \frac{d^2\theta_{des}}{dC_v^2}\dot{C}_v \tag{148}$$

$$\ddot{\theta}_{des} = \frac{d\theta_{des}}{dC_v}\ddot{C}_v + \frac{d^2\theta_{des}}{dC_v^2}\dot{C}_v^2 \tag{149}$$

As we would expect, these quantities depend on the first and second derivatives of C_v. The question is, what is the second derivative of a step function? The first derivative is an impulse but what

is the derivative of an impulse? The problem is that a step function is discontinuous and the quantities involving its first and second derivatives will exhibit "set-point kick". To overcome this, we windowed the step function. Then, if we defined the window correctly, we should get a function that resembles a step but is twice differentiable. We can then decrease the width of the window to appropriately approximate a step function and its first and second derivatives. Define the curvature piecewise continuously as:

$$C_v = \begin{cases} 0 & \text{for} \quad 0 \leq t < t_s \\ w(t)\frac{1}{R} & \text{for} \quad t_s \leq t < t_s + T \\ \frac{1}{R} & \text{for} \quad t_s + T \leq t \end{cases} \tag{150}$$

Where t_s is the start of the window and T is the width of the window. With this definition, we need C_v twice differentiable at the points t_s and $t_s + T$. Let us define $\ddot{w}(t)$ as:

$$\ddot{w}(t) = \frac{2\pi}{T} \sin\left(2\pi \frac{t - t_s}{T}\right) \tag{151}$$

Then integrating this expression we get:

$$\dot{w}(t) = \frac{1}{T}\left[1 - \cos\left(2\pi \frac{t - t_s}{T}\right)\right] \tag{152}$$

$$w(t) = \frac{t - t_s}{T} + \frac{1}{2\pi} \sin\left(2\pi \frac{t_s - t}{T}\right) \tag{153}$$

Figure 4.1 shows plots of these functions.

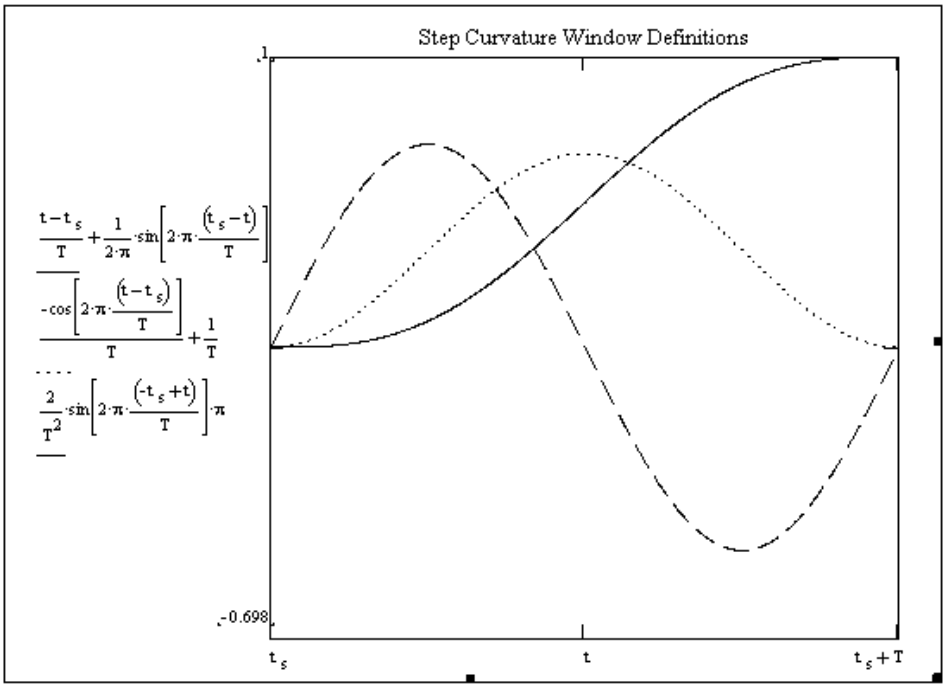

Figure 4.1 Window definitions for approximating step curvature input

This seems like a fair amount of work for some questionably useful terms. These must be included however otherwise, the results of the simulations using equations 350 - 352 will not match the results if equations 332 - 334 were used. We would, essentially, be simulating a different system.

We can plot the global trajectory using the following parametric coordinate definitions:

$$\dot{x}_{G\_des} = -v \sin \psi_{des} \tag{154}$$

$$\dot{y}_{G\_des} = v \cos \psi_{des} \tag{155}$$

The vehicle which has a lateral velocity $\dot{y}$ has the following coordinate definitions:

$$\dot{x}_G = -v \sin \psi + \dot{y} \cos \psi \tag{156}$$

$$\dot{y}_G = v \cos \psi - \dot{y} \sin \psi \tag{157}$$

In this case, x_G is the horizontal coordinate and y_G is the vertical.

Figure 4.2 shows a plot of y_{G_des} versus x_{G_des}, the desired global trajectory, when the cur vature is defined as a step input and when it is defined by equation 150 for $T = 0.5$, 1.0, and 2.0 s. The curvature starts at time $t = 2.0$ s and the total simulation time is 8.0 s with the trajectory proceeding counter-clockwise.

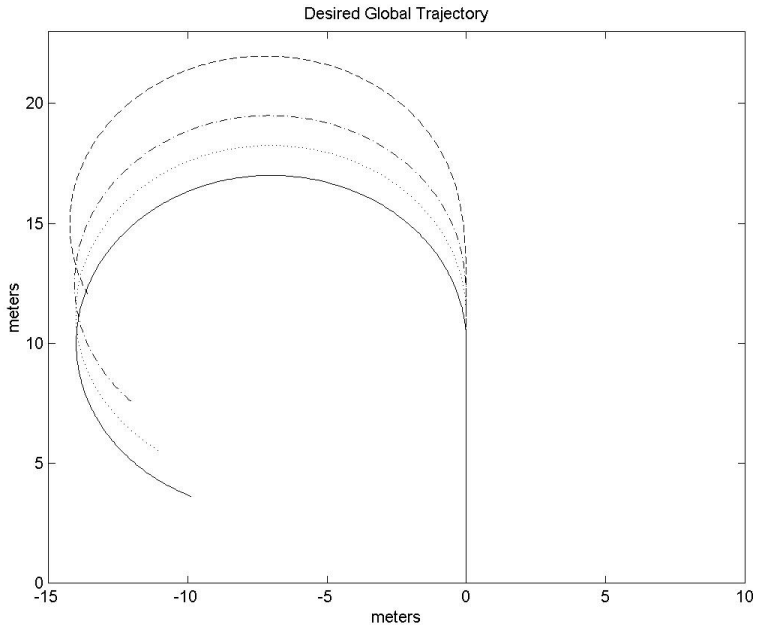

Figure 4.2 Desired global trajectory for 3 window lengths, $R = 7.0$ m

At first glance, this may seem like a poor way of defining the desired trajectory since the trajectory with a window width of only 2.0 s significantly differs from the step input case. We must remember however that it is the driver that is defining the desired trajectory and not the actual road since the driver could choose to drive into the ditch. When the curvature is windowed, the driver simply needs to start the turn earlier as is typical when a driving instructor tells the student to focus beyond the front of the car when driving. Such a result is shown in Figure 4.3.

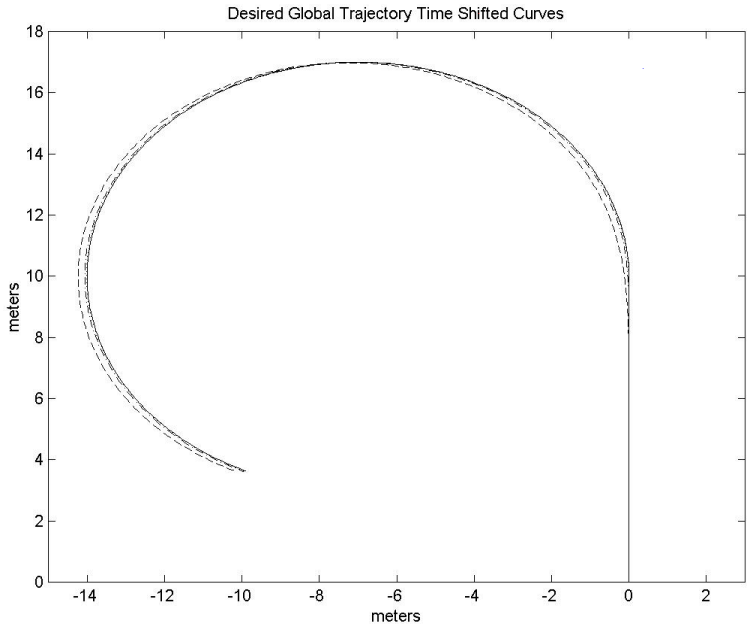

Figure 4.3 Desired global trajectory with shifted window, $R = 7.0\,\mathrm{m}$

Now that we have defined the curve the driver will try to follow, we can simulate the overall system.

4.1.2 Lateral State Observer. The system we simulated in this section is equation 115. Recall that the controllers were defined as:

$$\delta_{lat} = -\mathbf{k}_{lat}\tilde{\mathbf{x}}_{lat} + \delta_{ff} \tag{158}$$

$$\delta_{tilt} = -\mathbf{K}\tilde{\mathbf{z}} \tag{159}$$

The parameter values are listed in equations 99 and 110. The values of the observer gain matrix are listed in equation 111. The term $\begin{bmatrix} \mathbf{F}(C_v) \\ \mathbf{F}(C_v) \end{bmatrix}$ was described above. Finally, the maneuver radius and vehicle velocity were $R = 7.0$ m and $v = 5.0$ $\frac{\text{m}}{\text{s}}$ respectively. Now, let us look at the global trajectory of the vehicle when the controller is the lateral state observer (LSO) and how it compares to the desired trajectory as defined by the driver. This is shown in Figure 4.4.

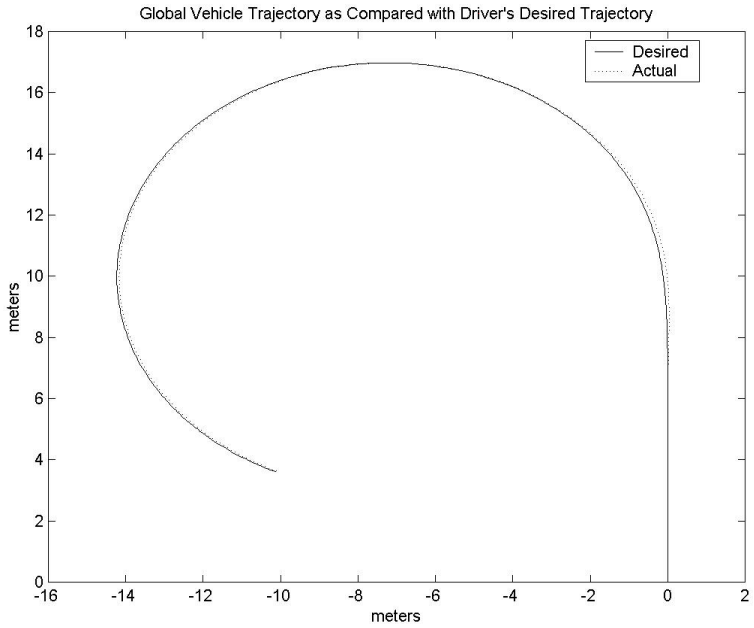

Figure 4.4 LSO controlled vehicle global trajectory

This shows the driver successfully following the road as it curves. Another important plot is the vehicle's lean angle shown in Figure 4.5.

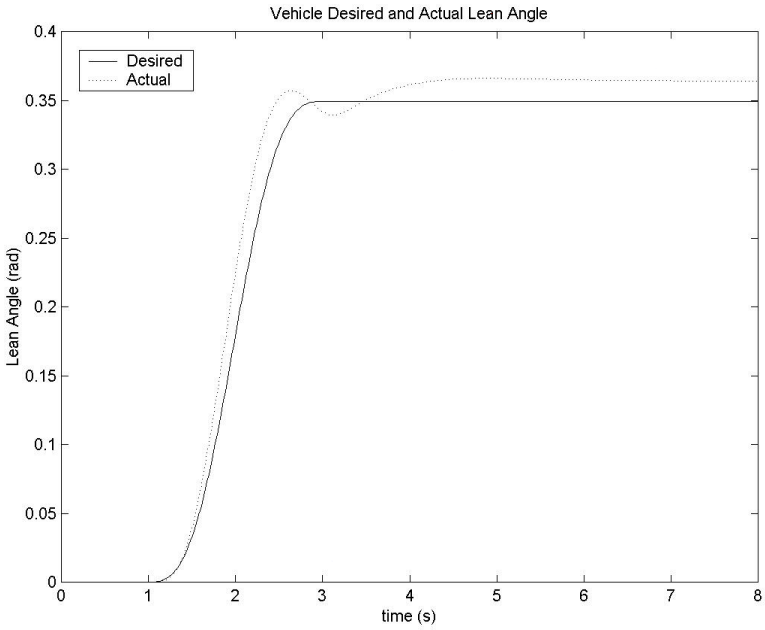

Figure 4.5 LSO controlled vehicle lean angle

There is no conflict that the desired and actual steady state lean angles are not equal because of the term for the desired motion, $\begin{bmatrix} \mathbf{F}(C_v) \\ \mathbf{F}(C_v) \end{bmatrix}$. Lastly, we look at the steering outputs in Figures 4.6 and 4.7.

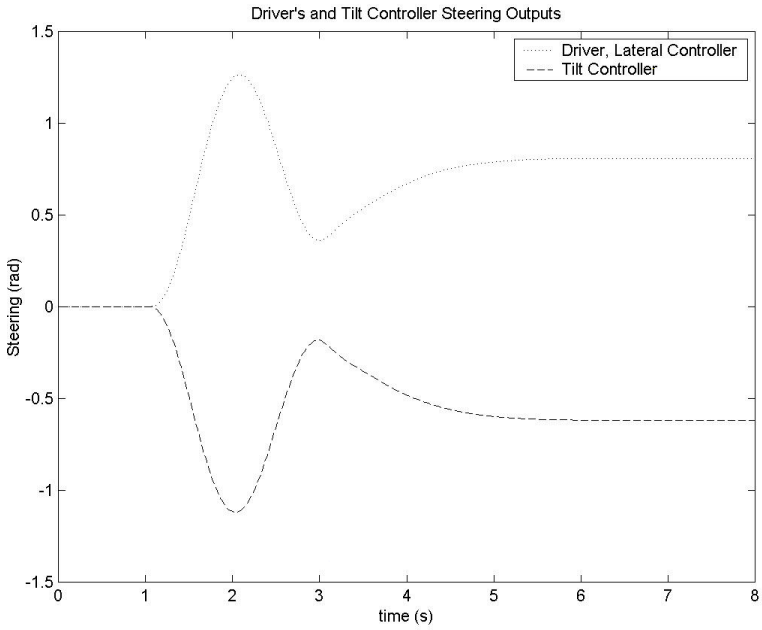

Figure 4.6 LSO controlled vehicle steering outputs

Figure 4.6 shows the two separate controllers opposing each other.

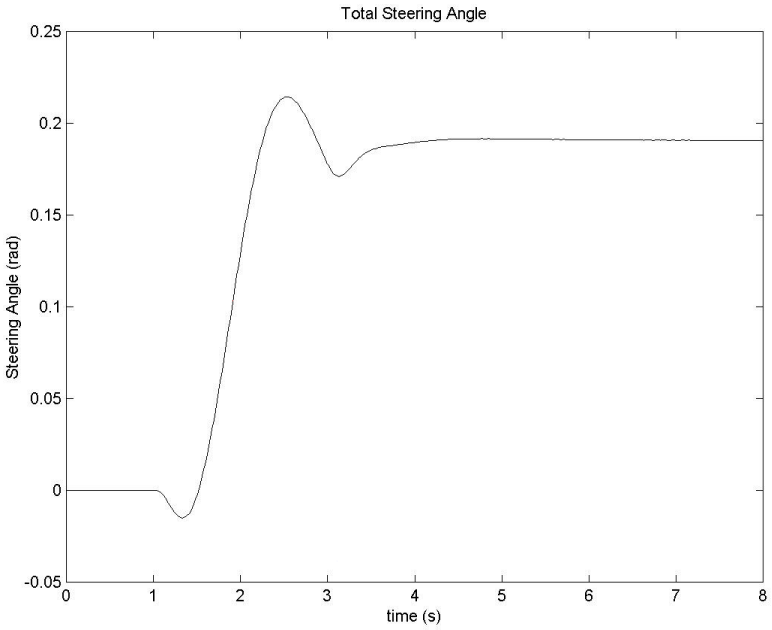

Figure 4.6 LSO controlled vehicle plant input

Figure 4.7 shows the characteristic counter-steering that is required for an inverted pendulum type control problem.

4.1.3 Desired Lean Angle, Steer-by-Wire. Next, we simulated the steer-by-wire type controller. This system, recall, was designed to track the driver's output when it was interpreted as the vehicle lean angle. A logical response to plot then is the step response of the system. If the closed loop is defined by equation 127, the step response to the desired lean angle is shown in figure 24. The controller gains were $k_p = -3.89$ and $k_d = -1.16$.

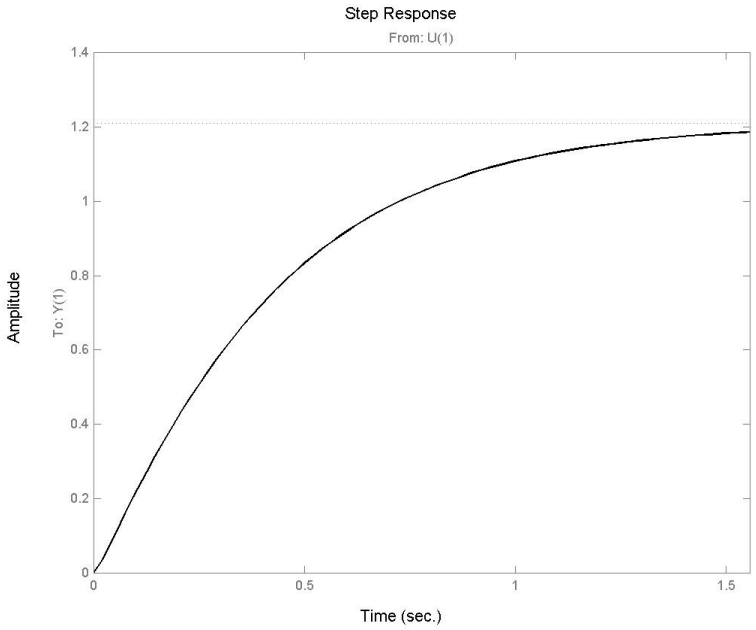

Figure 4.8 DLA controlled vehicle with derivative term, lean angle step response

As was shown in section III , the bandwidth of the system is decreased when the stabilizing derivative term is included. This decrease in bandwidth is apparent when comparing Figure 4.8 to Figure 4.9 which had the parameter values of $k_p = -3.89$ and $k_d = 0.0$.

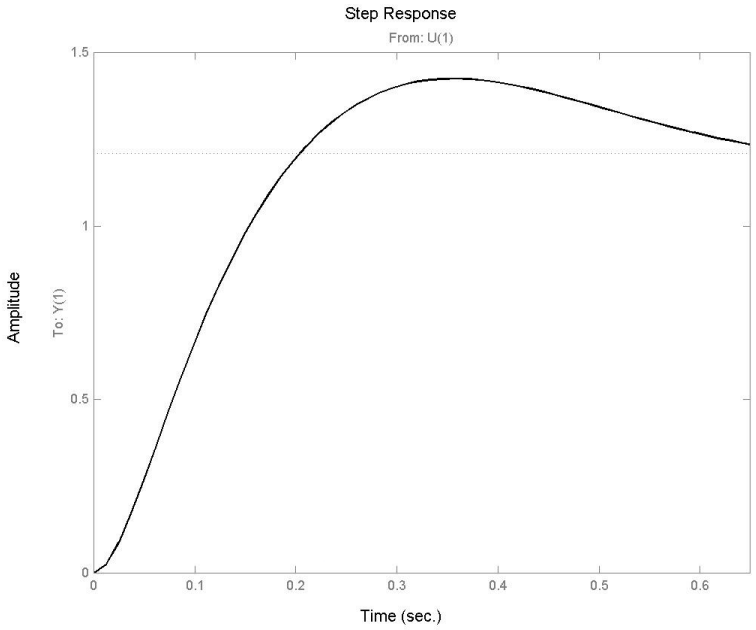

Figure 4.9 DLA controlled vehicle without derivative term, lean angle step response

Notice the decreased rise time. We can again simulate this response globally. The equation to simulate was:

$$\dot{\tilde{\mathbf{x}}} = \begin{bmatrix} \tilde{\mathbf{A}}_{11} & \tilde{\mathbf{A}}_{12} - \mathbf{B}_1\mathbf{K} \\ \tilde{\mathbf{A}}_{21} & \tilde{\mathbf{A}}_{22} - \mathbf{B}_2\mathbf{K} \end{bmatrix} \tilde{\mathbf{x}} + \begin{bmatrix} \mathbf{B}_1 \\ \mathbf{B}_2 \end{bmatrix} k_p\theta_{des} \tag{160}$$

Using a lateral controller of the form:

$$\theta_{des} = -\mathbf{K}_{lat}\tilde{\mathbf{x}} \tag{161}$$

Where K_{lat} was chosen such that equation 160 is stable.

$$K_{lat} = \begin{bmatrix} 1.0 & 1.2 & 2.8 & -0.6 & 5.8 & 2.0 \end{bmatrix} \tag{162}$$

In this case, $K = \begin{bmatrix} k_p & k_d \end{bmatrix} = \begin{bmatrix} -3.9 & -1.2 \end{bmatrix}$ is the tilt controller. The maneuver radius and vehicle velocity for the last three plots of this section Figures 4.10 - 4.12 were $R = 7.0\,\mathrm{m}$ and $v = 5.0\,\frac{\mathrm{m}}{\mathrm{s}}$ respectively. Figure 4.10 shows the global trajectory of the vehicle.

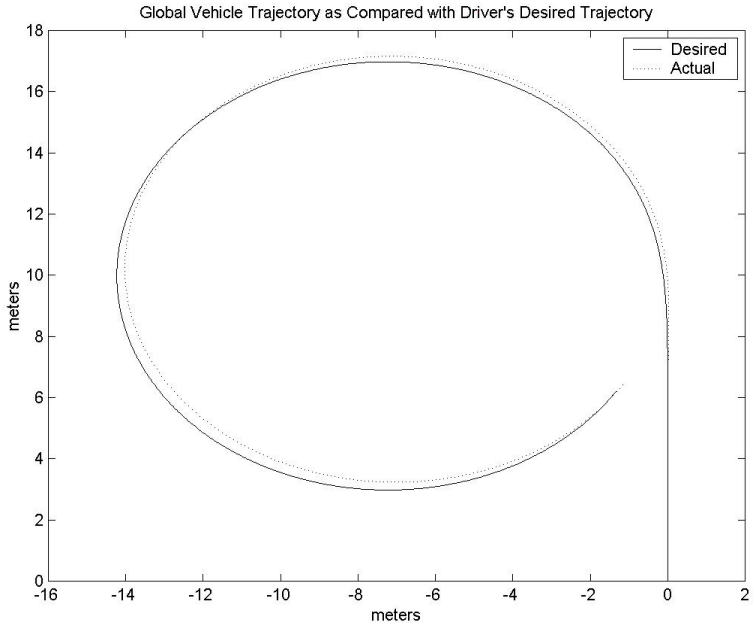

Figure 4.10 DLA controlled vehicle global trajectory

Figure 4.11 shows the tilting response compared with the output from the driver, θ_{des}.

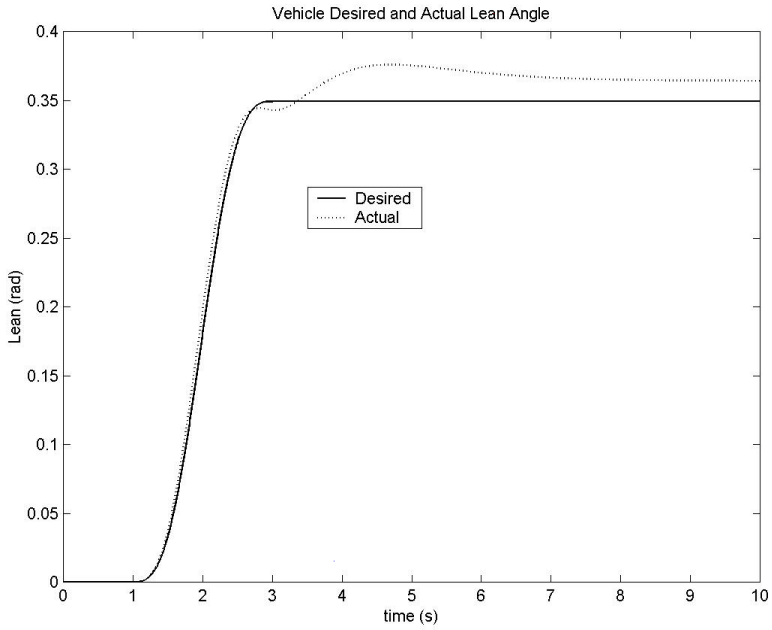

Figure 4.11 DLA controlled vehicle lean angle

The last figure of this section, figure 4.12, shows the front wheel angle for this simulation.

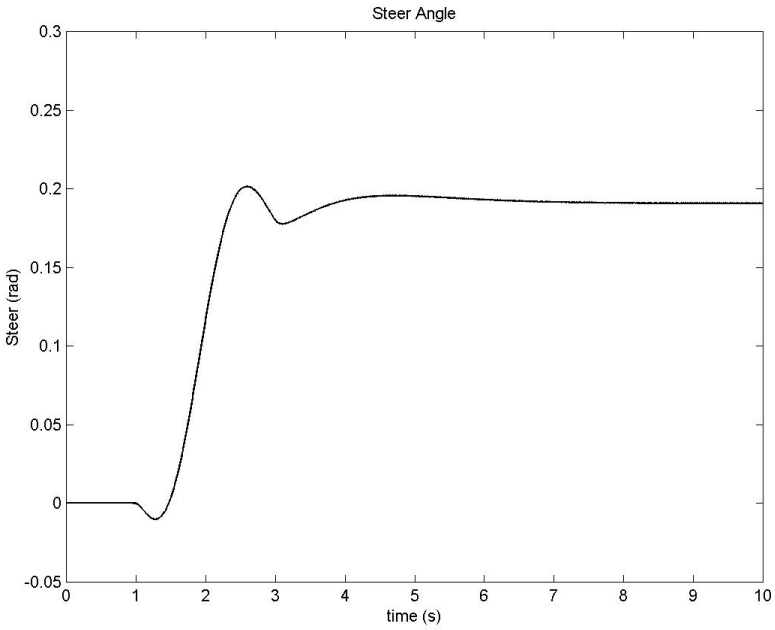

Figure 4.12 DLA controlled vehicle plant input

4.2 Visual Basic

It may seem that we are not meeting our objective of removing the driver from the tilt control loop for the Desired Lean Angle Steer-By-Wire system since the lateral controller of the previous simulations was designed as state feedback of all the error states. To show that it should still be possible to laterally control the vehicle when the driver's output is interpreted as θ_{des} and when the driver has no observation of the tilt angle, we wrote a real time simulator program with a graphical user interface.

4.2.1 Program Description. This program was written with Visual Basic to simulate the states of the vehicle. It continuously plotted a sliding bar to indicate the vehicles lateral translational position from the center of the lane. The user then positioned a joystick to keep the sliding bar close to the center stationary bar. Figure 4.13 shows the user interface.

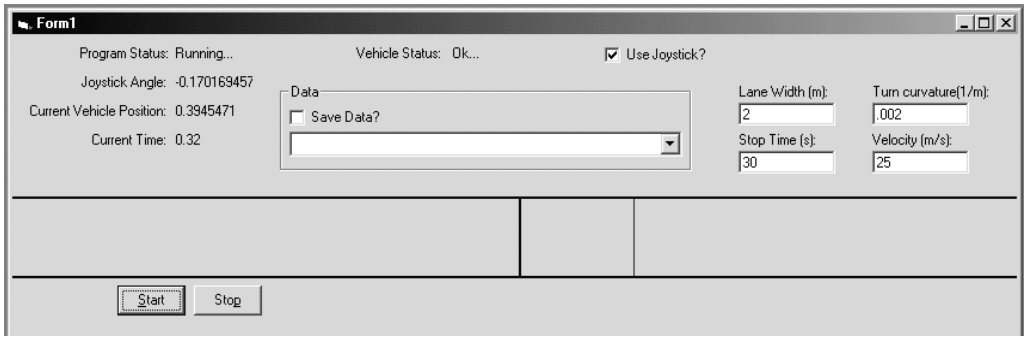

Figure 4.13 User interface for real time simulator

The thick vertical line in the center stays stationary and represents the centerline of the desired trajectory as shown in Figure 4.10. The thinner line on the right slides back and forth, as the user moved the joystick, indicating the lateral position of the center of gravity of the vehicle with respect to the centerline.

The plant was simulated as the linear model given by equations 350 to 352. These were integrated using Euler's forward method such that for any given state x:

$$x_n = T \cdot f(x_{n-1}) + x_{n-1} \tag{163}$$

Where T is the sample time of 0.003 s, and $f(x) = \dot{x}$. The simulator was programmed to stop if the lean angle exceeded about 40° or the lateral position exceeded the lane width. As we see in Figure 4.13, the driver can only respond to the vehicle's lateral position error and no other states with this simulator. The joystick lean angle was then directly interpreted as θ_{des} for the control law of equation 123 with the gains $k_p = -3.9$ and $k_d = -1.2$. Now, if the vehicle line appeared on the right side of the centerline, the user moved the joystick left pulling the vehicle back to the center. Likewise, the joystick would be moved right when the vehicle was to the left of the centerline. In this way, the user could keep the thinner line, indicating the vehicle position, close to the centerline.

If the user provided no input with the joystick, the vehicle line would quickly move to the edge of the window and the simulation would stop when it reached its limit.

4.2.2 Results. The results of one particular simulation are now presented. The parameters used in this case were $R = 20.0$ m, $v = 5.0 \frac{\text{m}}{\text{s}}$ and lane width = 2.0 m. Figure 4.14 shows the global position of the vehicle for a total running time of about 80 seconds.

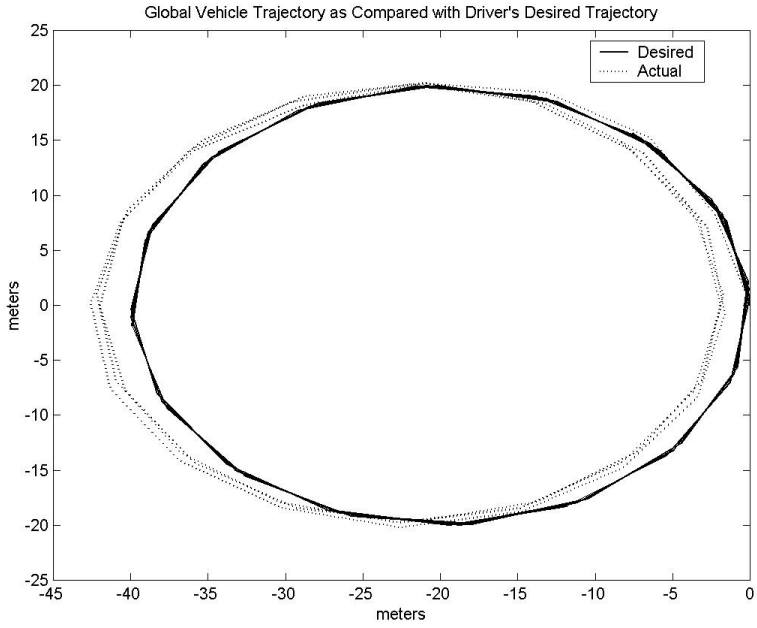

Figure 4.14 Real time simulator, vehicle global trajectory, 0 - 80s

The tracking may not be perfect but the lateral response certainly seems bounded and remains relatively close to the desired centerline trajectory. Figure 4.15 shows the same plot as figure 30 but for only the first 20 seconds.

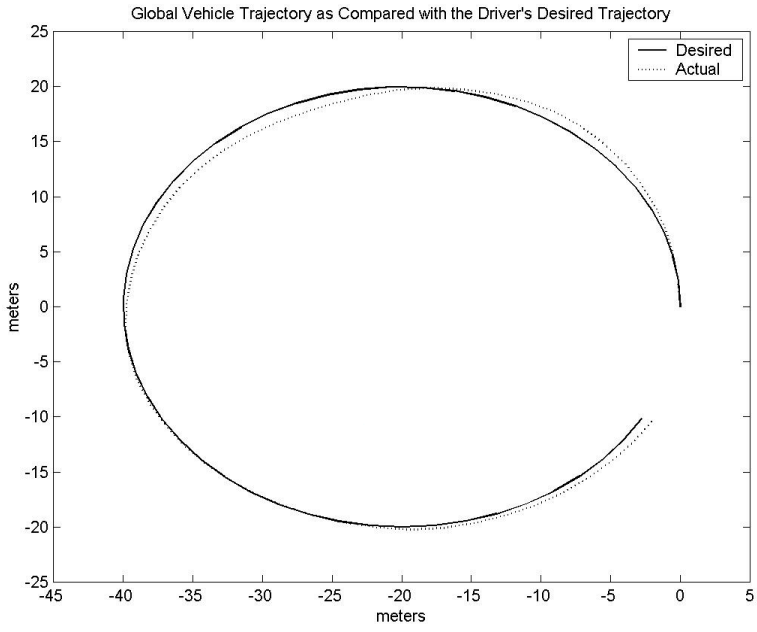

Figure 4.15 Real time simulator, vehicle global trajectory, 0 - 20s

Figure 4.16 shows the driver's input and the vehicle's actual lean angle. It again shows that there is a difference between the estimated steady state lean angle and the actual steady lean angle as we discussed in section 4.1.2 above.

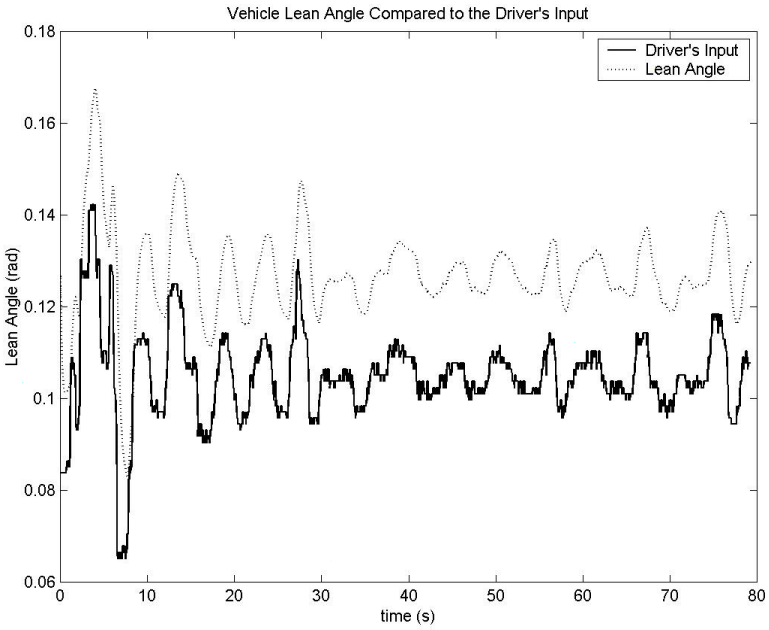

Figure 4.16 Real time simulator, vehicle lean angle, 0 - 80s

This data is rather oscillatory and future versions of the controller might be able to take this into account perhaps with Kalman filtering. The power spectrum of the lean angle data can better show this. Using the following specifications for the "spectrum" command in Matlab we obtained the power spectra of the tilt and desired tilt angle for the frequency data.

The specifications were:

- Sampling rate = 266Hz
- Length of DFT = 16384 for frequency resolution of $\frac{266 \cdot 2\pi}{16384} = 0.1$rad/s
- Hanning window of length 12000 samples
- Overlap of adjacent windows of 9000 samples (3/4 window length)

This was a long data sample, over 21,000 data points, so we could use long windowing of the data to include many cycles. We find that the desired lean angle has a peak at about 1.3 rad/s which is shown in Figure 4.17.

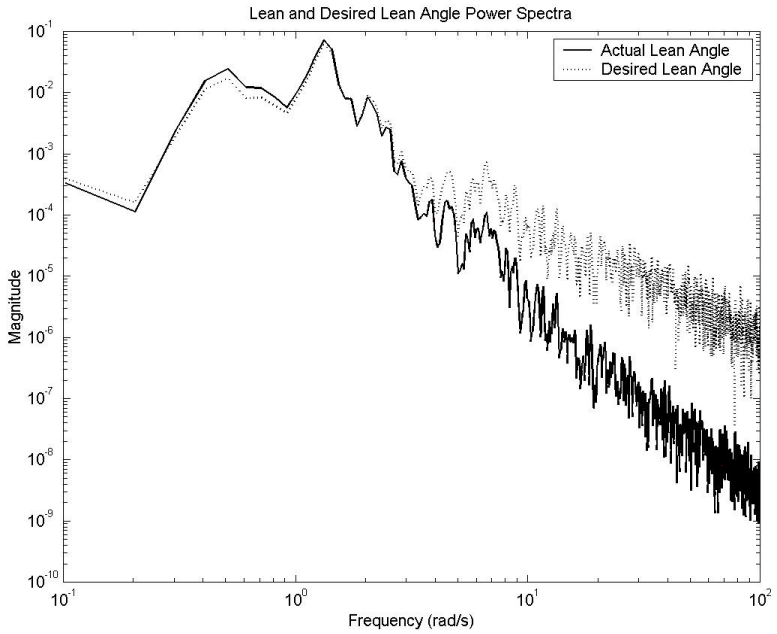

Figure 4.17 Real time simulator, vehicle lean angle power spectrum

Chapter V. Experimental Vehicle

5.1 Vehicle Description

We initially spent some time brainstorming the basic configuration to use for the vehicle. Because of the desire for a vehicle that would ultimately be used by consumers we opted for a vehicle that could be stable when the vehicle was stopped. This required a three or four wheel configuration instead of two. With only two wheels, something needs to hold the vehicle upright at a stop. On motorcycles, this is the driver's legs. With three or four wheels, we have the option of using the side-by-side wheels to hold the vehicle up with direct tilt control. We decided on the three wheel configuration with a single rear wheel because this met several objectives. These are discussed further below. First, we present some photos. Figure 5.1 shows the vehicle in the parking lot where the experiments were run.

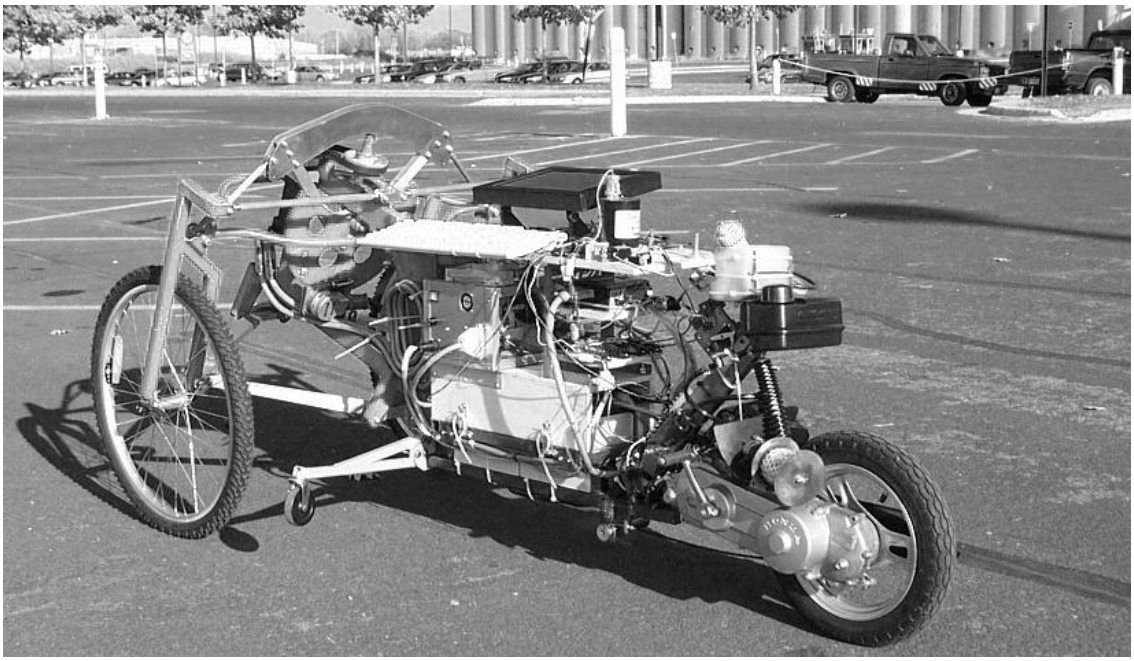

Figure 5.1 Vehicle in parking lot

A front view is shown in Figure 5.2. In this figure, the vehicle was in the lab.

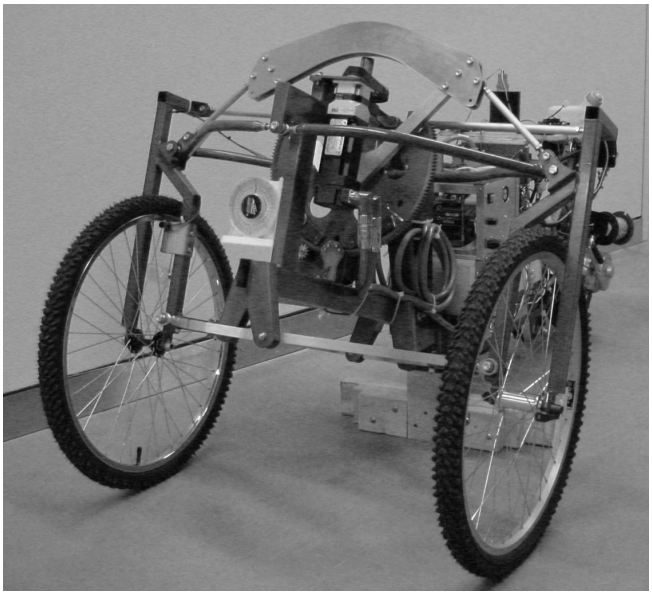

Figure 5.3 Vehicle front view

The last photo of the vehicle, Figure 5.3, is a close up view of the front chassis.

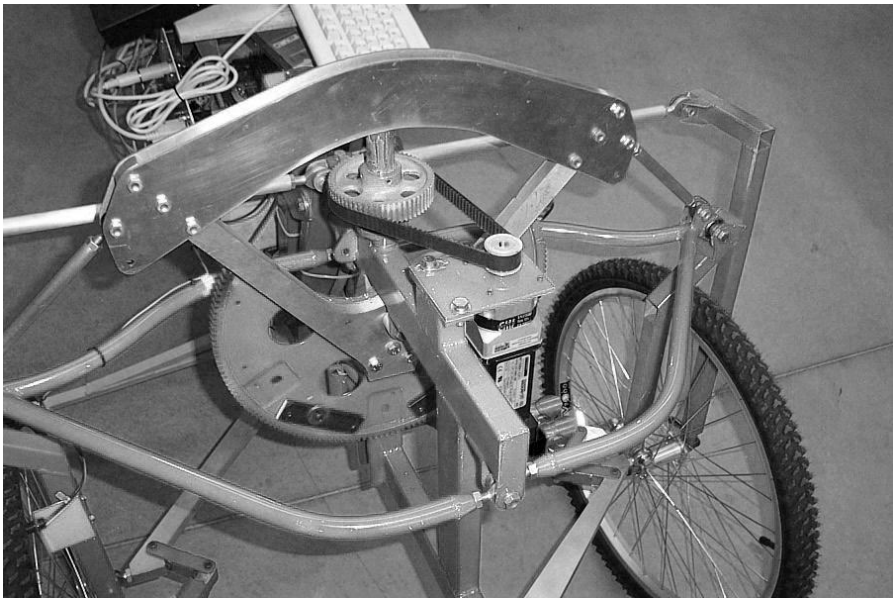

Figure 5.3 Front chassis view

5.1.1 Drive Unit. The power train we used was the rear drive unit from a 50cc Honda Spree scooter. Using this type of unit greatly simplified the design of the drive train since the unit had only two mount points that the frame needed to be built around. The unit was acquired from a local scooter scrap yard. This is shown in Figure 5.1.

5.1.2 Chassis. The configuration of a single rear wheel, necessitated that the front have two wheels. The end result is shown in Figures 5.1 - 5.3. A schematic view is given in Figure 5.4 and 5.5. A 4-bar linkage accommodated the leaning of the vehicle (numbered links in Figure 5.4). Links 2 and 4 always remain parallel to the ground plane and links 1 and 3 are parallel and at an angle θ from the vertical. The internal torques M_t, applied only in the Direct Tilt Control scheme, and M_δ are control inputs. In a non-leaning vehicle, links 1 and 5 form a rigid structure with link 6 providing suspension.

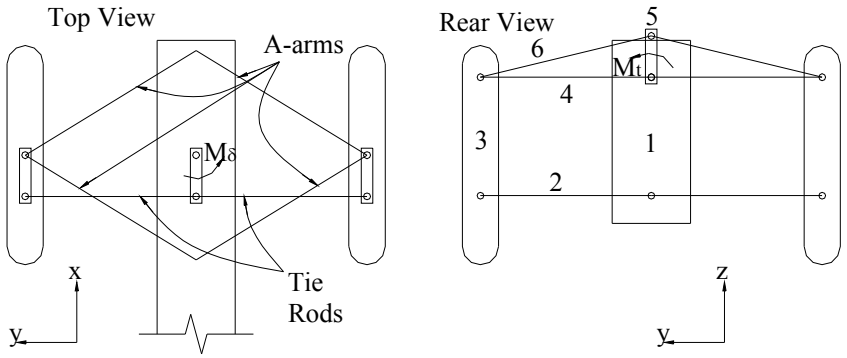

Figure 5.4 Schematic view of front chassis

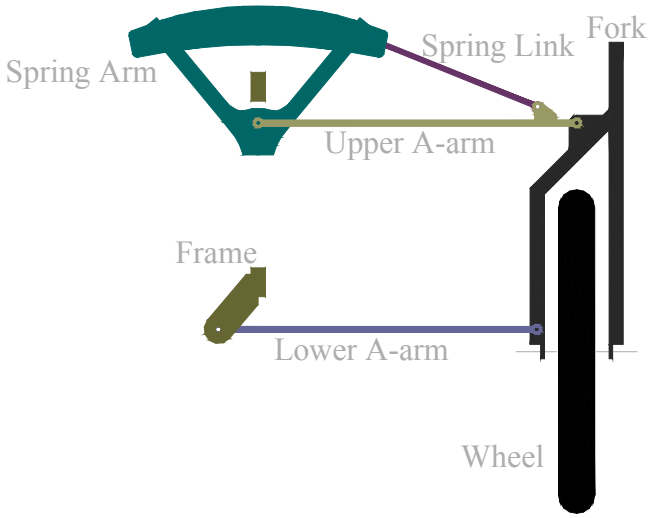

Figure 5.5 Vehicle Tilting Components

The correspondence between the links in Figures 5.4 and 5.5 are:

1. Frame
2. Lower A-arm
3. Fork (and wheel)
4. Upper A-arm
5. Spring arm
6. Spring Link

To link 5 in Figure 5.4, we mounted a 14-inch pitch diameter flex plate gear with 12-pitch. This is shown in the photos and is easily seen in Figure 5.3. If we were using "Direct Tilt Control", a torque, M_t, could be applied between links 1 (the vehicle body) and 5 (Spring arm and gear) to lean the vehicle through the gear. For "Steering Tilt Control", we used this gear to measure the angle between links 1 and 5 as the vehicle's lean angle. See the 5.1.8.3 section below.

5.1.3 Outriggers. Figure 5.1 shows the left side outrigger and castor wheel which were mounted directly behind the left front wheel. The upper limit of lean was about $\pm 15^\circ$ due to these outriggers on each side. The outriggers were a safety precaution to catch the vehicle when it crashed and acted like training wheels on a child's bike.

5.1.4 Electrical Power. Two 12 volt lead acid batteries were used to supply the 12 and 24 volt DC power that was required for the various components. These were chosen because of their ease of recharging and cost effectiveness (cheapest).

5.1.5 Computer.

5.1.5.1 Hardware. The computer components were interfaced using a PC/104 type bus that allowed for compact stacking of components.

CPU. The CPU card was a VersaLogic model EPM-CPU-6h with a clock speed of 266 MHz.

Harddrive. The harddrive held the boot files and operating system for the computer as well as our program and data files. See section 5.1.5.2 below for more details on data logging.

A/D and D/A Card. A VersaLogic model VCM-DAS-1 analog and digital input/output module was used. The module performed our analog-to-digital conversions, digital-to-analog conversions, and digital input. The card had a total of 16 A/D channels each with 16-bit resolution. The range of the channels could be set to either all ± 5 or all ± 10 volts. We set this to ± 5 with the 1 MHz, on board, low pass filter enabled. There were 2 D/A channels each with a resolution of 12-bits and set to 0 -10 volt range. Lastly, this card had 2, 8-bit digital input/output ports. One of these was used for the lean angle I/O, see 5.1.8.3.

RS-232 Card. To accommodate the extra serial connections we needed between components, we included a PCM-3640, 4-port RS-232 module. This allowed for communication between the steering motor controllers, digital gyro, and speed sensor microcontroller.

Power Supply. The power for the computer was provided by a Tri-M model HE104MAN-V4 power supply. The input to this was 12 volts DC from the vehicle batteries.

Miscellaneous. The non-critical components of the system computer included the keyboard, monitor and floppy drive. Each of these were standard items that need no further elaboration or specification.

5.1.5.2 Software. The operating system used was standard MS-DOS version 6.20. The real-time operating software we used for control and storing data to the harddrive was RTKernel 4.5 with the program written in the C language. Initially, the control algorithm was operating at 10 Hz. This was determined to be too slow and was ultimately increased to 500 Hz.

The data was logged to RAM as the vehicle was running then transferred to the harddrive when the vehicle stopped. The data for each sensor was logged to separate, single column, ASCII files. The elapsed time was also logged to its own file. Separate files were used because each running log task had a limited amount of allocated memory. Since the time was logged separately from the data, there was a slight lag between when the time data was logged and when the sensor data was logged. To determine the significance of this lag, we performed a run of the vehicle while logging the data as above, with one exception. The logging period was set to about 2 μs in order to consume as much CPU time as possible. The maximum lag was determined to be less than $0.2\mu s$ in this case. We considered this insignificant and the data was analyzed as if it were synchronous.

5.1.6 Steering. Steering was accomplished with a Kollmorgen Goldline Xt model number MT1506A1-E2C1 servomotor. This motor was controlled by a Kollmorgen Servostar Pico Drive

model PE205260 powered at 24 vdc. The position command (desired steering angle) sent to the amplifier was generated as a 0 - 10 volt analog signal from the D/A card with 12 bit resolution, see 5.1.5.1. The motor amplifier then used a 14 bit analog-to-digital conversion of this signal. The error for the motor's position control loop was calculated as the difference of the steering command and the actual position as measured by a 2048 count incremental encoder in the motor. A 1:10 gearhead on the motor was used to increase the torque and a timing belt connected the tie rod driving link to the motor. Figure 5.3 shows a zoomed version of the front steering. This view shows the steering motor along with the timing belt and the low ratio 18:62 sprockets. Along with this low sprocket ratio, we also tried a high, 1:1 ratio. To compare the torque capabilities of each sprocket ratio we recorded the position error, "pe", command from the steering amplifier for different runs of the vehicle with each ratio for the desired lean angle set to zero. The recorded value is the magnitude of the error between the commanded steering position and the actual steering position. This is converted to radians of steering and plotted as the power spectral density. Figure 5.6 shows this plot.

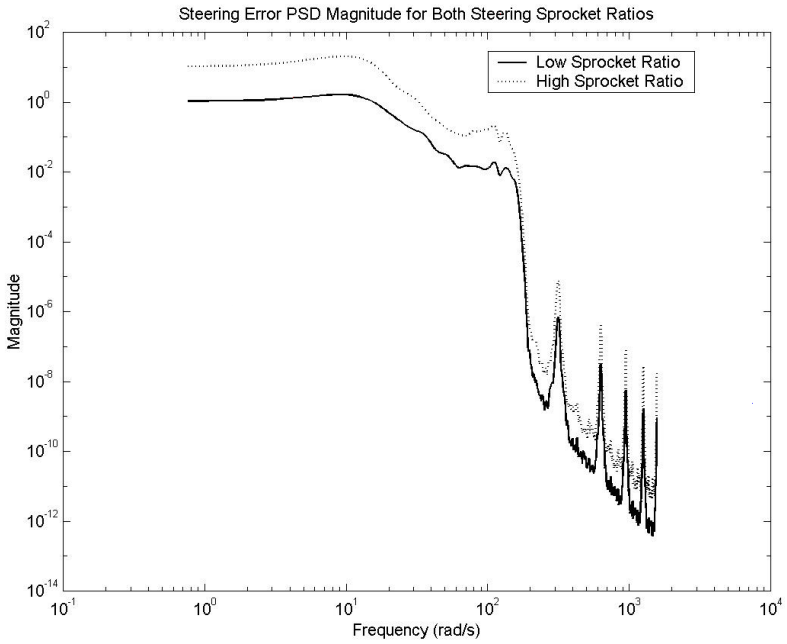

Figure 5.6 Steering error PSD for high and low sprocket ratios

We initially tried the high sprocket ratio on a few experiments but had poor results since the vehicle would tip over almost immediately. Figure 5.6 confirms this by showing the larger steering error when using the high sprocket ratio. From this, we concluded that the higher sprocket ratio did not have adequate torque. Because of this, we used the low sprocket ratio for our later experiments. The motor had a continuous torque rating of 1.35 Nm. The torque applied to the tie-rod linkage was then 13.5 Nm for the high sprocket ratio and 46.5 Nm for the low sprocket ratio. There was a trade of however for the increased torque. The trade off was a slower steering rate. The low ratio slowed down the steering rate considerably. The maximum steering rate was limited by a factor $\frac{10 \cdot 62}{18}$ or about 34.4. Instead of the maximum steering rate of 750-rpm that the motor was capable of with the 24 volt bus, we could attain only 21.8-rpm (2.3rad/s) with the gearing. Before any experiments were run, the unstable pole of the vehicle was estimated by the system model to have a

bandwidth of about 2.7rad/s. Thus, we should expect to see instances where the controller cannot stabilize the system. This is supported by certain results in the experimental section.

5.1.7 RC User Inputs.

5.1.7.1 Throttle and Rear Brake Channel. The throttle and rear brake on the drive unit was controlled with an RC servomotor from one channel of a Futaba 75 MHz radio transmitter/receiver. The servomotor used PD control to follow input signals from the transmitter. The servomotor directly controlled the position of the throttle cable on the carburetor. The rear brake was applied with a 5 resistor in series with a 12 volt DC motor applying tension to the brake cable. This motor was actuated with a switch that was closed when the RC servomotor was controlled fully backwards.

5.1.7.2 User Direction Input Channel. The user's direction command was taken from a variable potentiometer voltage divider read with the A/D card. The potentiometer was 10 kohm and its position was controlled with another RC servomotor on the other channel of the radio transmitter/receiver. The current source for the voltage divider was provided by a 5 volt IC regulator. The servomotor's full motion was not capable of the full motion of the potentiometer and so limited the voltage swing to about 1.6 - 3.8 volts. The A/D card with 16 bit resolution and ± 5 volt range yielding a 0.15 millivolt resolution was used to measure the signal after passing through an antialiasing filter, see section 5.1.9 below. To further remove noise in this signal, it was filtered through a third order Butterworth filter with a cutoff frequency of 1Hz. Figure 5.7 shows this data for a typical run of the vehicle.

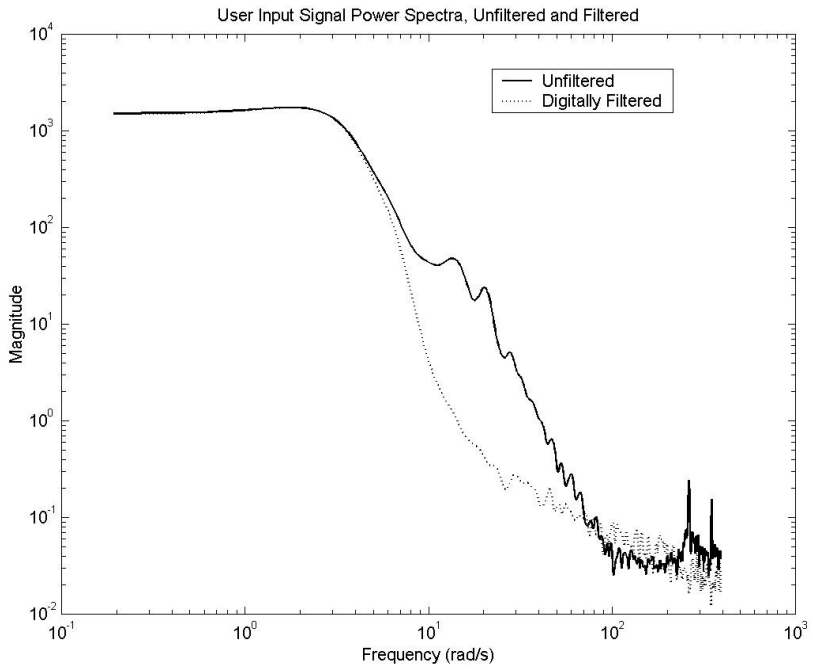

Figure 5.7 User input signal PSD, filtered and unfiltered

This shows the attenuation of noise in the input signal between 10 and 30 rad/s. Once the user input signal, u, was filtered, it was then set to a value between ± 1. Where $+1$ is full scale user input in one direction and -1 is full scale in the other. This is then converted to a desired maneuver curvature, C_v, by the following equation.

$$C_v = K_u(v)u \tag{164}$$

Notice that C_v depends on u and the velocity. If the vehicle is moving slowly, the lean angle should be close to upright. This means:

$$K_u(v) \to 0 \text{ as } v \to 0 \tag{165}$$

As the vehicle speeds up, C_v must be limited by the maximum feasible lean angle of the vehicle, 10° in our case due to the outriggers. Equation 166 relates the maximum curvature to the maximum lean.

$$C_v^{\max}(v) = \frac{g}{v^2}\tan(\theta_{\max}) \tag{166}$$

This is just equation 41. We then need to find a form of $K_u(v)$ to satisfy these conditions. The following definition is adequate.

$$K_u(v) = \begin{cases} 0 & \text{for} \quad 0 \le v < v_{win}^{\min} \\ C_v^{\max}(v_{win}^{\max}) + C_v^{\max}(v_{win}^{\max})\sin\left(\frac{\pi\left(2v - v_{win}^{\min} - v_{win}^{\max}\right)}{2\left(v_{win}^{\max} - v_{win}^{\min}\right)}\right) & \text{for} \quad v_{win}^{\min} \le v < v_{win}^{\max} \\ \frac{g}{v^2}\tan(\theta_{\max}) & \text{for} \quad v \ge v_{win}^{\max} \end{cases} \tag{167}$$

The two parameters, $v_{win}^{\min}$ and $v_{win}^{\max}$, in this equation were used to make a smooth transition in the curvature between 0 and the value listed on the last line. To make the transition, a sine window was used. $v_{win}^{\min}$ is the velocity at the start of the window. In our case this was when the speed sensor started registering at 1.5m/s, see 5.1.8.2 section below. The other parameter, $v_{win}^{\max}$, was the end of the windowing function. This was set to be 10m/s. $C_v^{\max}(v_{win}^{\max})$ is the maximum curvature at $v_{win}^{\max}$ and had a value of $0.00865\,\mathrm{m}^{-1}$.

5.1.8 Sensors.

5.1.8.1 Yaw.

The yaw rate of the vehicle was measured with both an analog and digital gyro.

Analog. The analog gyro was a Matsushita angular rate sensor model EWTS. This was used because it could be sampled faster than the digital gyro. The output range was 0.3 - 4.7 V and was measured with our A/D card. The sensitivity of the sensor was 25 millivolts per degree per second and had a bandwidth of 7 Hz defined as the output being above -7dB. See section 5.1.9 describing the analog filter.

Digital. An Andrews Autogyro was the digital gyro we used. This signal was communicated with the computer via an RS-232 port at 9600 baud. A sample rate of about 10 Hz was the fastest that could be achieved. This is why the analog gyro was also used since this would be too slow if it were used for a control input.

5.1.8.2 Speed. Vehicle speed was determined by measuring the time between spokes on the right front wheel. The spokes were sensed with a GS100701 commercial grade hall effect sensor acting as a current sink. The elapsed time was measured in microseconds with a Domino-52 microcontroller. This number was passed to our computer with a serial connection RS-232 port at 9600 baud rate and having a maximum sample rate of about 10 Hz. Because the time was measured between spokes, there was a finite minimum velocity that could be sensed. This was due to the limitation of the Domino-52 microcontroller's integer data type counter rolling over. In which case, the number passed to the computer was zero. The minimum velocity we could measure was about 1.5m/s.

5.1.8.3 Lean Angle. To measure the lean angle of the vehicle, we used an optical encoder. The encoder was a BEI model number H25D-SS-CW-8GC-7406R-LED-SM20. The relevant information in this is that it was an 8-bit absolute encoder. This was connected to the ring gear, listed in section 5.1.2 and shown in figure 36, with a 12-pitch and 1-inch pitch diameter pinion. This gave us a 14:1 increase in the resolution of the lean angle resulting in a final tilt angle resolution of about 0.0018-rads or 0.1°. To use the modified PD controller, described in section 3.2,

we needed the tilt angle of the vehicle along with the tilt rate. To estimate the tilt rate, we low pass filtered the data generated by the following discrete formula:

$$\frac{\Delta\theta}{\Delta t}(k) = \frac{\theta(k) - \theta(k-1)}{t(k) - t(k-1)} \tag{168}$$

The low pass filter we used was a second order Butterworth filter. This form was chosen because it seemed to fit the data fairly well when graphically comparing the tilt data to the tilt rate data. Figure 5.8 shows such a case where of the vehicle was oscillated back and forth in the lab. The Butterworth filter used in this case had a cutoff frequency of 1.25 Hz.

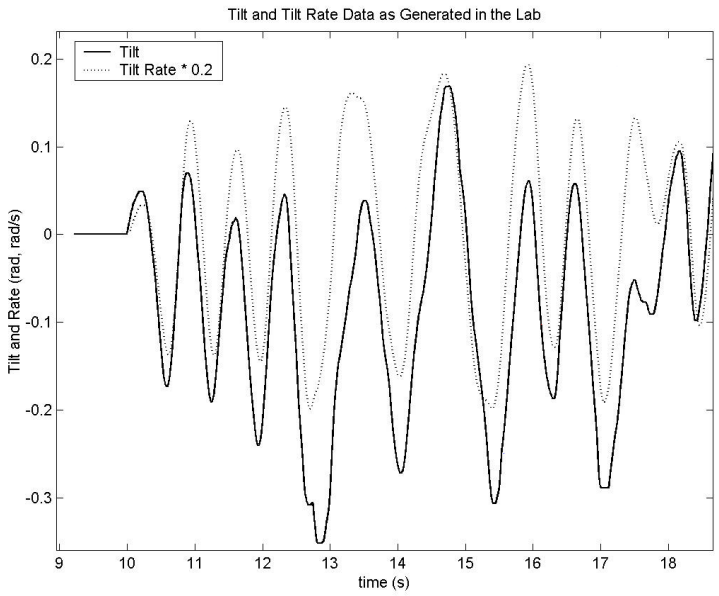

Figure 5.8 Tilt and tilt rate measurement

The data in this graph had a sample rate of 500Hz. It shows the problem with lag associated with filtering the derivative term estimate. As a reference, this method is similar to performing the digital conversion by Euler's backward method for the following derivative estimation:

$$\frac{s}{\tau s + 1} \tag{169}$$

Which is, of course, the derivative action with a first order low pass filter. The butterworth filter was tried in an effort to improve on the first order filter.

5.1.9 Antialiasing Filters. The analog signals of user input and analog yaw rate were sampled at 500 Hz. To reduce aliasing, first order low pass RC filters, were included on each of these channels. Since these filters needed to be made before we could run the vehicle, we needed to estimate the bandwidth of the system to make sure the filters did not attenuate the signals significantly. From equation 335 and an initial estimate of the parameters, we estimated the bandwidth of the system using a bode diagram to be about 30 Hz. From this, we chose the RC filter values of $R = 988$ and $C = 4.7\,\mu$F for the user input channel. The resulting bandwidth of this filter was 34 Hz. For the yaw rate gyro, an RC filter with values of $R = 1.5\,\text{k}$ and $C = 3.2\,\mu$F was used. This resulted in a filter bandwidth of 33 Hz. Thus, the system bandwidth of about 30Hz was within the bandwidth of our antialiasing filters. At the Nyquist frequency for the 500 Hz sample rate, the filters provided about 15 dB of attenuation and about 80 degrees of lag.

5.2 Parameter Estimation

The values of each of the parameters in the vehicle model had to be estimated. A brief description of how each value of the linearized model was estimated is listed.

5.2.0.1 m. The vehicle's mass was measured with two bathroom scales as the sum of weights on each tire.

$$m = \frac{2R_f + R_r}{g} = \frac{2 \cdot 58.0 + 95.0}{9.81} \cdot 4.45 = 96.0\,\text{kg} \tag{170}$$

The number 4.45 is the conversion from lbf to N.

5.2.0.2 l. This distance was measured with tape measure as the distance between the contact points of the front and rear tires.

$$l = 60.0\,\text{in} = 1.52\,\text{m} \tag{171}$$

5.2.0.3 l_f, l_r. These parameters were estimated with the following formula's:

$$l_f = \frac{R_r}{2R_f + R_r} l = \frac{95.0}{2 \cdot 58.0 + 95.0} \cdot 1.52 = 0.69\,\text{m} \tag{172}$$

$$l_r = \frac{2R_f}{2R_f + R_r} l = \frac{2 \cdot 58.0}{2 \cdot 58.0 + 95.0} \cdot 1.52 = 0.84\,\text{m} \tag{173}$$

5.2.0.4 h. Estimating this quantity took a little more effort. To do this, we measured the weight on the rear tire when it was held at various heights. Figure 5.9 shows a schematic of this process for the wheel reactions R^f and R^r.

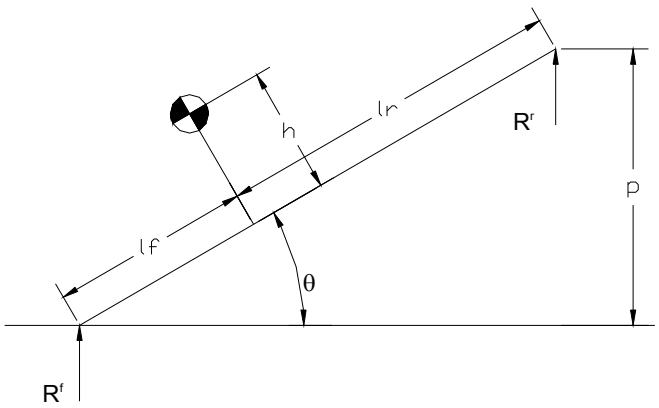

Figure 5.9 Center of gravity height estimation schematic

$p \pm 0.5$ (in)	$\frac{p}{\sqrt{p^2+l^2}}$, $(\tan\theta)$	$R_r \pm 2.0$ (lbs)
0.0	0.0	95.0
20 5/16	0.32	90.0
37 5/8	0.53	80.0
43 5/16	0.59	78.0
48 3/4	0.63	71.0

Table 5.1 Center of gravity height estimation data

The formula that relates h to R_r and p is:

$$h = \frac{Wl_f - R_r l}{W} \cdot \frac{1}{\tan\theta} = \frac{Wl_f - R_r l}{W} \cdot \frac{\sqrt{p^2+l^2}}{p} \tag{174}$$

Where $W = 2R_f + R_r$, is the total weight of the vehicle or as measured above, 211.0 lbs. By solving for R_r we get an expression that we can use with least squares to get an estimation of h.

$$R_r = -\frac{Wh}{l}\tan\theta + \frac{Wl_f}{l} = -\frac{Wh}{l} \cdot \frac{p}{\sqrt{p^2+l^2}} + \frac{Wl_f}{l} \tag{175}$$

Which is a linear expression for the pair $(\frac{p}{\sqrt{p^2+l^2}}, R_r)$. The slope of the trendline fitting this data will be an approximation to $-\frac{Wh}{l}$. The data we acquired is given in Table 5.1.

Figure 5.10 shows this data along with the least squares fitted trendline.

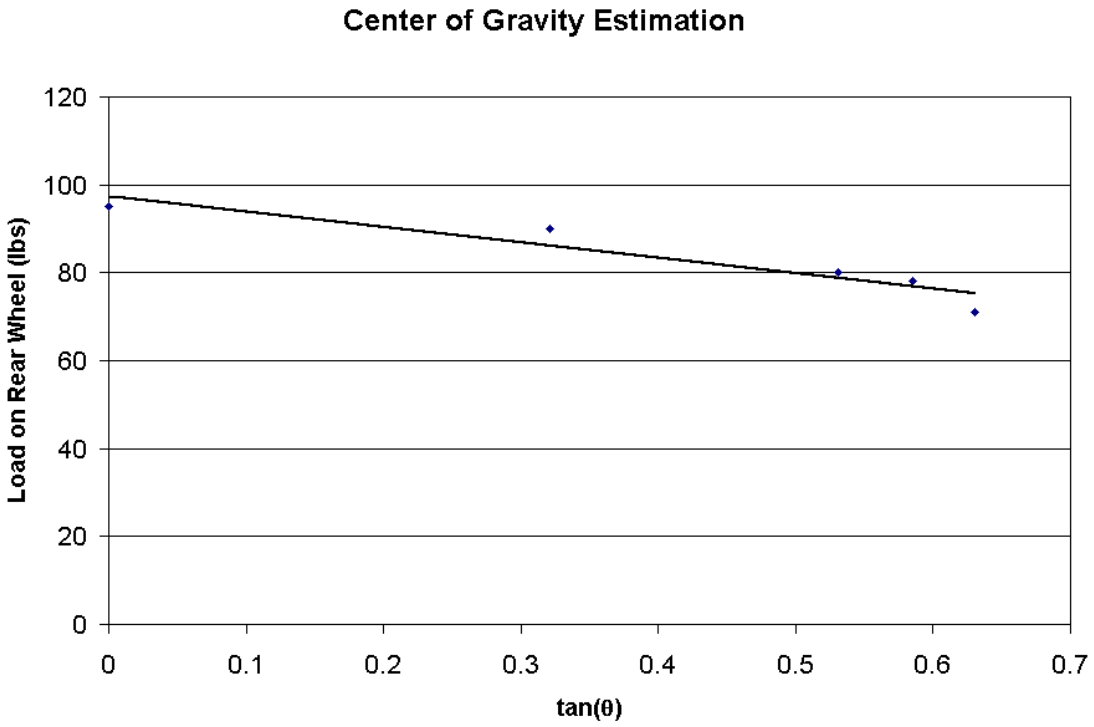

Figure 5.10 Center of gravity height estimation data

The fitted trend line was calculated using Microsoft Excel's trendline capability which uses least squares. Doing so, we find the parameters with the 95% confidence levels to be, $(-34.91 \pm 22.8, 97.24 \pm 10.9)$. The so obtained equation was $y = -34.91x + 97.24$. As a check to its validity, if we calculate the value of $\frac{Wl_f}{l}$ we get 95.0 lbs which is very close to the value 97.2 lbs as estimated by the trendline. From this, we can now calculate h.

$$h = \frac{-slope \cdot l}{W} = \frac{34.91 \cdot 60.0}{211.0} = 9.9\,\text{in} = 0.25\,\text{m} \tag{176}$$

5.2.0.5 I^{xx}. To estimate this value, we start the system (vehicle) from the initial condition $\mathbf{x} = \begin{bmatrix} 0 & 0 & 0 & 0 & \epsilon & \epsilon' \end{bmatrix}^{\mathbf{T}}$. Since the lateral modes are at a stable equilibrium position, we have isolated the parameter I^{xx} from the other unestimated parameters. We plotted data of the

vehicle tipping over from upright while the velocity was zero (vehicle stationary). This was done by holding the vehicle at an initial value and releasing it. Equation 315 then becomes:

$$\theta_{2d} = \frac{1}{I^{xx} + h^2 m \sin^2\theta} \left(mgh\left(\sin\theta\right) - h^2 m \left(\cos\theta \sin\theta\right) \theta_d^2 \right) \tag{177}$$

Since m, g, and h are now known, we can plot the response of this model to the initial conditions of the vehicle while varying I^{xx} to match the actual data. Figure 5.11 shows these results.

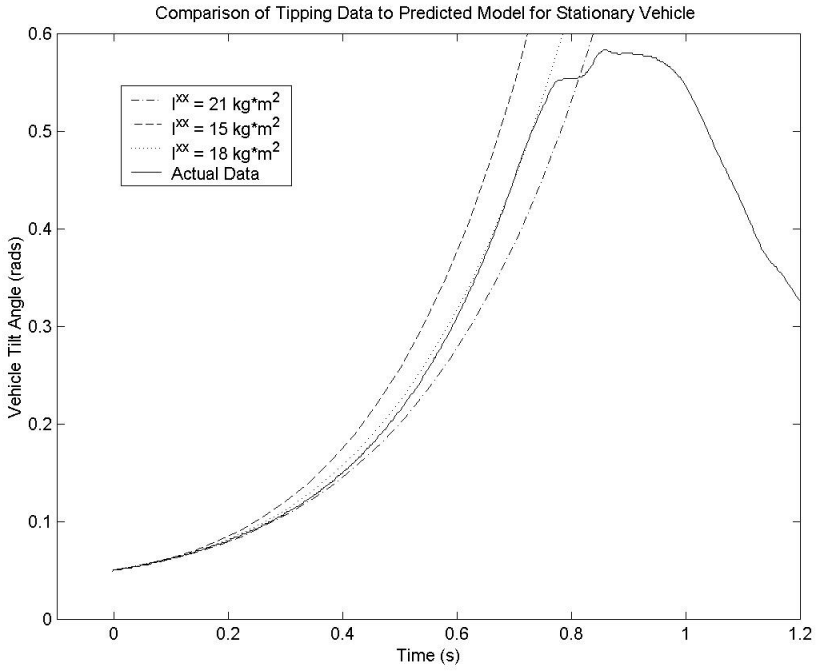

Figure 5.11 Predicted tipping response of vehicle for various values of I^{xx}

From this plot, we estimated I^{xx}.

$$I^{xx} = 18.0\,\mathrm{kg\,m^2} \tag{178}$$

5.2.0.6 $I^{zz}, C_f, C_r, \lambda_f, \lambda_r$. Unlike I^{xx}, these parameters needed to be estimated together. The lateral modes that are affected by these parameters are the vehicle's lateral translation and yaw. The limitations of our experiments prevented isolating each lateral mode as we isolated the tilting mode in estimating I^{xx}. This would in general be a difficult feat because of the vehicle's configuration. It would be theoretically possible to perform an experiment with only lateral translation if the vehicle had 4-wheel steering since in such a case we might be able to prevent yaw motion but this is far beyond the scope of this project. It might also be possible to look at the vehicle when in a steady state turn where there is a steady state yaw but no translation but again, this is beyond the scope of this project. Finally, since there was no method to lock the vehicle upright (remove the tipping mode), we could not isolate the lateral modes from the tipping mode. For this reason, closed loop control needed to be included when estimating these lateral parameters to get a long enough sample. The estimation of these parameters was then done by varying these parameters for a simulated model that was tracking the user's input to an actual vehicle experiment. Recall that the system block diagram is composed of two loops. The outer lateral loop is controlled by the driver. The inner tilting loop controls the tilting and so, tracks the response from the driver. To compare the simulated vehicle's response to the actual vehicle's response, we fed the recorded input of the driver and the recorded vehicle velocity, from an actual test run, into the simulation. The controller on the simulated vehicle then tracked this input using the same tilt control gains k_p, and k_d as was used for that particular experimental run. A block diagram of this setup is shown in Figure 5.12.

I^{zz}	$60.0\,\mathrm{kg\,m^2}$
C_f	$3500.0\frac{\mathrm{N}}{\mathrm{rad}}$
C_r	$5480.0\frac{\mathrm{N}}{\mathrm{rad}}$
λ_f	$1000.0\frac{\mathrm{N}}{\mathrm{rad}}$
λ_r	$2000.0\frac{\mathrm{N}}{\mathrm{rad}}$

Table 5.2 Lateral mode parameter values

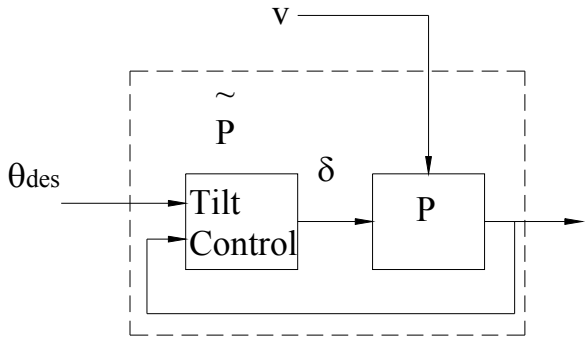

Figure 5.12 Lateral motion parameter estimation block diagram

In Figure 5.12, the plant P is the linearized model given in the section II and derived in appendix

C. The inputs θ_{des} and v were taken from the experimental data. We then varied the values of I^{zz}, C_f , C_r, λ_f , and λ_r to achieve the approximate best fit to the experimental yaw rate data. Using the values of these parameters given in Table 5.2, we plotted the simulated and actual tilting and yaw rate data in Figures 5.13 and 5.14.

From these plots we see that tracking fails when the vehicle tilts too far and the outriggers hit the ground. This occurs at values of about -0.25 and 0.35 rad in figure 46 and can be seen as the limits of motion.

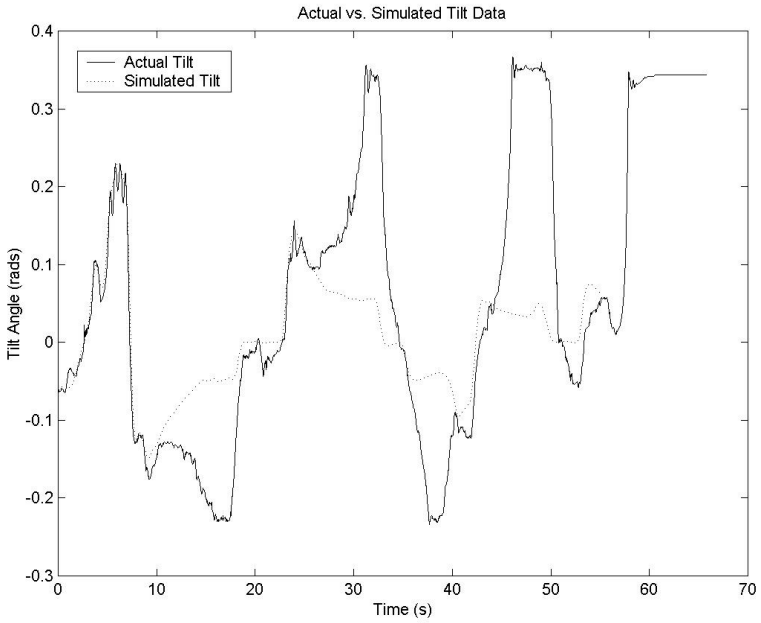

Figure 5.13 Simulated vehicle tilt for lateral mode parameter estimation

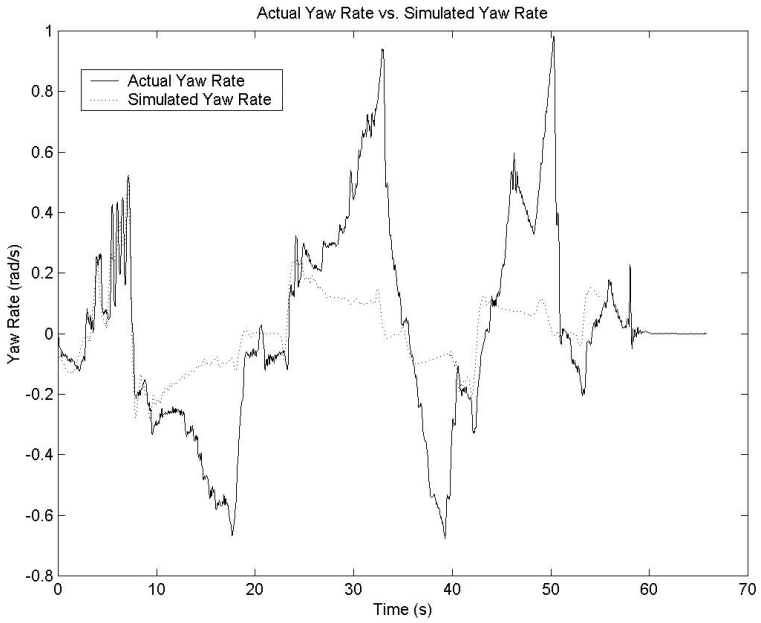

Figure 5.14 Simulated vehicle yaw rate for lateral mode parameter estimation

A 2nd order digital Butterworth filter was applied to the actual vehicle yaw rate data to provide more smoothing. The cutoff frequency was 3.8 Hz and the sample rate was 125 Hz.

The controller we implemented on the vehicle during these experimental runs was the desired lean angle, steer-by-wire type tilt controller with the gains of $k_p = -1.7$ and $k_d = -0.05$. The controller was implemented by interpreting the driver's output as a desired curvature as described in the Controls section. Using the approximate steady state lean angle definition, equation 41, we converted that signal to the desired lean angle.

$$\theta_{des} = \arctan \frac{v^2 C_v}{g} \tag{179}$$

The block diagram of the continuous time controller was shown inFigure 3.5. As described in section V, the controller was actually implemented digitally, in software cycling at 500Hz. The block diagram of the discrete control loop is:

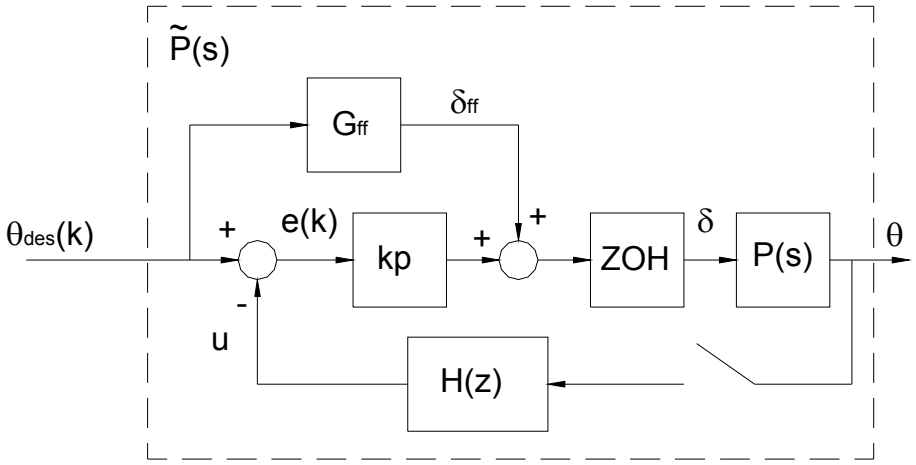

Figure 6.1 Control loop realization

The important point here is $H(z)$. This is the discrete equivalent of $H(s)$ given by equation 131. The method for estimating the derivative term of θ was described in the 5.1.8.3 section. Using

this method with Euler's backward approximation rule, (38:pp. 192), and the discrete Butterworth filter, $H_B(z)$, we get an explicit expression for $H(z)$.

$$H(z) = 1 + \frac{k_d}{k_p} H_B(z) s \Big|_{s \leftarrow \frac{z-1}{Tz}} = 1 + \frac{k_d}{k_p} H_B(z) \frac{z-1}{Tz} \tag{180}$$

$$H_B(z) = \frac{0.0201z^2 + 0.0402z + 0.0201}{z^2 - 1.561z + 0.641} \tag{181}$$

$$H(z) = \frac{1.30z^3 - 1.27z^2 + 0.35z - 0.30}{z^3 - 1.561z^2 + 0.641z} \tag{182}$$

In this case, and for all the data listed in this section, a Butterworth filter with a cutoff frequency of 25Hz was used. This was done to reduce the lag associated with the estimate of the tilting rate, $\dot{\theta}$, but it also allowed more noise. Because there was more noise, setting k_d too large destabilized the system. This is discussed further in the section 6.4 below. The block G_{ff} creates the feedforward steering term required to produce a control output even when $e(k)$ was zero. The value of δ_{ff} was calculated using equation 36 and 179 above.

$$\delta_{ff} = \frac{l}{R} = lC_v \simeq \frac{lg}{v^2} \tan\theta_{des} \simeq k_{ff}\theta_{des} \tag{183}$$

When running the vehicle, we started by holding the vehicle upright for a short time while accelerating. This was done just long enough for the vehicle to be moving when it was released. All plots shown in this section are of the vehicle in motion. The data logger was setup to start saving data only when the speed sensor registered a non-zero velocity, see section V.

6.1 Model Validation

We have already done some comparison between the simulated model and actual vehicle for the purpose of parameter estimation. To estimate the moment of inertia, I^{xx}, we performed an open loop simulation with a stationary vehicle. Also, to estimate the lateral mode parameters, I^{zz}, C_f, C_r, λ_f , λ_r, we used data taken from a closed loop run and compared it to a simulation with the estimated parameters. Now in this section, we again used data from a closed loop run of the vehicle to compare to simulation. The fact that the experiments must be performed on a closed loop system limits some of the usefulness since the plant cannot be observed explicitly but since we are dealing with an unstable plant, we have no choice. The driver in this case was giving commands via the radio controller that were in turn interpreted as a desired curvature, by equation 41, as a desired tilt angle. The tilt controller then performs the closed loop balancing about this desired tilt angle. Figure 6.2 shows the tilt and desired tilt for one such run.

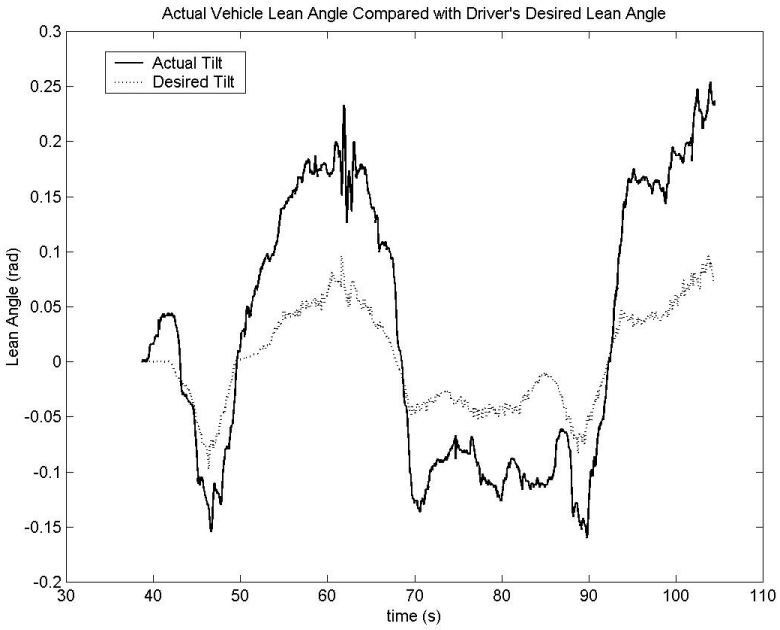

Figure 6.2 Actual vehicle tilting response

In this run, we see that we actually ran out of memory space for data without the vehicle tipping over. Also, notice the error between the desired tilt and actual tilt. This was due to disturbances and the errors incurred in the approximations necessary to derive the expression 36. Figure 6.3 shows the speed of the vehicle for this particular run.

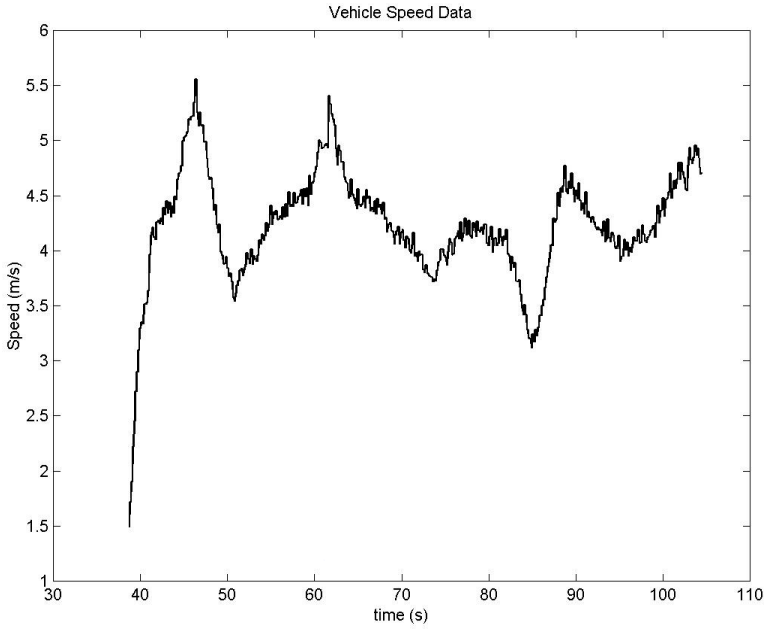

Figure 6.3 Actual vehicle speed response

We can verify equation 18 by plotting the right side of the equation for the tilt and speed data for this run along with the yaw rate data from the analog gyro. This is shown in Figure 6.4.

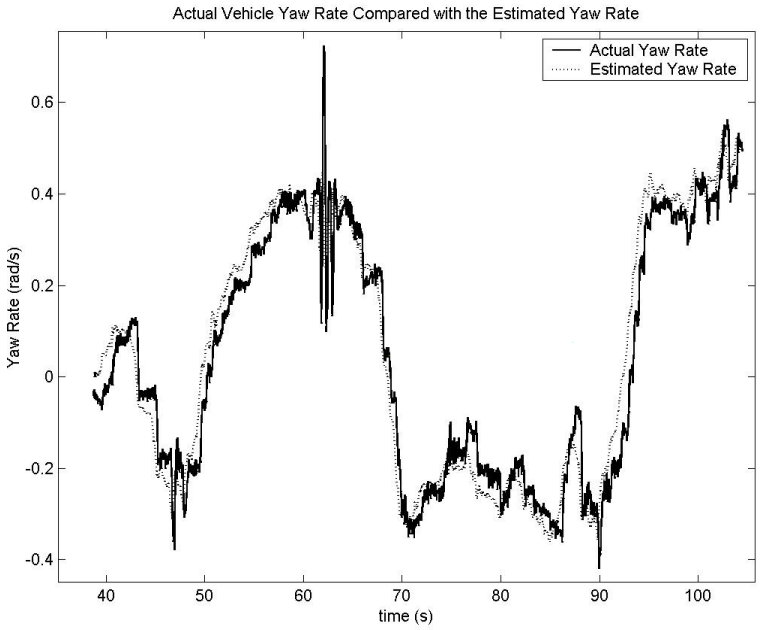

Figure 6.4 Actual vehicle yaw rate

Thus, we see a good agreement between the estimated yaw rate, from equation 18, and the actual yaw rate. If we refer back toFigure 2.4, we see that equation 40 given by:

$$\dot{\psi}_{ss} = \frac{g}{v} \tan \theta_{ss} \tag{184}$$

should be a good approximation to equation 18 and thus equation 40 is valid. Next, we'll look at some frequency response data and compare it to the model described in section 3.2.

The computations for this section are performed using Matlab and require some elaboration. The simulated model's response calculation is straight forward using the 'Control System Toolbox', 'bode' command. The experimental data however required some processing specifications. The command to perform the spectral analysis was the 'spectrum' command from the 'Signal Processing Toolbox' which uses the periodogram method for computing the power spectra and correlation func-

tions, see (39:pp. 375-378,516-519). From the ratio of the cross-correlation to the auto-correlation functions we get the estimate of the transfer function. The specifications used for the data in this section are:

- Sampling rate = 125Hz
- Length of DFT = 4096 for frequency resolution of $\frac{125 \cdot 2\pi}{4096} = 0.2$rad/s
- Hanning window of length 700 samples
- Overlap of adjacent windows of 525 samples (3/4 window length)

Figures 6.5 and 6.6 show the transfer function estimated in this way from the desired steering angle output by the tilt controller to the vehicle tilt data. This is the "P" block shown inFigure 3.3 when the output is the lean angle.

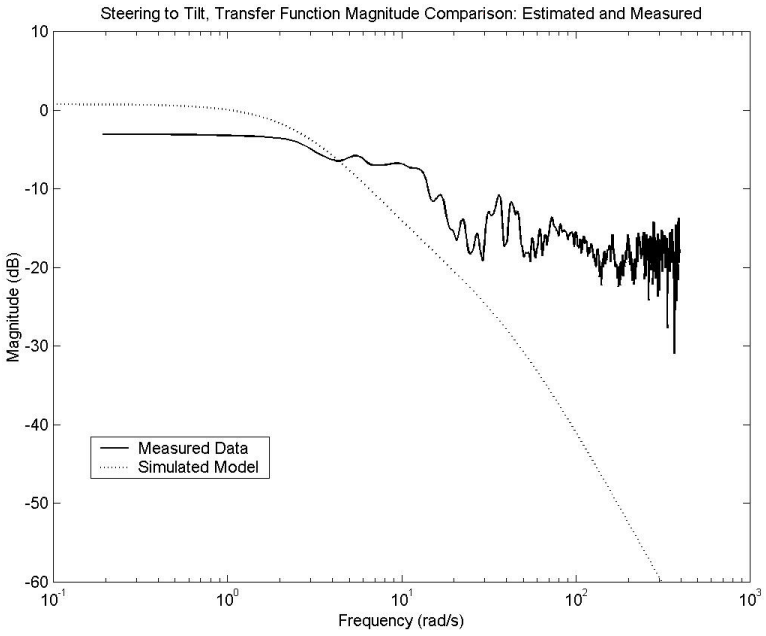

Figure 6.5 Estimated transfer function magnitude: desired steer angle to vehicle tilt

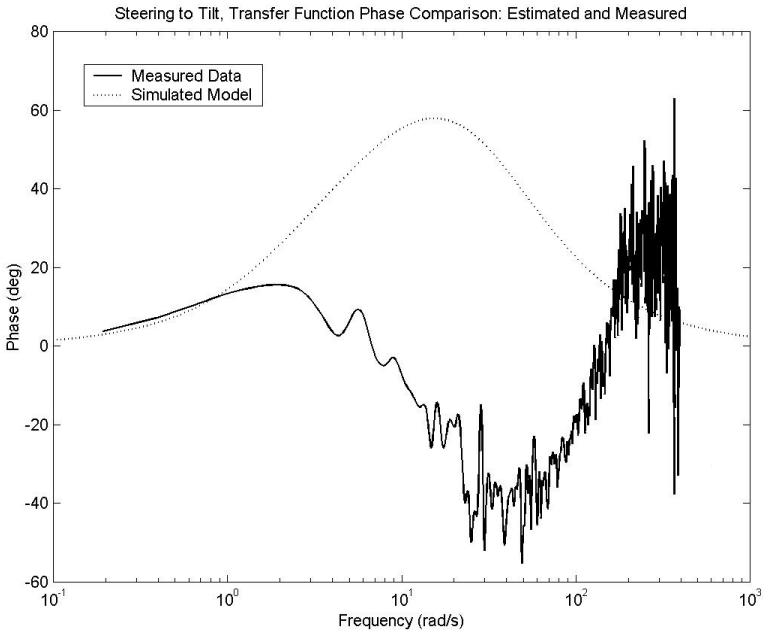

Figure 6.6 Estimated transfer function phase: desired steer angle to vehicle tilt

As we will see in the last two sections of this chapter, the deviation of the experimental plot from the theoretical plot is at frequencies that we can account for by disturbances. Figure 6.6 shows the non-minimum phase nature of the transfer function $\frac{\theta(s)}{\delta(s)}$ due to the unstable pole. Figures 6.7 and 6.8 show the transfer function estimated from the desired steering angle to the vehicle yaw rate data. This is the "P" block shown in Figure 3.3 when the output is the yaw rate.

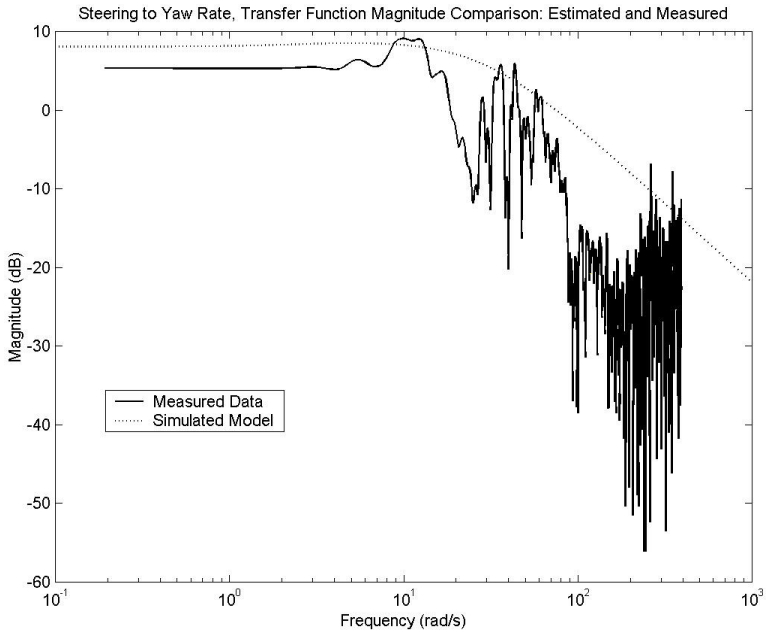

Figure 6.7 Estimated transfer function magnitude: desired steering to yaw rate

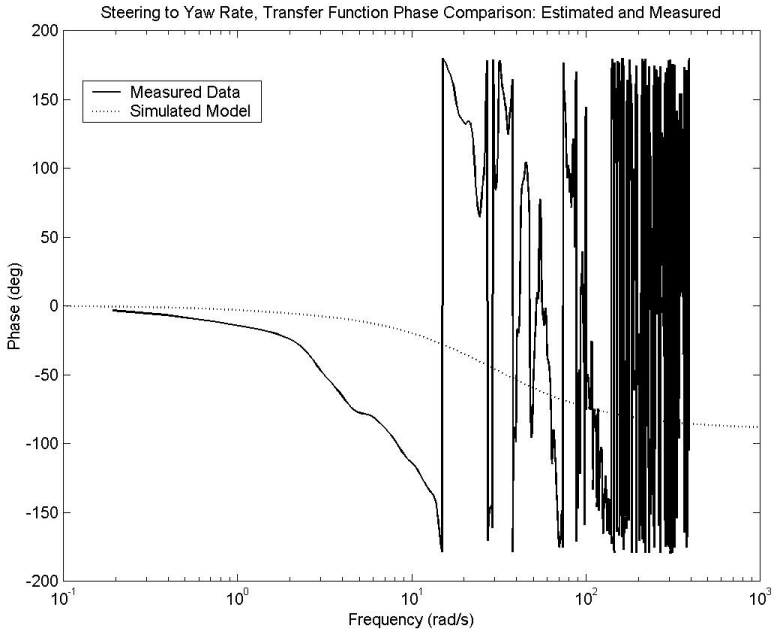

Figure 6.8 Estimated transfer function phase: desired steering to yaw rate

Recall, from the description of the steering, that there were significant dynamics in the steering due to torque and speed limitations of our steering servomotor. These dynamics are not accounted for in the simulated model but do affect the measured data. The speed limitation in the steering will be elaborated upon in section 6.4 below. Also, the simulated model was calculated using a constant speed and was strictly open loop where as the actual vehicle had varying velocity and needed to be closed loop to get a long enough sample. The next few plots show the estimated transfer functions for the diver's output, $\theta_{des}(s)$, to the tilt and yaw rate. In this case, we are estimating and measuring the transfer function of the closed, tilt controlled, loop which is shown as the inner loop, $\tilde{P}$, in Figure 3.3. Figures 6.9 and 6.10 are the response of the function, $\frac{\theta(s)}{\theta_{des}(s)}$.

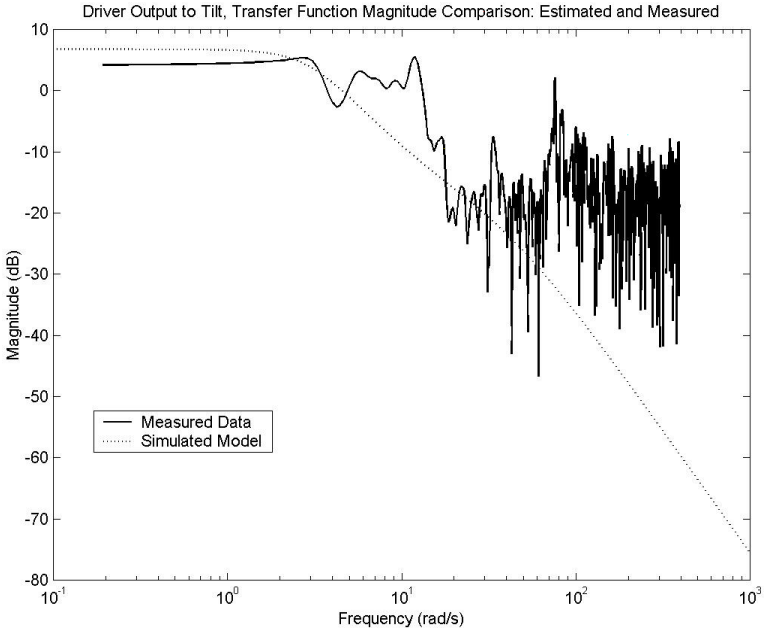

Figure 6.9 Estimated transfer function magnitude: driver output to vehicle tilt

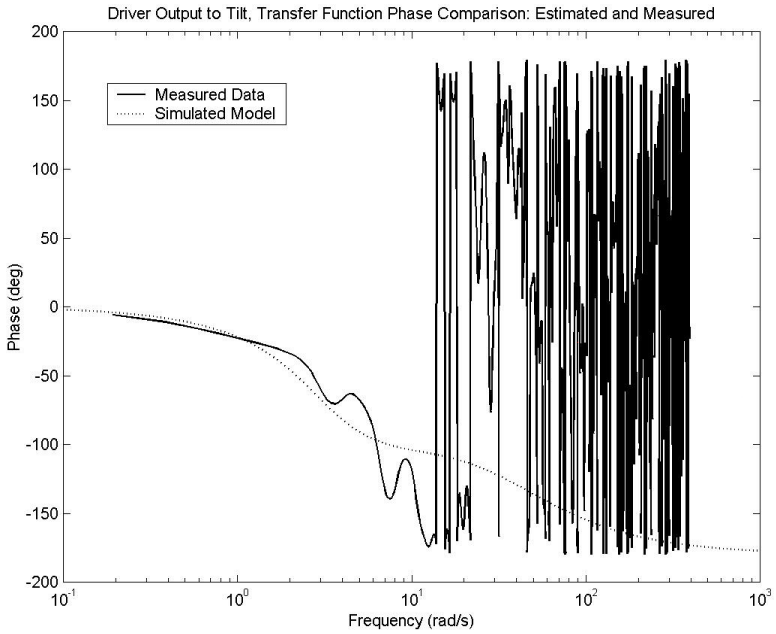

Figure 6.10 Estimated transfer function phase: driver output to vehicle tilt

Notice the difference between Figures 6.10 and 6.6. The controller seems to have corrected the non-minimum phase nature of the tilting as we desired. Figures 6.11 and 6.12 show the frequency response of the block " $\tilde{P}$" of Figure 3.3 when the output is the yaw rate.

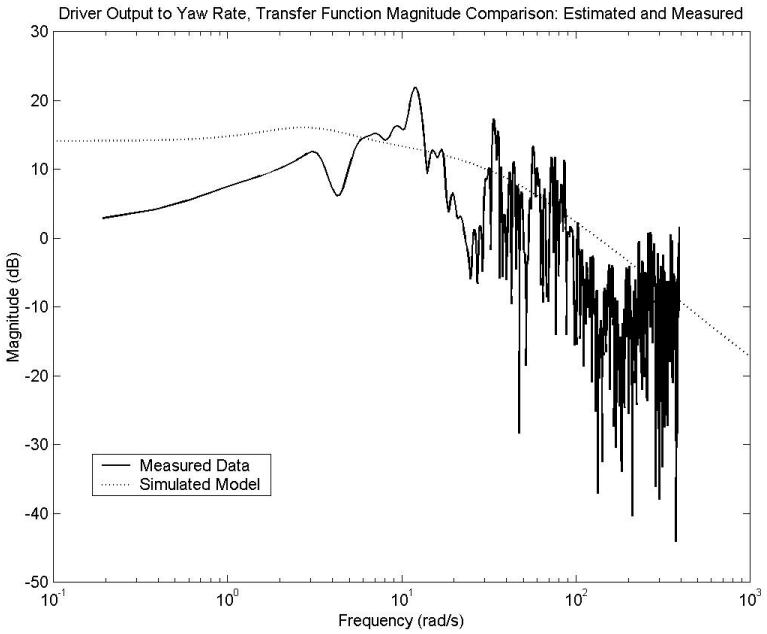

Figure 6.11 Estimated transfer function magnitude: driver output to yaw rate

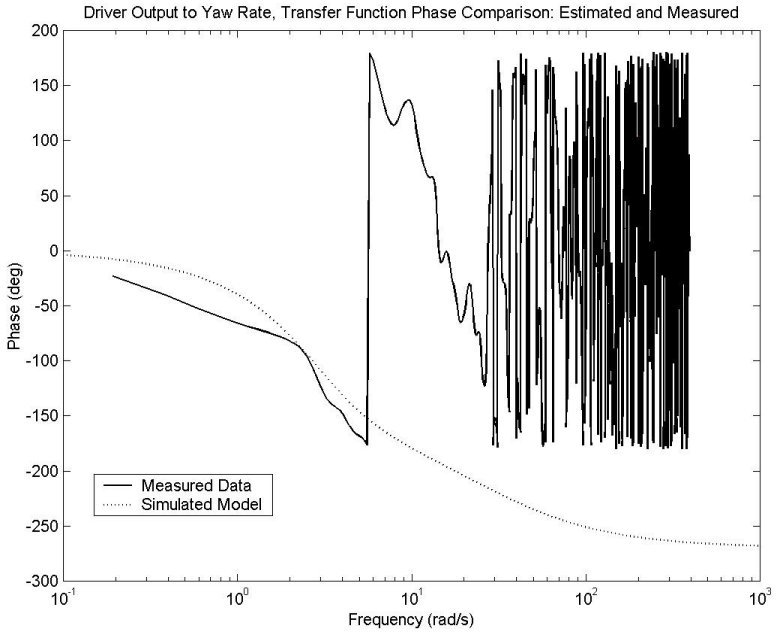

Figure 6.12 Estimated transfer function phase: driver output to yaw rate

There seems to be more difference between the simulated model and the yaw rate response than for the lean angle. Part of this could be from the fact that we did not have a very reliable method for estimating the lateral mode parameters, I^{zz}, C_f, C_r, λ_f, and λ_r (see section 5.2). From the measured data, there is some unaccounted dynamics of the yaw rate occurring at around 10rad/s. The closed loop tilting dynamics though match the model rather well for both the magnitude and phase. We now move on to describing other runs of the vehicle.

6.2 Vehicle Open Loop Response

In order to demonstrate the unstable nature of the vehicle, we ran a few experiments without any steering control. This shows the unstable open loop nature of the vehicle and the necessity of using some form of control, whether it is automatic or driver initiated. To do these runs, the steering servomotor was simply turned off so that the front wheels were free. The experiment was then run as any of the other experiments and the vehicle would simply tip over due to the unstable tilting pole. Figure 6.13 shows the tiltangle from such a run.

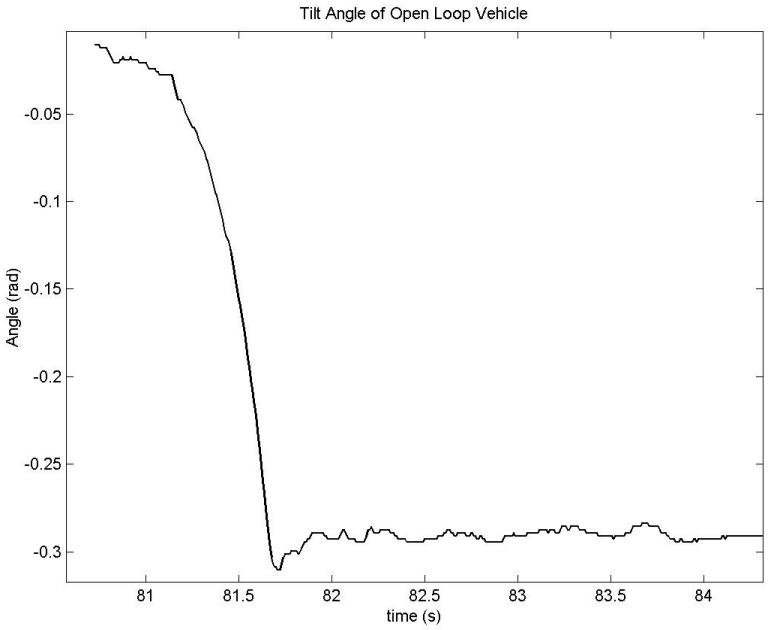

Figure 6.13 Open loop tilting response

We see that the vehicle immediately starts tipping over similar to an inverted pendulum. Within about one second, it has already fallen over. The next two plots show the recorded speed and yaw rate respectively for this particular run.

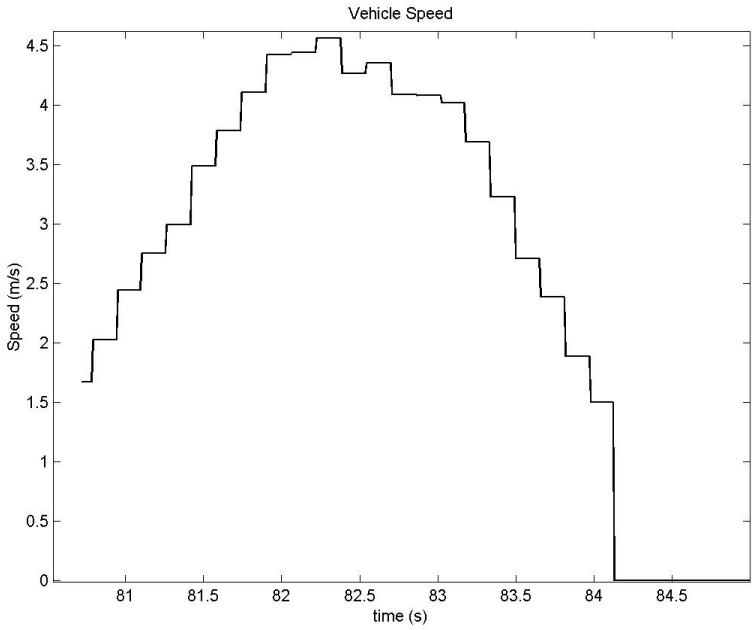

Figure 6.14 Open loop speed response

We can see that the data is not recorded until the speed reaches about 1.5m/s. At this time, from Figure 6.3, the vehicle is still mostly upright.

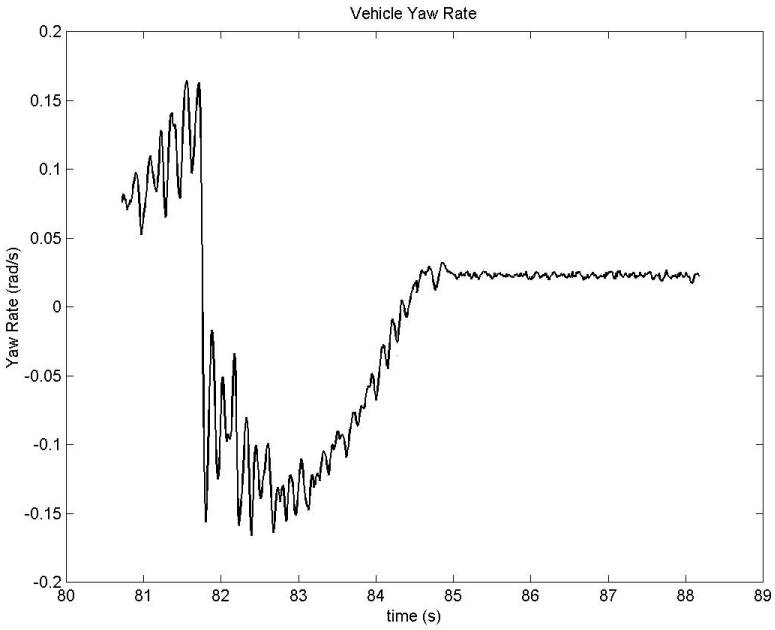

Figure 6.15 Open loop yaw rate response

In figure 6.15 the vehicle was initially, slowly yawing in the positive direction while it was tipping over. This was due, we believe, to a slight amount of positive steer angle in the front wheels. As expected, this caused the vehicle to tip in the opposite direction. When it tipped far enough, the trail effect of the steering configuration caused the wheels to turn in the opposite direction. This only occurs at larger lean angles because of the friction in the steering joints. When the trail finally caused the wheels to turn, the result was the large negative yaw rate at around 82 seconds in the figure. As the vehicle slows down, the yaw rate then returns to zero. The actual steering values were not recorded for this vehicle so we could not verify this with the steering data. Future prototypes should include a sensor to measure this.

We did a few more similar runs of the vehicle with the steering turned off and had similar results. This confirms that the vehicle is indeed unstable in the tilting mode. In terms of dynamical systems, the upright equilibrium point is unstable and the trajectory quickly diverges from it.

6.3 Vehicle Closed Loop Response

To contrast the unstable behavior displayed by the open loop experiment, we now show closed loop runs where this instability was controlled.

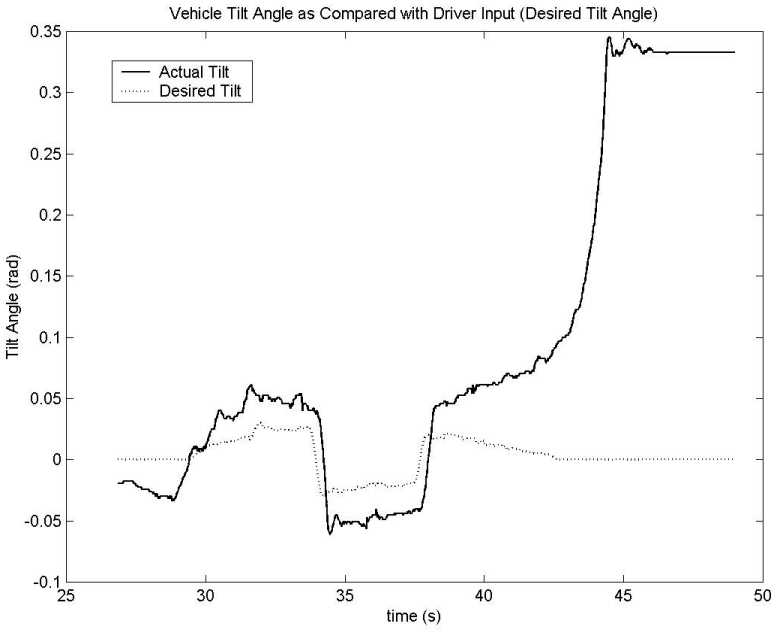

Figure 6.16 Closed loop tilting response

Figure 6.16 shows the actual and desired tilting for one particular run. From the desired tilt angle in this plot, we see that the driver is indicating both directions and the actual tilt angle is following. As was shown in equation 137, there should be a steady state error between θ_{des} and θ_{ss} for a step input in θ_{des}. This is expected since the closed loop, Figure 3.5, represents a type 0 system. We can elaborate on this for the data of Figure 6.16. The continuous time representation of Figure 6.1 is:

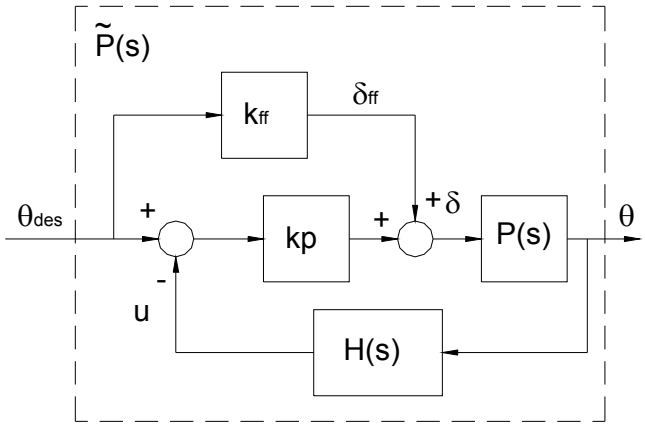

Figure 6.17 Continuous time control loop representation

The feed forward term is needed to make the desired trajectory from the driver an equilibrium solution of the dynamics and is not necessarily included to reduce the steady state error as is often times the case. Recall from section II that the dynamics require a non-zero steady state steer angle and yaw rate for a non-zero steady state lean angle. Based on the control law equation 123, when the actual tilt equals the desired tilt the steering is zero. Which, based on equation 30, is not an equilibrium solution of the dynamics. It is for this reason that the feed forward term is included. We estimated this feed forward with equation 36 which is a simplified estimate. Now, using block diagram simplification, Figure 6.17 becomes:

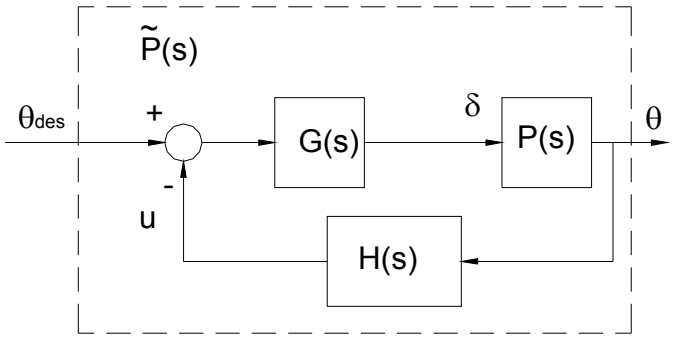

Figure 6.18 Continuous time control loop simplification

Where $G(s) = H^{-1}(s)\, k_{ff} + k_p$, $H(s)$ is given by equation 131, and $P(s)$ is given by equation 129. Now let us find e_{ss}, the difference between the desired and actual tilt at steady state. Dropping the s notation:

$$\begin{aligned} e &= \theta_{des} - \theta = \theta_{des} - \frac{GP}{1+GPH}\theta_{des} \\ &= \frac{1+GPH-GP}{1+GPH}\theta_{des} \end{aligned} \tag{185}$$

Now let θ_{des} be a step input with magnitude θ_{des_ss} then with the Final Value Theorem:

$$\begin{aligned} e_{ss} &= \lim_{s\to 0} sE(s) = \lim_{s\to 0} s\frac{1+GPH-GP}{1+GPH}\frac{\theta_{des\_ss}}{s} \\ &= \theta_{des\_ss}\lim_{s\to 0}\frac{1+GPH-GP}{1+GPH} \qquad (186) \\ &= \theta_{des\_ss}\lim_{s\to 0}\frac{1+(H-1)GP}{1+GPH} \qquad (187) \end{aligned}$$

For the data presented in this section, $k_p = -1.46$ and $k_d = -0.2$. If we refer to the tilt data in Figure 6.16 between 34 - 38 seconds, the desired tilt angle is approximately a step input with a gain of -0.02rad. The velocity in this region is about 5m/s, therefore $k_{ff} = \frac{lg}{v^2} \simeq 0.6$. We can now use this to evaluate equation 186 to get:

$$e_{ss} = -3.67 \cdot \theta_{des\_ss} \tag{188}$$

To compare this to the data, we plot the expression 189 versus time in Figure 6.19

$$\frac{e_{ss}}{\theta_{des}} = \frac{\theta_{des} - \theta}{\theta_{des}} \tag{189}$$

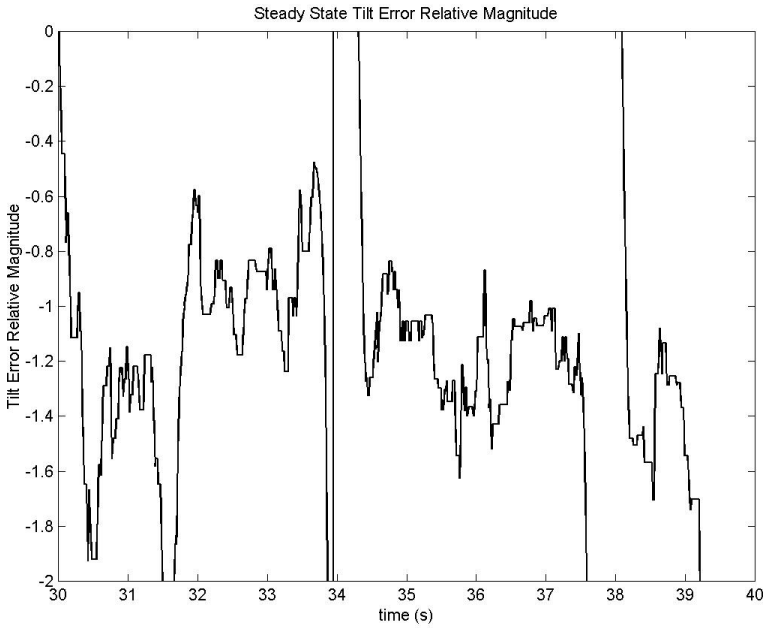

Figure 6.19 Relative tilt error magnitude for approximate step input

For the data between 34 - 38 seconds, we expect a value of -3.67 instead of the -1.2 as shown. This difference has two causes. First, the feed forward steering term was an approximation to the nonlinear equilibrium solution derived in section II. Second, the expected model, $P(s)$, is not exactly correct due to linearization and inaccuracies in parameter estimation. Both of these issues combine to make the actual equilibrium solution to the dynamics slightly different from the value indicated by the driver's θ_{des}. This difference, for now, is simply a parameter that the driver would adjust for as he or she learned how the vehicle responds to steering commands. To compare this to a typical non-leaning automobile, different vehicles turn at slightly different rates for any given steering wheel angle. Of course, different tires will influence this but also the differences in gearing between the steering wheel and the front wheels. This requires some learning on the part of the driver to account for how different vehicles behave.

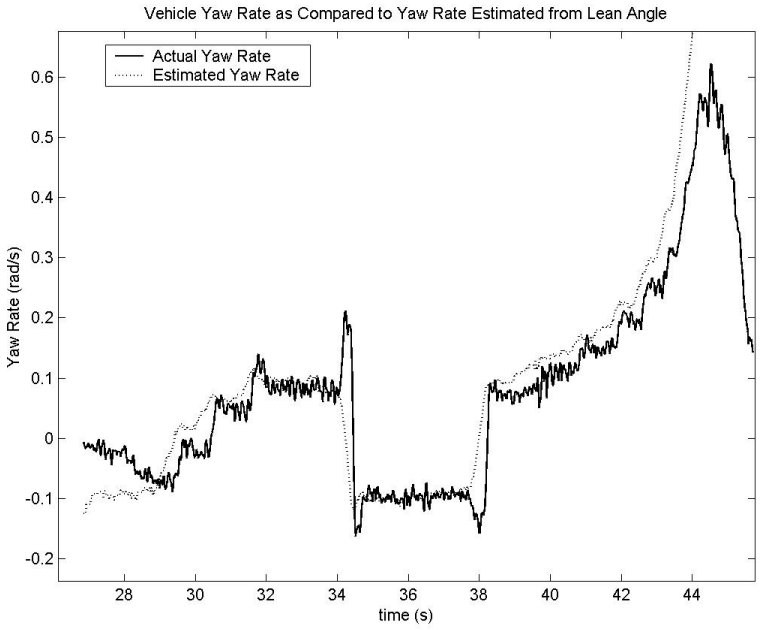

Figure 6.20 Closed loop yaw rate response

Figure 6.20 shows the vehicle yaw rate following the driver's commands. The estimated yaw rate in this figure was calculated using the expression $\dot{\psi} = \dot{v}C_v$ where the method for obtaining the signal, C_v, was described in section 5.1.7.2.

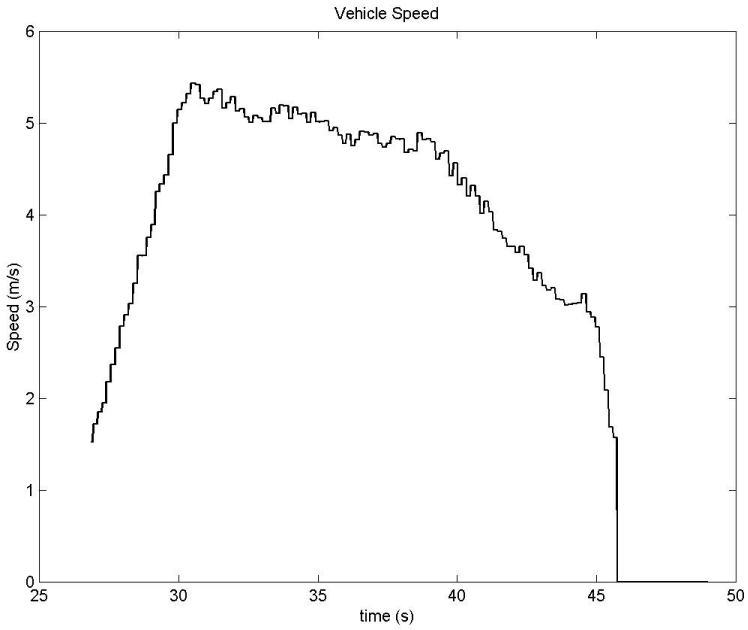

Figure 6.21 Closed loop speed response

Figure 6.21 shows the vehicle's speed throughout this run. This shows that the vehicle actually tipped over before the vehicle stopped. By about 42 seconds, the vehicle was already tipping over while the speed was still around 3 m/s. The last two sections of this chapter will discuss in more detail the failures of the controller. For now, let us focus on the region where the controller is operating as designed. The next plot of this section is of the noise in the steering positioning for this run.

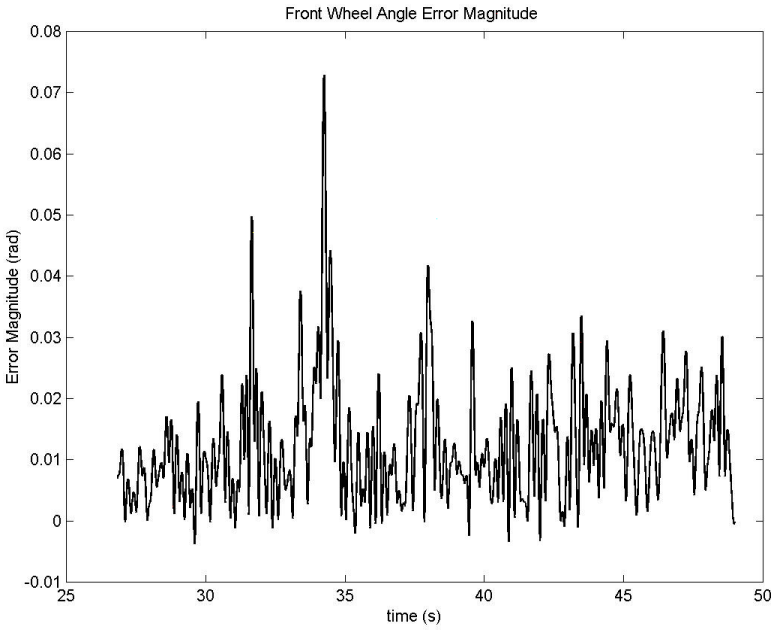

Figure 6.22 Closed loop steering error data

From figure 6.22 we see that the noise in the steering is mostly small, around 1° or 2°. It can however, even in this run with small lean angles, become as much as 4° as seen at around 35 seconds. Now that we have discussed some of the important details of these closed loop data plots, we can present some more data from different closed loop runs. The last 6 plots of this section show the data of tilt, desired tilt, and yaw rate for 6 separate runs. The units in these plots are radians for the tilt and desired tilt and radians per second for the yaw rate data.

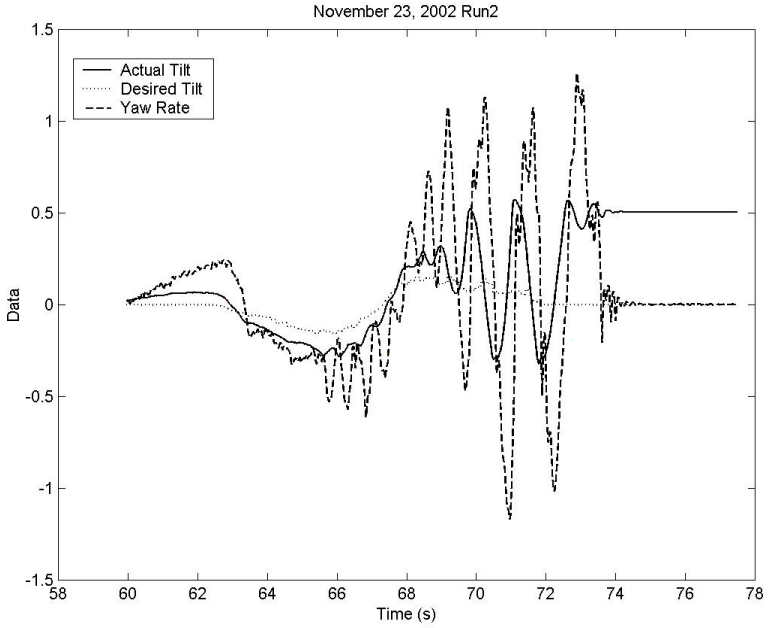

Figure 6.23 November 23, 2002 run 2 data

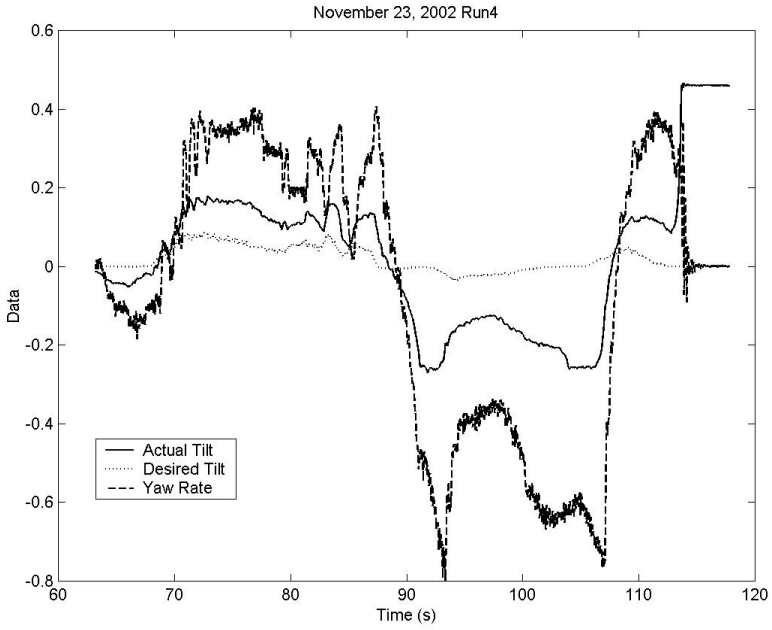

Figure 6.24 November 23, 2002 run 4 data

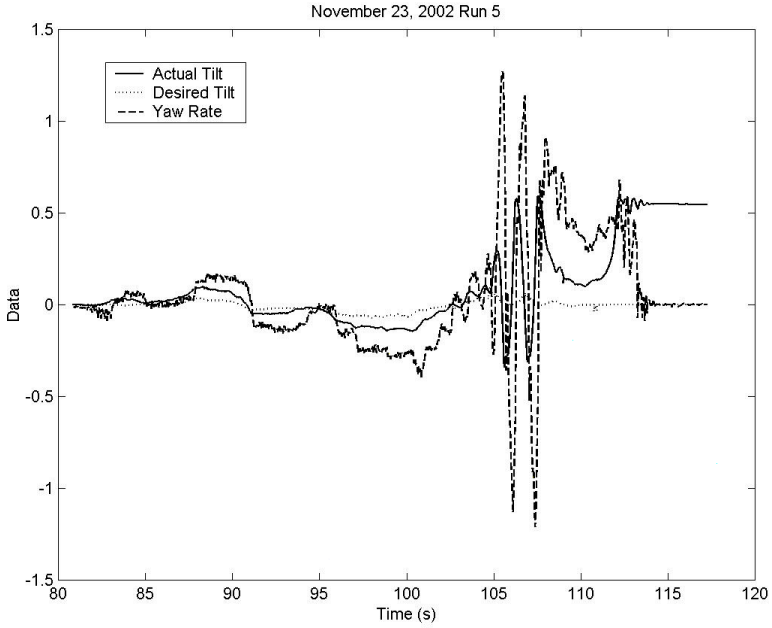

Figure 6.25 November 23, 2002 run 5 data

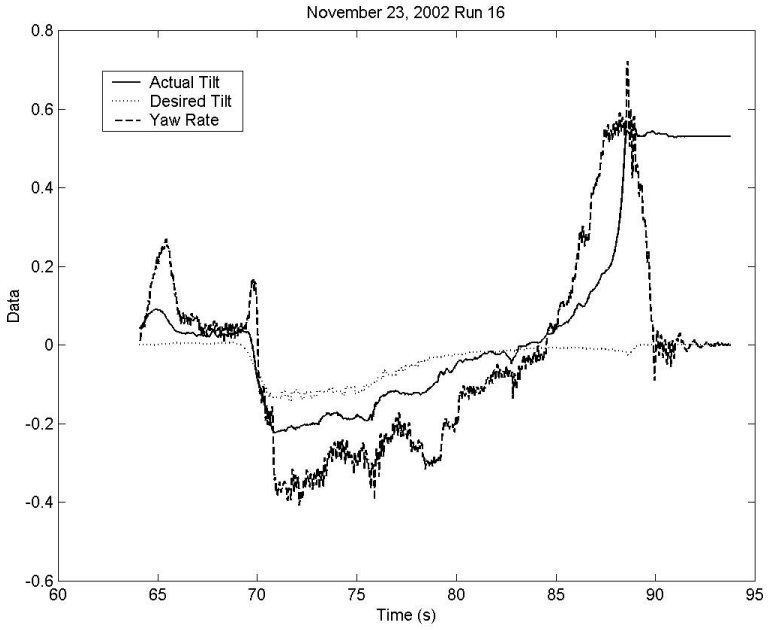

Figure 6.26 November 23, 2002 run 16 data

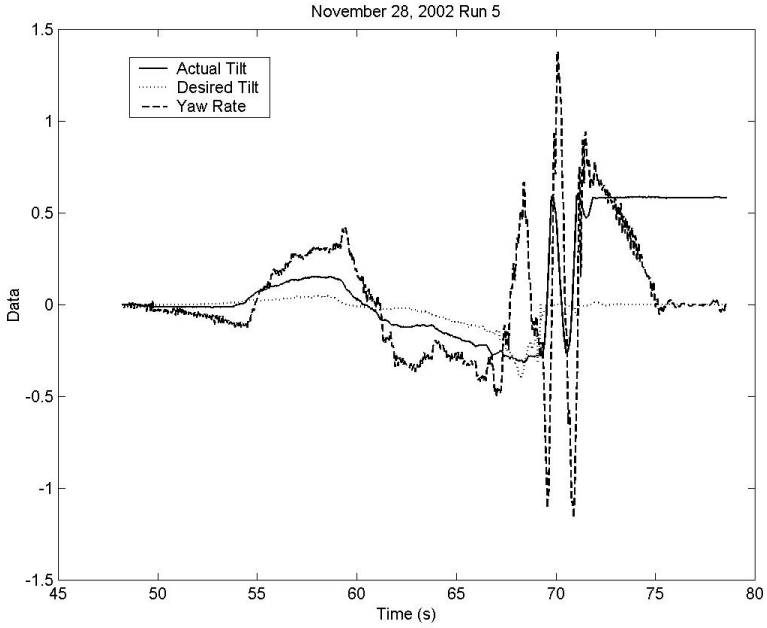

Figure 6.27 November 28, 2002 run 5 data

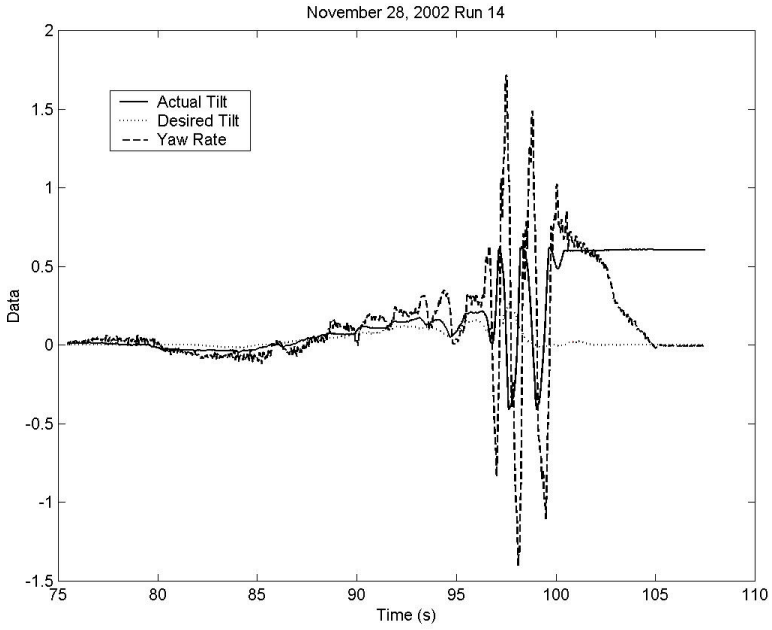

Figure 6.28 November 28, 2002 run 14 data

These last few plots show both the stabilization that occurs when the controller is used to close the loop. They also show some instabilities that usually result in ultimate failure of the system. We elaborate on these instabilities in the last two sections.

6.4 Unstable Oscillations

A few of the plots show some instability. There seems to be a distinct frequency in the vehicle tilting that can be excited and causes the controller to lose control. Figure 6.29 shows this happening.

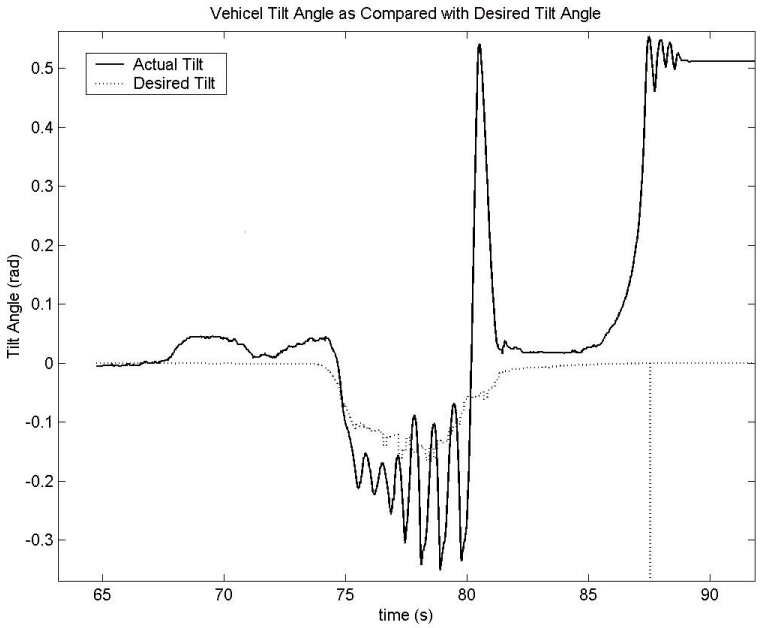

Figure 6.29 Vehicle tilting data, apparent instability

For the time up to about 75s, the system seemed to be behaving well. The controller was responding to disturbances in the tilt and maintaining a zero lean angle. After 75s however, the desired lean angle became nonzero and the vehicle started oscillating. When the vehicle was running upright, the disturbances to the wheel vertical reactions have little effect on the tilting. When the vehicle starts to tilt at some nominal nonzero angle these disturbances become increasingly more

significant because the tilting of the vehicle is inherently nonlinear. The question is why could the controller not correct for these distrubances? To help answer this, let us look at the resonant frequency of these oscillations. This can be found with the power spectral density plot, shown in Figure 6.30.

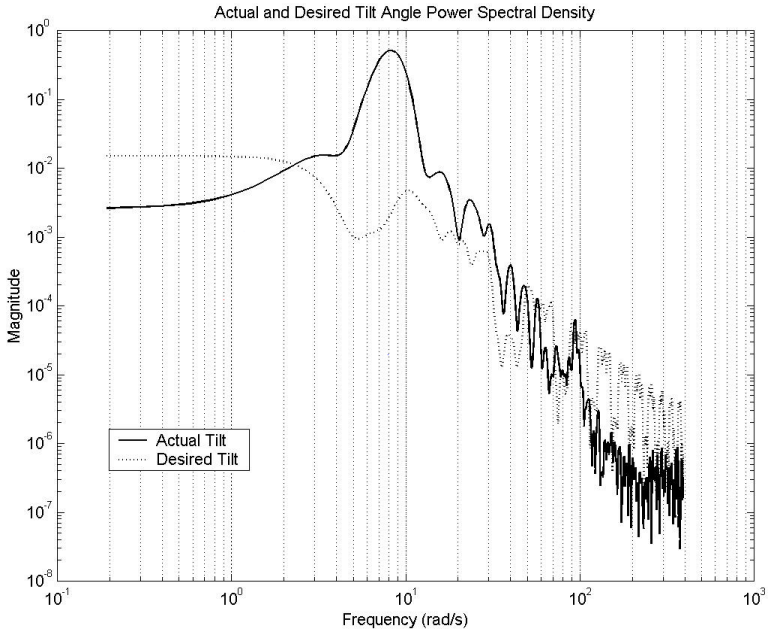

Figure 6.30 Vehicle tilt angle PSD of unstable region

The same command was used to generate the spectra of this section as in the 6.1 section but with the following settings:

- Sampling rate = 125Hz
- Length of DFT = 4096 for frequency resolution of $\frac{125 \cdot 2\pi}{4096} = 0.2$rad/s
- Hanning window of length 400 samples
- Overlap of adjacent windows of 300 samples (3/4 window length)

The oscillations show up as the peak at about 8.0 rad/s. As was shown in the "Steering" portion of chapter V, the maximum steering rate was about 21 rpm or 2.2 rad/s which is much too slow to correct for the frequency excited in the tilting. Figure 6.31, shows the steering angle error (see the "Steering" section of chapter V) along with the vehicle tilt.

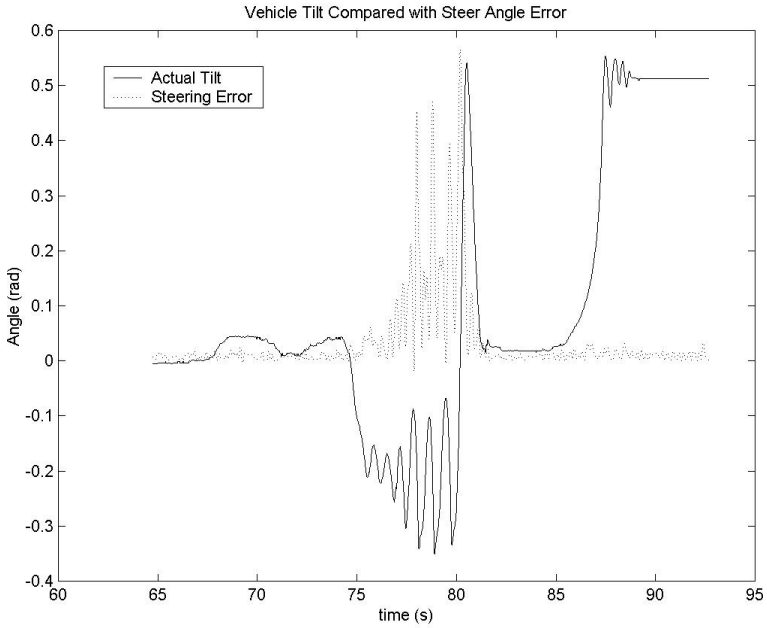

Figure 6.31 Vehicle steering error data

This steering error data shown in Figure 6.31 was obtained from the steering servomotor controller at a rate of about 12.5 Hz. For the vehicle configuration, the steering was limited to about $\pm 20°$. We can see saturation of steering occurring in the plot of the steer command, Figure 6.32, for the given maneuver.

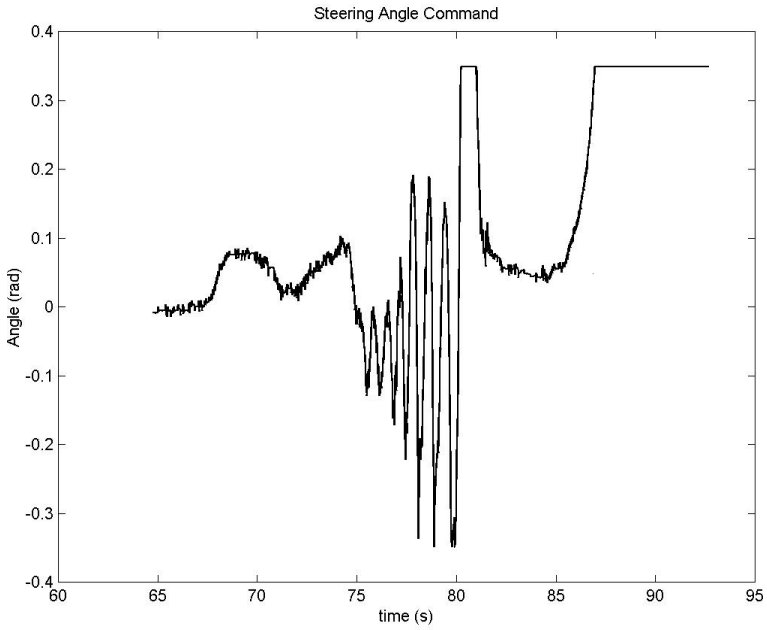

Figure 6.32 Steering angle command

To support that this disturbance is the cause of the oscillations in the tilting, we need to show that there is significant energy in the power spectrum of the steering error data at 8 rad/s. The problem is that the steering error data obtained from the steering amplifier is the absolute value of the error. This means that the bandwidth of the data could be one half what is actually calculated (for a rectified sine wave, the apparent frequency is twice the actual frequency). Figure 6.33 shows the PSD of the tilt and the steering error.

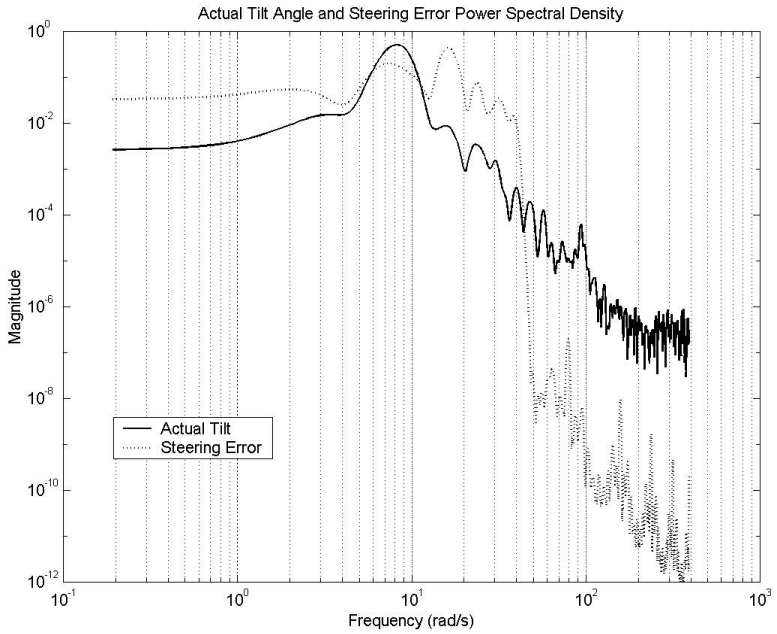

Figure 6.33 Steering error and tilt angle PSDs

Since the steering error data had a lower sampling rate, 12.5 Hz as compared to the 125 Hz of the tilt angle, Matlab's "resample" command was used to increase this rate. Because of this, we cannot observe frequencies higher than about 6Hz (37rad/s) in the error data. Notice the peak in the error spectrum at about 16.0 rad/s. This is twice the frequency of the tilt data peak and suggests that if the actual steering error could be recorded instead of its absolute value, the peak in the spectrum would be at about 8.0 rad/s. The next useful step is to analyze the open loop frequency response data.

To show that the closed loop actually contains an unstable pole from the frequency response data in this region, we need to do some manipulation of the signals of θ and θ_{des}. Start by manipulating the block diagram, Figure 6.1 to get Figure 6.34.

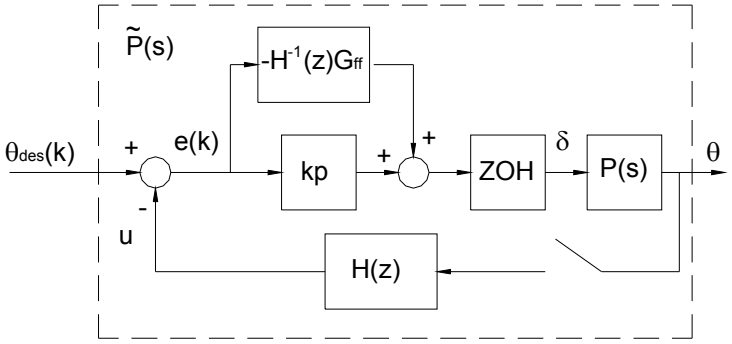

Figure 6.34 Control loop simplification 1

Now, let the inner feedforward loop be $G_1(z)$.

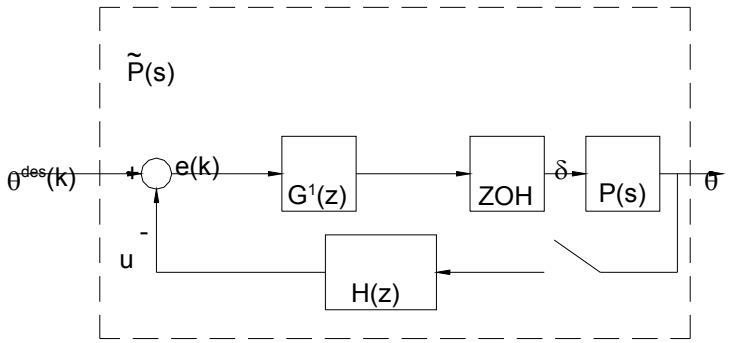

Figure 6.35 Control loop simplification 2

Then the closed loop is:

$$\frac{\theta}{\theta_{des}} = \frac{G_1 P}{1 + G_1 P H} \tag{190}$$

For the frequency data to yield information on the stability, we need to determine when $1 + G_1 P H$ approaches a singularity. This occurs when $G_1 P H = -1$. So, we need to plot the frequency data of, $G_1 P H$. We now need the signals that will estimate this quantity. Since $u = H(z)\theta$ we get:

$$\frac{u}{\theta_{des}} = \frac{G_1PH}{1 + G_1PH} \tag{191}$$

The error signal $e(k)$ is:

$$e = \theta_{des} - H\theta = \theta_{des} - H\frac{G_1P}{1 + G_1PH}\theta_{des} \tag{192}$$

$$\frac{e}{\theta_{des}} = 1 - \frac{G_1PH}{1 + G_1PH} = \frac{1}{1 + G_1PH} \tag{193}$$

By combining equations 191 and 193 we get:

$$\frac{u}{e} = \frac{u}{\theta_{des}} \cdot \left(\frac{e}{\theta_{des}}\right)^{-1} = \frac{G_1PH}{1 + G_1PH} \cdot \frac{1 + G_1PH}{1} = G_1PH \tag{194}$$

Therefore, we need to use the spectra of the signals u and e to determine the stability of the closed loop. Both these signals are readily available. $H(z)$ is known from equation 182. θ and θ_{des} are the recorded data. Figures 6.36 and 6.37 show these frequency response plots for the estimate of G_1PH.

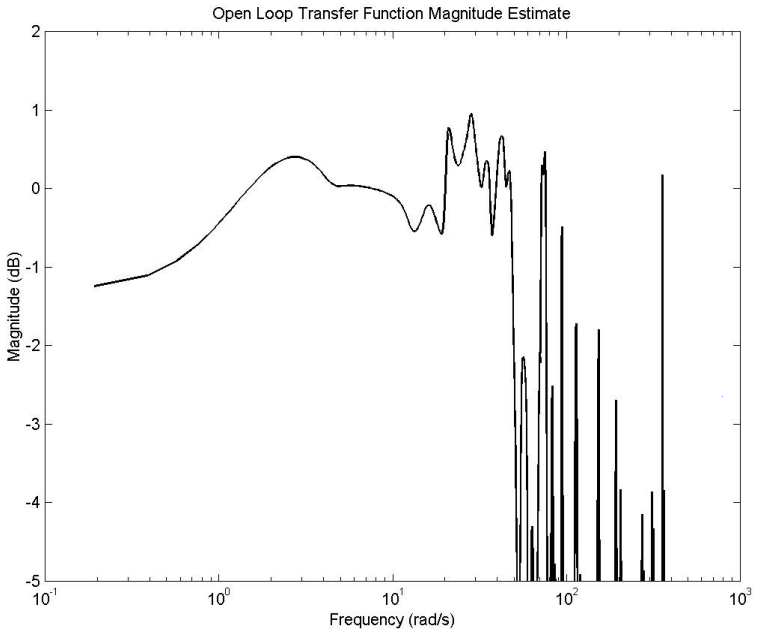

Figure 6.36 Open loop magnitude data, $\frac{u}{e}$

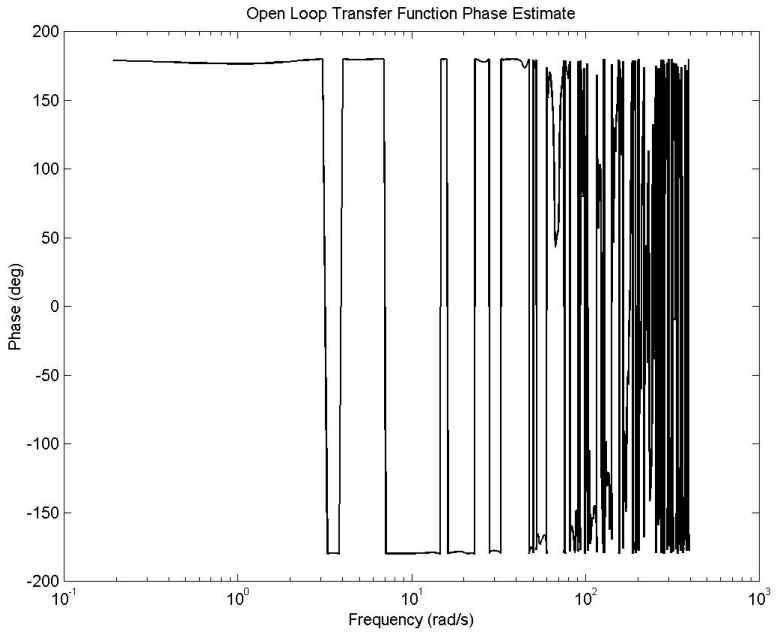

Figure 6.37 Open loop phase data, $\frac{u}{e}$

The phase plot may seem unusual since it is always around 180° but recall that the data used in this section was from the unstable region between 75 and 81 seconds as shown in Figure 6.29. This shows that the signal u always lags signal e by very close to 180° when the oscillations start, meaning that there is a poor phase margin. From the two plots, we can see the instability is just above the steering motor's rate limit. The phase becomes 180° at around 3 rad/s at which frequency the magnitude plot is at about 0.4dB which indicates instability.

6.5 Unmodeled Dynamics

Another source of noise to the system was from the connection between the front chassis and the rear frame. This connection had a significant wobble mode due to flexing that was not modeled but showed up in the data. In order to estimate the frequency of this noise source, I performed an

experiment in the lab that consisted of forcing the front chassis of the vehicle in order to perturb this dynamic mode at its resonant frequency. The resulting tilt angle data is shown in Figure 6.38.

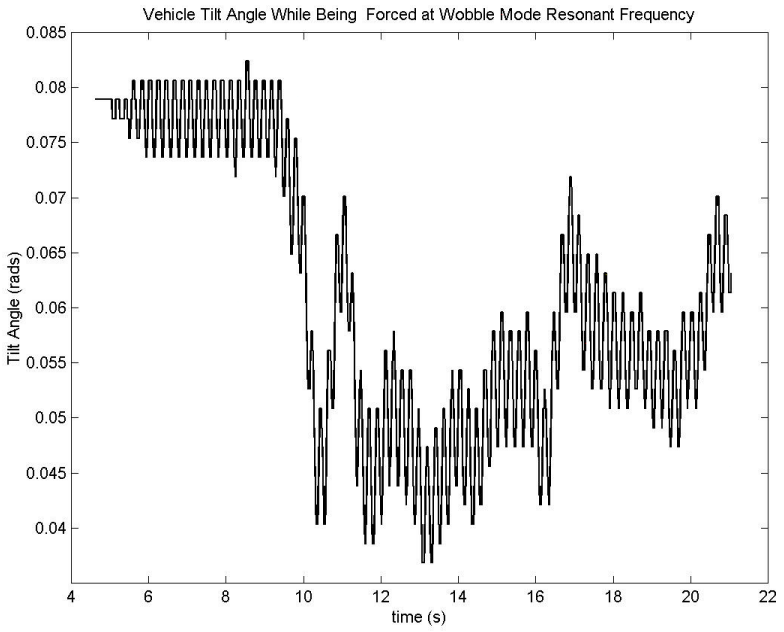

Figure 6.38 Wobble mode perturbation, Tilt angle response

The power spectrum of this data indicates the resonant frequency of this particular unmodeled dynamic mode.

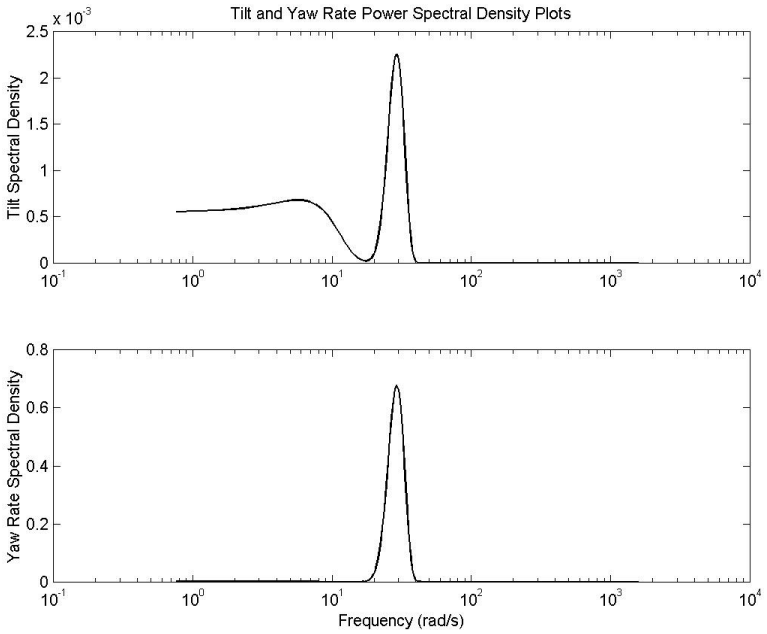

Figure 6.39 Wobble mode perturbation, tilt angle and yaw rate PSD

The sample rate for this data was 500Hz. The resonant frequency of the wobble mode shows up around 30rad/s or between 4 and 5 Hz. Referring back to Figure 6.5 we see this showing up in the tilting power spectrum. The last few plots of this section show the affects of this mode in the data for a separate run of the vehicle.

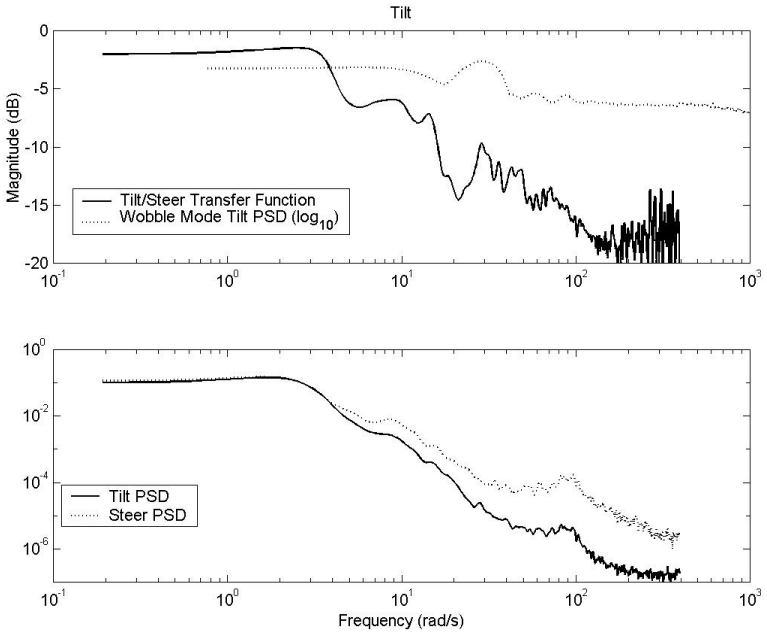

Figure 6.40 Wobble mode influence on tilt angle data

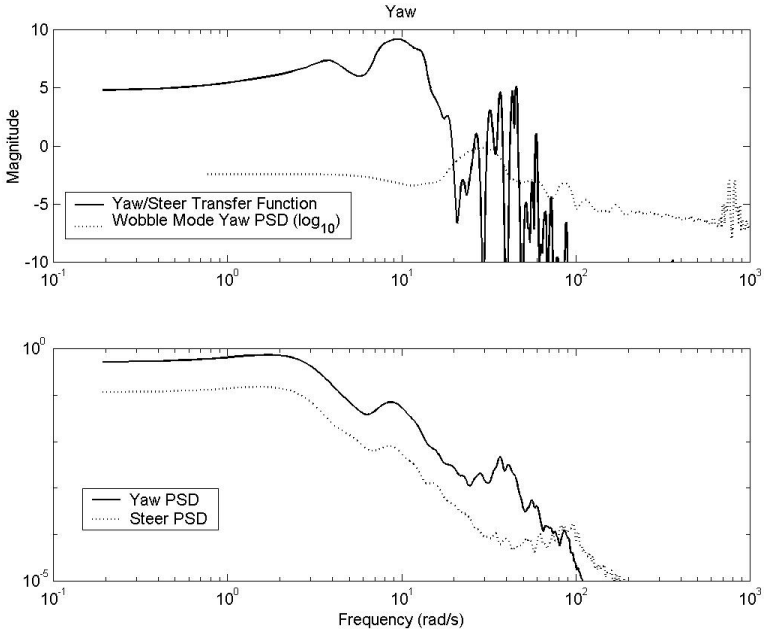

Figure 6.41 Wobble mode influence on yaw rate data

The base 10 logarithm of the power spectrum of the wobble mode is shown in the upper plot of these two figures along with the estimated open loop transfer function, seen in figures 87 and 88. The lower plot shows the power spectra of the tilt and steer data and the yaw rate and steer data. The estimated transfer function is the ratio of these two. The affect of the wobble mode seems more significant in the yaw rate data than the tilt data. By comparing the two spectra in the lower plot of the tilt data, we see the tilting PSD follows the steering PSD quite closely. Thus, frequencies in the tilt data are mostly accounted for by the steering. Looking however to the yaw data, we see some energy in the frequencies around 30 rad/s that is not accounted for by the steering spectrum. This is at the frequency of the wobble mode and so, seems to be the source of this noise. This is further supported by Figure 6.15 which was an open loop run of the vehicle. The oscillations are evident in the time plot of the data and is shown in the power spectrum as well at around 30rad/s in Figure 6.42.

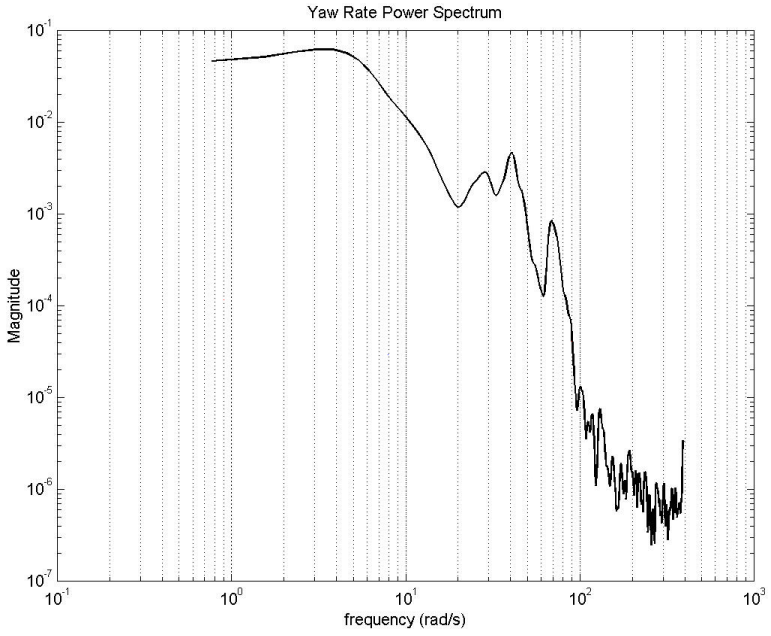

Figure 6.42 Open loop yaw rate PSD

Chapter VII. Summary and Conclusions

Starting with the assumption that we wanted to design a narrow vehicle, as discussed in the introduction section, we saw that ultimately leaning would be required. The objective was to design a first iteration steering based tilt controller to use to further analyze vehicle leaning and increase our understanding of the requirements for tilt control. A model of such a leaning vehicle was developed and a discussion of the expected equilibrium states followed. In that discussion, we found that the expected relation between yaw rate and lean angle was a natural result of the system model, see equation 41.

We then went on to explore possible controllers to stabilize this model. The first controller we analyzed, the independent lateral and tilt controller, had problems due to the strict independence of the controllers. The next controller we analyzed was a classical state estimator. The idea was for the tilt controller to know what the lateral controller was doing. This required some creative modeling to make the system observable and made for a large sixth order controller. Since this was a new project, we wanted to start with a controller that was not so complex. The controller we spent the most time analyzing was a modified version of a controller suggested in (4). In that steer-by-wire design, the user's output was interpreted as a desired lean angle. A modified PD control was implemented so that the vehicle tracked the user's signal.

This interpretation was the most useful shift in our understanding during this project. This interpretation was that the user's output could be considered a desired quantity for any scalar signal describing the vehicle's trajectory. In our case a natural signal to use was the lean angle since it was easily measured and with little noise. The controller then caused the vehicle to track this signal.

With a vehicle model developed, we went on to explore the affects of these controllers in simulation. The systems were implemented in Simulink and also with a real time simulator in Visual Basic. Counter steering, which is a general behavior of the inverted pendulum type problem,

was seen in each of the systems as expected. Refer to Figures 4.7 and 4.12. Also, the tracking nature of the PD control was shown in Figure 4.11. The ability for the driver to perform lateral control of the vehicle by outputting a signal interpreted as a desired lean angle was not obvious. To demonstrate that this could work, we programmed a real time simulator in Visual Basic. From that section, we saw that lateral tracking could be achieved.

While this control design and analysis was occurring, we also started work on constructing our experimental vehicle. The three wheeled design included a single rear drive wheel consisting of a 50cc scooter drive train and a two-wheeled front chassis. The vehicle was an invaluable tool in analyzing the control system and highlighting the fundamental challenges of such a narrow vehicle. From the experimental section, we verified that the controller did indeed provide stability. The vehicle, which simply tipped over without the steering control, was stable when the steering was on. For modest inputs, the vehicle followed the user direction commands as a desired lean angle. Refer to sections 6.1, 6.2, and 6.3.

Fundamental problems were also noticed from the experiments. One problem was that significant unmodeled dynamics existed in the vehicle. This mode of motion was not accounted for in the modeling or simulation sections, but was easily seen in the experimental vehicle. This motion was evident in a few of the power spectra of the experiments. For example in Figure 6.5 there was some energy appearing at around 30 rad/s, the frequency of this mode. Although this appeared to be at a high enough frequency not to significantly affect the leaning of the vehicle, see Figure 6.39, it did have significant affects on the yaw rate. If a controller were designed to include the yaw rate data, this disturbance would need to be corrected.

The most serious problem however was the limitations of the steering loop. The steering motor and controller were setup as a position control loop to track the output from the tilt controller. The motor itself had a turning rate limit of about 750 rpm, so that with the gearing, the steering loop velocity saturated at about 21 rpm. The gearing was necessary as shown in Figure 5.6 to achieve the

required torque. When trying to follow a user's input, an unstable motion could be excited that was at a frequency too fast for our steering motor to control but within the bandwidth of the plant, refer to Figures 6.33 and 6.5. Obviously this is not a satisfactory situation and needs to be corrected. This was the reason for using strong filtering on the driver's input and then also windowing the signal in an effort to prevent the excitation of this mode. Unfortunately the excitation of this mode was most likely from external disturbances such as the road as the vehicle was in motion.

Future work on this project needs to start with correcting this steering problem. The steering loop should be able to track the input from the driver for frequencies up to the bandwidth of the plant. This bandwidth was around 10 rad/s. We need to be sure our steering motor can turn the front wheels at a rate of at least 100 rpm. From Figure 6.30 the disturbance in the lean angle has a frequency of 8 rad/s which is about 76 rpm. The torque requirements were between 13.5 Nm for the high ratio and 50 Nm, the rated torque with the low steering sprocket ratio. With this higher bandwidth, we should see significant improvement in the vehicle handling since this was the main cause for instability.

Along with improving the steering bandwidth, another improvement could be made in measuring the front wheel angle. With the current vehicle only the steering error magnitude is obtained and only at a low sample rate. By obtaining the actual front wheel angle at the same sample rate as the tilt angle, we could perform better analysis of the data. This is not a strict requirement for the implementation but a practical improvement that would make experimentation and analysis of the data easier.

The steering loop is the first and most important correction to the vehicle. The next should be the wobble mode between the front and rear frames. This creates noticeable disturbances and can easily be corrected by stiffening this connection. Lastly, a method for measuring the actual angle of the front wheels is needed. When this is done, the yaw rate will be a reliable signal and it

might be possible to incorporate this signal into the controller. This brings up the last suggestion for future work, improving the robustness.

After these improvements are made, more experiments should be run to evaluate the robustness and performance of the system. It's possible that the robustness will be adequate but in the likely event that it's not, further work on the controller design will be required. Work can also be done on improving the performance of the controller. With corrections to the hardware problems, it might be possible to implement a PID controller to reduce the steady state error in the lean angle and so improve performance.

In closing, our initial runs of the vehicle may have seemed mediocre. However, these problems were attributable to easily corrected problems. This means that steering tilt control of a narrow vehicle should be feasible and work should continue towards the practical implementation on a vehicle.

Appendix A. Coordinate Systems

In order to derive the dynamic model, we need to first define our coordinate systems. We start our definitions at the inertial frame origin point P. This is defined to be at a point directly below the center of gravity, point B, when the vehicle is upright. This is shown in figure A1.

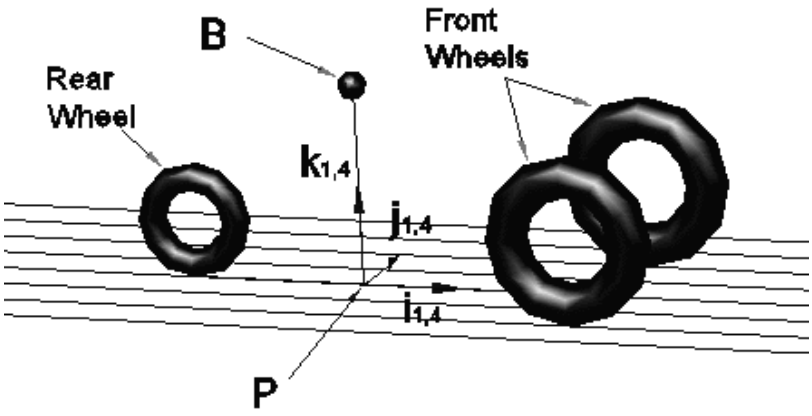

Figure A-1 Coordinates sytems 1 and 4

We consider system 1 to be the inertial frame while system 4 is non-inertial in that it has an instantaneous rotation of $\dot{\psi}$ in the $\mathbf{k}_1$ direction and instantaneous translation of $\dot{y}$ in the $\mathbf{j}_1$ direction.

The next useful coordinate system is system 3. This system is fixed to the vehicle body and is formed by a rotation of θ in the $-\mathbf{i}_4$ direction. This is shown in Figure A-2.

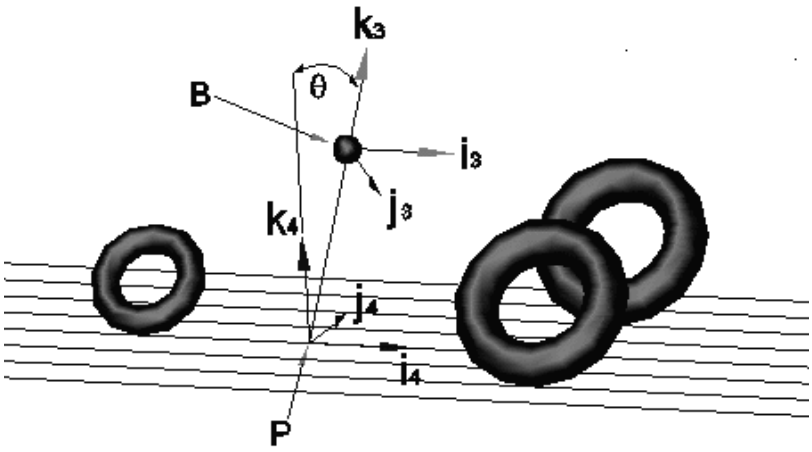

Figure A-2 Vehicle body, body fixed coordinate systems 3 and 4

Coordinate frame 4 rotates with the yawing motion of the body while frame 3 rotates with the rolling motion of the body. The directions of $\mathbf{i}_3$ and $\mathbf{i}_4$ are parallel. The last two coordinate frames that are significant for this paper are associated with the front wheels. The front wheels have one degree of freedom with respect to the vehicle body. We define two more coordinate frames to deal with this. The first is the steering axis of the front wheels which is oriented at an angle β from the $\mathbf{k}_3$ axis. This is shown in Figure A-3 as $\mathbf{k}_5$.

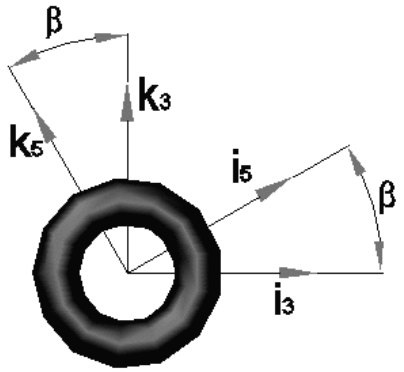

Figure A-3 Vehicle body, body fixed coordinate system 5 with respect to system 3

The **j** direction for both systems in Figure A-3 is into the page. This is normal to the plane of symmetry of the wheel as shown. The last system is defined from the steering angle δ as shown in Figure A-4. When the front wheel is steered about axis $\mathbf{k}_5$, this allows us to define the last coordinate frame, system 6. This frame is viewed in the next figure from the $\mathbf{i} - \mathbf{j}$ plane.

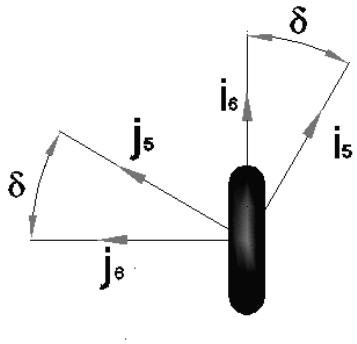

Figure A-4 Front wheel, body fixed coordinate system 6 with respect to system 5

The motion of the vehicle is most often described using vectors in 3D space. Often these vectors will be listed in column form with the coordinate system basis listed as a subscript, see appendix section B. This is shown in the last two expressions in the following example where the vector is shown as a linear combination of basis vectors $\mathbf{i}_3$, $\mathbf{j}_3$, $\mathbf{k}_3$ and as a column vector.

$$x \cdot \mathbf{i}_3 + y \cdot \mathbf{j}_3 + z \cdot \mathbf{k}_3 = \begin{bmatrix} x & y & z \end{bmatrix}_3^{\mathbf{T}} \tag{195}$$

To convert from one coordinate system to another we use rotation matrices. The rotation matrices for these coordinate frames are:

$$\mathbf{R}_3^4 = \begin{bmatrix} 1 & 0 & 0 \\ 0 & \cos\theta & -\sin\theta \\ 0 & \sin\theta & \cos\theta \end{bmatrix}, \; \mathbf{R}_5^3 = \begin{bmatrix} \cos\beta & 0 & \sin\beta \\ 0 & 1 & 0 \\ -\sin\beta & 0 & \cos\beta \end{bmatrix}, \; \mathbf{R}_6^5 = \begin{bmatrix} \cos\delta & \sin\delta & 0 \\ -\sin\delta & \cos\delta & 0 \\ 0 & 0 & 1 \end{bmatrix} \tag{196}$$

As an example, consider the column vector notation of the height of the center of gravity in system 3 and system 4. In system 3 the height is given as:

$$^P\mathbf{r}^B = \begin{bmatrix} 0 & 0 & h \end{bmatrix}_3^{\mathbf{T}}$$

See appendix section B. To express this vector in system 4 we multiply by the rotation matrix $\mathbf{R}_4^3 = \begin{bmatrix} 1 & 0 & 0 \\ 0 & \cos\theta & \sin\theta \\ 0 & -\sin\theta & \cos\theta \end{bmatrix}$ which is the transpose of matrix $\mathbf{R}_3^4$.

$$^P\mathbf{r}^B = \mathbf{R}_4^3 \cdot \begin{bmatrix} 0 & 0 & h \end{bmatrix}_3^{\mathbf{T}} = \begin{bmatrix} 0 & h\sin\theta & h\cos\theta \end{bmatrix}_4^{\mathbf{T}}$$

Thus we can represent any vector quantity in any convenient coordinate frame. Changing between multiple frames is accomplished by successive multiplications by rotation matrices. For example, to change from system 4 to system 6 requires the composite rotation matrix $\mathbf{R}_6^4$.

$$\mathbf{R}_6^4 = \mathbf{R}_6^5\mathbf{R}_5^3\mathbf{R}_3^4 = \begin{bmatrix} \cos\beta\cos\delta & \cos\theta\sin\delta + \cos\delta\sin\theta\sin\beta & -\sin\theta\sin\delta + \cos\theta\cos\delta\sin\beta \\ -\cos\beta\sin\delta & \cos\theta\cos\delta - \sin\theta\sin\beta\sin\delta & -\cos\delta\sin\theta - \cos\theta\sin\beta\sin\delta \\ -\sin\beta & \cos\beta\sin\theta & \cos\theta\cos\beta \end{bmatrix} \tag{197}$$

We can verify that this is an orthogonal transformation matrix by multiplying $\mathbf{R}_6^4$ by its transpose $\mathbf{R}_4^6$. The result should be the identity matrix, $\mathbf{I}$, since there should be no change to the representation of the vector. This is indeed the case since:

$$\mathbf{R}_6^4\mathbf{R}_4^6 = \begin{bmatrix} 1 & 0 & 0 \\ 0 & 1 & 0 \\ 0 & 0 & 1 \end{bmatrix} \tag{198}$$

Appendix B. Symbols and Notation

B.1 Notation

- $\mathbf{i}_n, \mathbf{j}_n, \mathbf{k}_n$ – Unit vectors in right hand coordinate system n
- $[x]_n$ – Column vector coordinates with respect to coordinate basis n
- $\mathbf{R}^n_m$ – Rotation matrix, converts coordinates in system n to coordinates in system m
- $\mathbf{r}^I$, $\mathbf{v}^I$ – Position and velocity of point I respectively
- ${}^J\mathbf{r}^I$, ${}^J\mathbf{v}^I$ – Position and velocity of point I with respect to J respectively
- ${}^m\boldsymbol{\omega}^n$ – Angular velocity of frame n with respect to frame m
- $\frac{{}^n d}{dt}\mathbf{x}$ – Time derivative of vector $\mathbf{x}$ with respect to frame n
- b, flw, frw, rw – Subscripts indicating vehicle body, front left or right wheels, and rear wheel respectively
- Q_n – Quantity for body n, eg. m_b is the mass of the vehicle body
- $\breve{Q}$ – Intermediate definition, expressions as listed
- ξ - Temporary place keeper variables

B.2 Vehicle Specific Symbols

B.2.1 Constant Terms.

- fw – Subscript indicating either or both front wheels
- $G_b, G_{flw}, G_{frw}, G_{rw}$ – Point of of center of gravity of individual bodies
- B – Point of center of gravity of the total vehicle
- P – Point in ground plane directly below B (parallel to $\mathbf{k}_3$ direction) in coordinate basis 3

- h – Distance in $\mathbf{k}_3$ direction from point P to point B, $h = 0.25\,\mathrm{m}$
- $\tilde{h}$ – Distance in $\mathbf{k}_3$ direction from point P to point G_b
- g_x – Distance in $\mathbf{i}_3$ direction from point B to point G_b
- g_z – Distance in $\mathbf{k}_3$ direction from point B to point G_b
- l_f, l_r – Distance in $\mathbf{i}_3$ direction from points B to G_{fw} and B to G_{rw} respectively, $l_f = 0.69\,\mathrm{m}$, $l_r = 0.84\,\mathrm{m}$
- $\tilde{l}_f, \tilde{l}_r$ – Distance in $\mathbf{i}_3$ direction from points G_b to G_{fw} and G_b to G_{rw} respectively
- r_{fw} – Radius of front wheels
- r_{rw} – Radius of rear wheel
- b – Wheel stance
- m_b, m_{fw}, m_{rw} – Mass of individual bodies, $m_b = 190.4\,\mathrm{lb}, m_{fw} = 7.8\,\mathrm{lb}, m_{rw} = 5.0\,\mathrm{lb}$
- m – Total mass of vehicle ($m = m_b + 2m_{fw} + m_{rw}$), $m = 211.0\,\mathrm{lb} = 96\,\mathrm{kg}$
- R_f, R_r – Measured weights at each front and rear wheel respectively, $R_f = 58.0\,\mathrm{lb}$, $R_r = 95.0\,\mathrm{lb}$
- $I_b^{xx}, I_b^{yy}, I_b^{zz}$ – Moments of inertia of vehicle body about $\mathbf{i}_3$, $\mathbf{j}_3$, and $\mathbf{k}_3$ directions
- I_b^{xz} – This term was included in the model derivation but was ultimately dropped by assuming
- $I_{fw}^{xx}, I_{fw}^{yy}, I_{fw}^{zz}$ – Moments of inertia of front wheels about $\mathbf{i}_6$, $\mathbf{j}_6$, and $\mathbf{k}_6$ directions
- $I_{rw}^{xx}, I_{rw}^{yy}, I_{rw}^{zz}$ – Moments of inertia of rear wheel about $\mathbf{i}_3$, $\mathbf{j}_3$, and $\mathbf{k}_3$ directions
- I^{xx} – Sum of moments of inertia of individual bodies about each body fixed $\mathbf{i}$ direction ($I^{xx} = I_b^{xx} + 2I_{fw}^{xx} + I_{rw}^{xx}$), $I^{xx} \simeq 18.0\,\mathrm{kg\,m^2}$
- I^{yy} – Sum of moments of inertia of individual bodies about each body fixed $\mathbf{j}$ direction ($I^{yy} = I_b^{yy} + 2I_{fw}^{yy} + I_{rw}^{yy}$)

- I^{zz} – Sum of moments of inertia of individual bodies about each body fixed $\mathbf{k}$ direction ($I^{zz} = I_b^{zz} + 2I_{fw}^{zz} + I_{rw}^{zz}$), $I^{zz} \simeq 60.0\,\mathrm{kg\,m^2}$
- J – Intermediate definition for nonlinear model, $J = I^{xx} + mh^2 \sin^2\theta$
- κ – Intermediate definition for linear model, $\kappa = 1 + \frac{mh^2}{I^{xx}}$
- C_f, C_r – Tire slip angle gains for front and rear tires respectively, $C_f \simeq 3500.0\frac{\mathrm{N}}{\mathrm{rad}}$, $C_r \simeq 5480.0\frac{\mathrm{N}}{\mathrm{rad}}$
- λ_f, λ_r – Tire camber gains for front and rear tires respectively, $\lambda_f \simeq 1000.0\frac{\mathrm{N}}{\mathrm{rad}}$, $\lambda_r \simeq 2000.0\frac{\mathrm{N}}{\mathrm{rad}}$

B.2.2 State and State Dependent Terms.

- v – Vehicle velocity, parallel to $\mathbf{i}_4$ direction, considered a parameter
- R – Turn radius of vehicle maneuver, see (7)
- C_v – Curvature of maneuver, $C_v = \frac{1}{R}$, for straight roads, $C_v = 0$, see (7)
- $\tilde{C}_v$ – Input from user indicating desired vehicle trajectory, (interpret as desired road curvature)
- $y, \dot{y}, \ddot{y}$ – Vehicle lateral displacement, velocity, and acceleration, parallel to $\mathbf{j}_4$ direction
- $\psi, \dot{\psi}, \ddot{\psi}$ – Vehicle yaw, yaw velocity, and yaw acceleration, parallel to $\mathbf{k}_4$ direction
- $\theta, \dot{\theta}, \ddot{\theta}$ – Vehicle lean, lean velocity, and lean acceleration, parallel to $\mathbf{i}_4$ direction
- $\delta, \dot{\delta}, \ddot{\delta}$ – Front wheel angle, angular velocity, and acceleration, parallel to $\mathbf{k}_6$ direction
- $\mathbf{x}$ – State variables $\mathbf{x} = \begin{bmatrix} \dot{y} & \dot{\psi} & \theta & \dot{\theta} \end{bmatrix}^{\mathbf{T}}$
- ψ_{des} – Desired vehicle yaw rate for particular road curvature, $\psi_{des} = v \cdot C_v$
- θ_{des} – Desired vehicle lean for particular road curvature, $\tan\theta_{des} = \frac{v^2 \cdot C_v}{g}$
- $e_1, \dot{e}_1, \ddot{e}_1$ – Lateral position error
- $e_2, \dot{e}_2, \ddot{e}_2$ – Yaw error

- $e_3, \dot{e}_3, \ddot{e}_3$ – Lean angle error
- $\boldsymbol{\omega}_b, \boldsymbol{\omega}_{flw}, \boldsymbol{\omega}_{frw}, \boldsymbol{\omega}_{rw}$ – Angular velocity of individual vehicle bodies
- $\omega_{fw}^{spin}, \omega_{rw}^{spin}$ – Angular velocity of front and rear wheels about axes $\mathbf{j}_6$ and $\mathbf{j}_3$ respectively
- $\mathbf{H}_b, \mathbf{H}_{flw}, \mathbf{H}_{frw}, \mathbf{H}_{rw}$ – Angular momentum of individual vehicle bodies
- $P_{flw}^y, P_{frw}^y, P_{rw}^y$ – Wheel/body reactions in $\mathbf{j}_4$ direction
- $P_{flw}^z, P_{frw}^z, P_{rw}^z$ – Wheel/body reactions in $\mathbf{k}_4$ direction
- M_{flw}^x, M_{frw}^x – Front wheel/body moments in $\mathbf{i}_6$ direction
- M_{rw}^x – Rear wheel/body moments in $\mathbf{i}_3$ direction
- M_{rw}^z – Rear wheel/body moments in $\mathbf{k}_3$ direction
- M_δ – Input steering torque on front wheels combined
- F_f, F_r – Lateral forces between tires and road, acting in $\mathbf{j}_4$ direction
- N_{fw}, N_{rw} – Normal reaction forces between tires and road, acting in $\mathbf{k}_4$ direction
- g – Acceleration of gravity ($9.81 \frac{\mathrm{m}}{\mathrm{s}}$)

Appendix C. Dynamic Model Derivation

The development of the general equations of motion is illustrated for each body. After these equations are listed I use a few simplifying assumptions to make the problem more tractable and to develop the first iteration controller for the problem. The equations are developed in terms of the state variables $y, \dot{y}, \psi, \dot{\psi}, \theta, \dot{\theta}, \delta$, and $\dot{\delta}$, see section B.

General equations of motion using Newton-Euler Method are (34:pp. 431):

$$m\mathbf{a}^G = \mathbf{F} \tag{199}$$

$$\frac{d}{dt}\mathbf{H}^G = \mathbf{M} \tag{200}$$

In these equations, each term is a vector in 3D space. Finding expressions for these can be quite complex and tedious. To simplify the process, assumptions must be made. These assumptions will be explained as the equations are developed.

C.1 Vehicle Body

C.1.1 Translational Balance. The body is considered rigid and to have motion in three dimensions. Equation 199 for the vehicle body is derived by differentiating the velocity of the body's center of gravity, $\mathbf{v}^{G_b}$. The expression is found explicitly by using the Transport Theorem (34:pp. 117).

$$\mathbf{v}^{G_b} = \mathbf{v}^B + {}^B\mathbf{v}^{G_b},\ {}^B\mathbf{v}^{G_b} = \frac{{}^1d}{dt}{}^B\mathbf{r}^{G_b} = \frac{{}^3d}{dt}{}^B\mathbf{r}^{G_b} + \boldsymbol{\omega}_b \times {}^B\mathbf{r}^{G_b} \tag{201}$$

$$\mathbf{v}^B = \mathbf{v}^P + {}^P\mathbf{v}^B,\ {}^P\mathbf{v}^B = \frac{{}^1d}{dt}{}^P\mathbf{r}^B = \frac{{}^3d}{dt}{}^P\mathbf{r}^B + \boldsymbol{\omega}_b \times {}^P\mathbf{r}^B \tag{202}$$

The cross product terms arise due to the Transport Theorem. It is not immediately obvious, but the time derivatives, $\frac{{}^3d}{dt}{}^B\mathbf{r}^{G_b}$, and $\frac{{}^3d}{dt}{}^P\mathbf{r}^B$ are both zero. We can show that this is true by calculating

the position of point B, the center of gravity, with respect to some other known, constant point. Consider the point directly below the center of gravity of the vehicle body in system 3 (this is not point P which is directly below point B). Let the position vectors of each body be defined from this point as:

$$\tilde{\mathbf{r}}^{G_{flw}} = \begin{bmatrix} \tilde{l}_f \\ -\frac{b}{2}\cos\theta \\ r_{fw} - \frac{b}{2}\sin\theta \end{bmatrix}_3, \ \tilde{\mathbf{r}}^{G_{frw}} = \begin{bmatrix} \tilde{l}_f \\ \frac{b}{2}\cos\theta \\ r_{fw} + \frac{b}{2}\sin\theta \end{bmatrix}_3 \tag{203}$$

$$\tilde{\mathbf{r}}^{G_{rw}} = \begin{bmatrix} -\tilde{l}_r \\ 0 \\ r_{rw} \end{bmatrix}_3, \ \tilde{\mathbf{r}}^{G_b} = \begin{bmatrix} 0 \\ 0 \\ \tilde{h} \end{bmatrix}_3 \tag{204}$$

Using these expressions, we can use the definition of the center of gravity to calculate its position. Doing this, we get:

$$\tilde{\mathbf{r}}^{B} = \frac{1}{m}\begin{bmatrix} 2m_{fw}\tilde{l}_f - m_{rw}\tilde{l}_r \\ 0 \\ m_b\tilde{h} + 2m_{fw}r_{fw} + m_{rw}r_{rw} \end{bmatrix}_3 \tag{205}$$

Thus, the relative position of the center of gravity of the overall vehicle with respect to the center of gravities of the other bodies is constant in leaning. The relative position vector from point B to point G_b is then found to be:

$${}^{B}\tilde{\mathbf{r}}^{G_b} = \frac{1}{m}\begin{bmatrix} m_{rw}\tilde{l}_r - 2m_{fw}\tilde{l}_f \\ 0 \\ 2(\tilde{h} - r_{fw})m_{fw} + (\tilde{h} - r_{rw})m_{rw} \end{bmatrix}_3 = \begin{bmatrix} g_x \\ 0 \\ \dot{g}_z \end{bmatrix}_3 \tag{206}$$

Next make the following observations:

$$l_f = \tilde{l}_f - g_x \tag{207a}$$

$$l_r = \tilde{l}_r + g_x \tag{207b}$$

$$h = \tilde{h} - g_z \tag{207c}$$

With these substitutions, we get:

$$g_x = \frac{1}{m_b}\left(m_{rw} l_r - 2 m_{fw} l_f\right) \tag{208a}$$

$$g_z = \frac{1}{m_b}\left(2(h - r_{fw}) m_{fw} + (h - r_{rw}) m_{rw}\right) \tag{208b}$$

$$h = \frac{1}{m}\left(m_b \tilde{h} + 2 m_{fw} r_{fw} + m_{rw} r_{rw}\right) \tag{208c}$$

Next we can express the positions of each body's center of gravity with respect to the overall vehicle's center of gravity.

$${}^{P}\mathbf{r}^{B} = \begin{bmatrix} 0 \\ 0 \\ h \end{bmatrix}_3, \; {}^{B}\mathbf{r}^{G_b} = \begin{bmatrix} g_x \\ 0 \\ g_z \end{bmatrix}_3 \tag{209a}$$

$${}^{B}\mathbf{r}^{G_{flw}} = \begin{bmatrix} l_f \\ \frac{b}{2}\cos\theta \\ r_{fw} + \frac{b}{2}\sin\theta - h \end{bmatrix}_3, \; {}^{B}\mathbf{r}^{G_{frw}} = \begin{bmatrix} l_f \\ -\frac{b}{2}\cos\theta \\ r_{fw} - \frac{b}{2}\sin\theta - h \end{bmatrix}_3 \tag{209b}$$

$${}^{B}\mathbf{r}^{G_{rw}} = \begin{bmatrix} -l_r \\ 0 \\ r_{rw} - h \end{bmatrix}_3 \tag{209c}$$

Combining equations 201 and 202, we get the velocity of the center of gravity of the vehicle body.

$$\mathbf{v}^{G_b} = \mathbf{v}^P + \boldsymbol{\omega}_b \times {}^P\mathbf{r}^B + \boldsymbol{\omega}_b \times {}^B\mathbf{r}^{G_b} \tag{210}$$

The components of the individual terms of this expression in column vector form are:

$$\mathbf{v}^P = \begin{bmatrix} v \\ \dot{y} \\ 0 \end{bmatrix}_4 = \mathbf{R}_3^4 \begin{bmatrix} v \\ \dot{y} \\ 0 \end{bmatrix}_4 = \begin{bmatrix} v \\ \dot{y}\cos\theta \\ \dot{y}\sin\theta \end{bmatrix}_3 \tag{211a}$$

$$\begin{aligned} \boldsymbol{\omega}_b &= {}^1\boldsymbol{\omega}^4 + {}^4\boldsymbol{\omega}^3 = \begin{bmatrix} 0 \\ 0 \\ \dot{\psi} \end{bmatrix}_4 + \begin{bmatrix} -\dot{\theta} \\ 0 \\ 0 \end{bmatrix}_4 = \begin{bmatrix} -\dot{\theta} \\ 0 \\ \dot{\psi} \end{bmatrix}_4 \\ &= \mathbf{R}_3^4 \begin{bmatrix} -\dot{\theta} \\ 0 \\ \dot{\psi} \end{bmatrix}_4 = \begin{bmatrix} -\dot{\theta} \\ -\dot{\psi}\sin\theta \\ \dot{\psi}\cos\theta \end{bmatrix}_3^T \end{aligned} \tag{211b}$$

Point P always remains in the ground plane hence its velocity, $\mathbf{v}^P$, when represented in system 1 or 4, does not have a component in the vertical direction. We now need to differentiate expression 210 to get the acceleration of the center of gravity of the body.

$$\begin{aligned} \frac{{}^1d}{dt}\mathbf{v}^{G_b} &= \mathbf{a}^{G_b} = \frac{{}^1d}{dt}\left(\mathbf{v}^P + \boldsymbol{\omega}_b \times {}^P\mathbf{r}^B + \boldsymbol{\omega}_b \times {}^B\mathbf{r}^{G_b}\right) \\ &= \frac{{}^1d}{dt}\mathbf{v}^P + \frac{{}^1d}{dt}\left(\boldsymbol{\omega}_b \times {}^P\mathbf{r}^B\right) + \frac{{}^1d}{dt}\left(\boldsymbol{\omega}_b \times {}^B\mathbf{r}^{G_b}\right) \end{aligned} \tag{212}$$

We differentiate each term to get:

$$\begin{aligned}
\frac{{}^1d}{dt}\mathbf{v}^P &= \mathbf{a}^P = \frac{{}^4d}{dt}\mathbf{v}^P + {}^1\boldsymbol{\omega}^4 \times \mathbf{v}^P \\
&= \begin{bmatrix} \dot{v} \\ \ddot{y} \\ 0 \end{bmatrix}_4 + \begin{bmatrix} 0 \\ 0 \\ \dot{\psi} \end{bmatrix}_4 \times \begin{bmatrix} v \\ \dot{y} \\ 0 \end{bmatrix}_4 \\
&= \begin{bmatrix} \dot{v} - \dot{\psi}\dot{y} & v\dot{\psi} + \ddot{y} & 0 \end{bmatrix}_4^{\mathbf{T}}
\end{aligned} \tag{213}$$

To differentiate the cross product terms, we again apply the transport theorem and the product rule to get:

$$\begin{aligned}
\frac{{}^1d}{dt}\left(\boldsymbol{\omega}_b \times {}^P\mathbf{r}^B\right) &= \frac{{}^3d}{dt}\left(\boldsymbol{\omega}_b \times {}^P\mathbf{r}^B\right) + {}^1\boldsymbol{\omega}^3 \times \left(\boldsymbol{\omega}_b \times {}^P\mathbf{r}^B\right) \\
&= \frac{{}^3d}{dt}\left(\boldsymbol{\omega}_b \times {}^P\mathbf{r}^B\right) + \boldsymbol{\omega}_b \times \left(\boldsymbol{\omega}_b \times {}^P\mathbf{r}^B\right)
\end{aligned} \tag{214}$$

Using the product rule, the first term on the right becomes:

$$\frac{{}^3d}{dt}\left(\boldsymbol{\omega}_b \times {}^P\mathbf{r}^B\right) = \boldsymbol{\omega}_b \times \left(\frac{{}^3d}{dt}{}^P\mathbf{r}^B\right) + \left(\frac{{}^3d}{dt}\boldsymbol{\omega}_b\right) \times {}^P\mathbf{r}^B \tag{215}$$

Using the fact that $\frac{{}^3d}{dt}{}^P\mathbf{r}^B = 0$, $\frac{{}^1d}{dt}\left(\boldsymbol{\omega}_b \times {}^P\mathbf{r}^B\right)$ becomes:

$$\frac{{}^1d}{dt}\left(\boldsymbol{\omega}_b \times {}^P\mathbf{r}^B\right) = \left(\frac{{}^3d}{dt}\boldsymbol{\omega}_b\right) \times {}^P\mathbf{r}^B + \boldsymbol{\omega}_b \times \left(\boldsymbol{\omega}_b \times {}^P\mathbf{r}^B\right) \tag{216}$$

Explicitly, these terms are:

$$\frac{{}^3d}{dt}\boldsymbol{\omega}_b = \begin{bmatrix} -\ddot{\theta} \\ -\left(\sin\theta\right)\ddot{\psi} - \dot{\psi}\dot{\theta}\left(\cos\theta\right) \\ \left(\cos\theta\right)\ddot{\psi} - \dot{\psi}\dot{\theta}\left(\sin\theta\right) \end{bmatrix}_3 \tag{217}$$

$$\left(\frac{^3d}{dt}\boldsymbol{\omega}_b\right) \times {}^P\mathbf{r}^B = \begin{bmatrix} h\left(-\left(\cos\theta\right)\dot{\psi}\dot{\theta} - \left(\sin\theta\right)\ddot{\psi}\right) \\ h\ddot{\theta} \\ 0 \end{bmatrix}_3$$

$$= \begin{bmatrix} h\left(-\left(\cos\theta\right)\dot{\psi}\dot{\theta} - \left(\sin\theta\right)\ddot{\psi}\right) \\ h\left(\cos\theta\right)\ddot{\theta} \\ -h\left(\sin\theta\right)\ddot{\theta} \end{bmatrix}_4 \tag{218}$$

$$\boldsymbol{\omega}_b \times \left(\boldsymbol{\omega}_b \times {}^P\mathbf{r}^B\right) = \begin{bmatrix} -h\left(\cos\theta\right)\dot{\psi}\dot{\theta} \\ -h\left(\cos\theta\sin\theta\right)\dot{\psi}^2 \\ -ht_d^2 - h\left(\sin^2\theta\right)\dot{\psi}^2 \end{bmatrix}_3$$

$$= \begin{bmatrix} -h\left(\cos\theta\right)\dot{\psi}\dot{\theta} \\ -h\left(\sin\theta\right)\dot{\psi}^2 - h\left(\sin\theta\right)\dot{\theta}^2 \\ -h\left(\cos\theta\right)\dot{\theta}^2 \end{bmatrix}_4 \tag{219}$$

Equation 217 is found by differentiation of the coordinates of $\boldsymbol{\omega}_b$ when expressed in system 3. With these definitions, equation 216 is:

$$\frac{^1d}{dt}\left(\boldsymbol{\omega}_b \times {}^P\mathbf{r}^B\right) = \begin{bmatrix} -h\left(\cos\theta\right)\dot{\psi}\dot{\theta} + h\left(-\left(\cos\theta\right)\dot{\psi}\dot{\theta} - \left(\sin\theta\right)\ddot{\psi}\right) \\ h\left(\cos\theta\right)\ddot{\theta} - h\left(\sin\theta\right)\dot{\psi}^2 - h\left(\sin\theta\right)\dot{\theta}^2 \\ -h\left(\sin\theta\right)\ddot{\theta} - h\left(\cos\theta\right)\dot{\theta}^2 \end{bmatrix}_4 \tag{220}$$

We use the same process to get a similar expression for the last term of equation 212:

$$\frac{^1d}{dt}\left(\boldsymbol{\omega}_b \times {}^B\mathbf{r}^{G_b}\right) = \begin{bmatrix} -2\left(\cos\theta\right)\dot{\psi}\dot{\theta}g_z - \dot{\psi}^2 g_x - \left(\sin\theta\right)g_z\ddot{\psi} \\ g_x\ddot{\psi} + \left(\cos\theta\right)g_z\ddot{\theta} - \left(\sin\theta\right)\dot{\psi}^2 g_z - \left(\sin\theta\right)\dot{\theta}^2 g_z \\ -\left(\sin\theta\right)g_z\ddot{\theta} - \left(\cos\theta\right)\dot{\theta}^2 g_z \end{bmatrix}_4 \tag{221}$$

Combining equations 213, 220, and 221 we get the final expression for the acceleration of the center of gravity of the vehicle body.

$$\begin{aligned} \mathbf{a}^{G_b} &= \frac{^1d}{dt}\mathbf{v}^{G_b} \\ &= \begin{bmatrix} \dot{v} - \dot{\psi}\dot{y} - \dot{\psi}^2 g_x - \xi_z\ddot{\psi}\sin\theta - 2\xi_z\dot{\psi}\dot{\theta}\cos\theta \\ v\dot{\psi} + \ddot{y} + g_x\ddot{\psi} + \xi_z\ddot{\theta}\cos\theta - \xi_z\dot{\psi}^2\sin\theta - \xi_z\dot{\theta}^2\sin\theta \\ -\xi_z\left(\ddot{\theta}\sin\theta + \dot{\theta}^2\cos\theta\right) \end{bmatrix}_4 \qquad (222) \\ \xi_z &= h + g_z \qquad (223) \end{aligned}$$

C.1.1.1 Resultant Force. The A-arms of the vehicle chassis are approximated as massless bodies and together with the forks and the vehicle body, form a parallelogram linkage, see section V. This allows us to assume that they (the A-arms) work to create an independent force and a couple acting on the vehicle body. In system 4, the resultant force is:

$$\begin{aligned} \mathbf{F}_b &= {}^b\mathbf{P}^{flw} + {}^b\mathbf{P}^{frw} + {}^b\mathbf{P}^{rw} + {}^b\mathbf{F}^{grav} \\ &= \begin{bmatrix} P^x_{flw} \\ P^y_{flw} \\ P^z_{flw} \end{bmatrix}_4 + \begin{bmatrix} P^x_{frw} \\ P^y_{frw} \\ P^z_{frw} \end{bmatrix}_4 + \begin{bmatrix} P^x_{rw} \\ P^y_{rw} \\ P^z_{rw} \end{bmatrix}_4 + \begin{bmatrix} 0 \\ 0 \\ -m_b g \end{bmatrix}_4 \end{aligned} \tag{224a}$$

C.1.1.1 Resultant Force.

$$m_b\mathbf{a}^{G_b} = {}^b\mathbf{P}^{flw} + {}^b\mathbf{P}^{frw} + {}^b\mathbf{P}^{rw} + {}^b\mathbf{F}^{grav} \tag{225}$$

C.1.2 Moment Balance. The next step is to find an expression for equation 200 for the vehicle body. To do this, we need an expression for $\mathbf{H}_b$.

$$\begin{aligned}\mathbf{H}_b &= \mathbf{I}_b\boldsymbol{\omega}_b = \begin{bmatrix} I_b^{xx} & 0 & -I_b^{xz} \\ 0 & I_b^{yy} & 0 \\ -I_b^{xz} & 0 & I_b^{zz} \end{bmatrix}_3 \cdot \begin{bmatrix} -\dot{\theta} \\ -(\sin\theta)\,\dot{\psi} \\ (\cos\theta)\,\dot{\psi} \end{bmatrix}_3 \\ &= \begin{bmatrix} -(\cos\theta)\,\dot{\psi}I_b^{xz} - \dot{\theta}I_b^{xx} \\ -(\sin\theta)\,\dot{\psi}I_b^{yy} \\ \dot{\theta}I_b^{xz} + (\cos\theta)\,\dot{\psi}I_b^{zz} \end{bmatrix}_3 \end{aligned} \tag{226}$$

The inertia tensor is defined with respect to the body fixed coordinates system 3 (see appendix A). The axes of this system are not necessarily the principle axes. This is because there is only one plane of symmetry, at the $(x,z)_3$ plane. This plane of symmetry allows us to assume that the products of inertia involving the y term are zero. If either of the $(x,y)_3$ or $(y,z)_3$ planes were also planes of symmetry, then the system 3 axes would be principle axes and hence the quantity I_b^{xz} would be zero. We will, however, ultimately assume that the system 3 coordinates are sufficiently close to the principle axes. This will allow us to approximate I_b^{xz} to be zero.

To differentiate $\mathbf{H}_b$ in the inertial frame and find Euler's equations of motion, we again use the Transport Theorem ((34:pp. 117)).

$$\frac{{}^1d}{dt}\mathbf{H}_b = \frac{{}^3d}{dt}\mathbf{H}_b + \boldsymbol{\omega}_b \times \mathbf{H}_b \tag{227}$$

$$\frac{{}^3d}{dt}\mathbf{H}_b = \begin{bmatrix} -\left((\cos\theta)\,\ddot{\psi} - \dot{\psi}\dot{\theta}\sin\theta\right)I_b^{xz} - \ddot{\theta}I_b^{xx} \\ -\left((\sin\theta)\,\ddot{\psi} + \dot{\psi}\dot{\theta}\cos\theta\right)I_b^{yy} \\ \ddot{\theta}I_b^{xz} + \left((\cos\theta)\,\ddot{\psi} - \dot{\psi}\dot{\theta}\sin\theta\right)I_b^{zz} \end{bmatrix}_3 \tag{228}$$

$$\boldsymbol{\omega}_b \times \mathbf{H}_b = \begin{bmatrix} -(\sin\theta)\,\dot{\psi}\dot{\theta}I_b^{xz} + (\sin\theta)\,\dot{\psi}^2\,(\cos\theta)\,(-I_b^{zz} + I_b^{yy}) \\ \left(\dot{\theta}^2 - \left(\cos^2\theta\right)\dot{\psi}^2\right) I_b^{xz} + \dot{\theta}\,(\cos\theta)\,\dot{\psi}\,(I_b^{zz} - I_b^{xx}) \\ (I_b^{yy} - I_b^{xx})\,\dot{\psi}\dot{\theta}\sin\theta - (\sin\theta)\,\dot{\psi}^2\,(\cos\theta)\,I_b^{xz} \end{bmatrix}_3 \tag{229}$$

Equation 227 then becomes:

$$\begin{aligned} {}^1\frac{d}{dt}\mathbf{H}_b &= \begin{bmatrix} -I_b^{xz}\,(\cos\theta)\,\ddot{\psi} - \ddot{\theta}I_b^{xx} + (\sin\theta)\,\dot{\psi}^2\,(\cos\theta)\,(-I_b^{zz} + I_b^{yy}) \\ -\xi_1 I_b^{yy} + \left[\dot{\theta}^2 - \left(\cos^2\theta\right)\dot{\psi}^2\right] I_b^{xz} + \dot{\theta}\,(\cos\theta)\,\dot{\psi}\,(I_b^{zz} - I_b^{xx}) \\ \xi_2 I_b^{zz} + (I_b^{yy} - I_b^{xx})\,\dot{\psi}\dot{\theta}\sin\theta + \left(\ddot{\theta} - (\sin\theta)\,\dot{\psi}^2\,(\cos\theta)\right) I_b^{xz} \end{bmatrix}_3 \qquad (230) \\ \xi_1 &= (\sin\theta)\,\ddot{\psi} + \dot{\psi}\dot{\theta}\cos\theta \qquad (231) \\ \xi_2 &= (\cos\theta)\,\ddot{\psi} - \dot{\psi}\dot{\theta}\sin\theta \qquad (232) \end{aligned}$$

C.1.2.1 Resultant Moment.

$$\begin{aligned} \mathbf{M}_b &= {}^b\mathbf{M}^{flw} + {}^b\mathbf{M}^{frw} + {}^b\mathbf{M}^{rw} - \mathbf{M}_\delta + \\ &\quad {}^{B}\mathbf{r}^{G_b} \times {}^b\mathbf{F}^{grav} + {}^{B}\mathbf{r}^{G_{flw}} \times {}^b\mathbf{P}^{flw} + {}^{B}\mathbf{r}^{G_{frw}} \times {}^b\mathbf{P}^{frw} + {}^{B}\mathbf{r}^{G_{rw}} \times {}^b\mathbf{P}^{rw} \\ &= \begin{bmatrix} M_{flw}^x \\ 0 \\ 0 \end{bmatrix}_6 + \begin{bmatrix} M_{frw}^x \\ 0 \\ 0 \end{bmatrix}_6 + \begin{bmatrix} M_{rw}^x \\ 0 \\ M_{rw}^z \end{bmatrix}_3 - \begin{bmatrix} 0 \\ 0 \\ M_\delta \end{bmatrix}_5 \\ &\quad + {}^{B}\mathbf{r}^{G_b} \times {}^b\mathbf{F}^{grav} + {}^{B}\mathbf{r}^{G_{flw}} \times {}^b\mathbf{P}^{flw} + {}^{B}\mathbf{r}^{G_{frw}} \times {}^b\mathbf{P}^{frw} + {}^{B}\mathbf{r}^{G_{rw}} \times {}^b\mathbf{P}^{rw} \end{aligned} \tag{233}$$

The moment is given in system 6 for simplicity sake. It becomes very complicated in system 3 and will require some simplifying assumptions before it can be used. This is postponed until the equations for the wheels are developed.

C.1.2.2 Moment Balance Expression.

$$\begin{aligned}\frac{^1d}{dt}\mathbf{H}_b &= {}^b\mathbf{M}^{flw} + {}^b\mathbf{M}^{frw} + {}^b\mathbf{M}^{rw} - \mathbf{M}_\delta \\ &\quad + {}^B\mathbf{r}^{G_b} \times \mathbf{F}_b^{grav} + {}^B\mathbf{r}^{G_{flw}} \times {}^b\mathbf{P}^{flw} + {}^B\mathbf{r}^{G_{frw}} \times {}^b\mathbf{P}^{frw} + {}^B\mathbf{r}^{G_{rw}} \times {}^b\mathbf{P}^{rw}\end{aligned} \tag{234}$$

C.2 Front Wheels

The explicit expressions for the front wheels moment balance, become far too complex to be usable for this paper. Some of the steps are listed however to illustrate both how the procedure could be completed and why the simplifying assumptions need to be made.

C.2.1 Translational Balance. The translational balance, equation 199 for each of the front wheels, is found in a similar manner as for the vehicle body by replacing ${}^B\mathbf{r}^{G_b}$ with ${}^B\mathbf{r}^{G_{flw}}$ and ${}^B\mathbf{r}^{G_{frw}}$. Restating equation 209b.

$${}^B\mathbf{r}^{G_{flw}} = \begin{bmatrix} l_f \\ \frac{b}{2}\cos\theta \\ r_{fw} + \frac{b}{2}\sin\theta - h \end{bmatrix}_3, \quad {}^B\mathbf{r}^{G_{frw}} = \begin{bmatrix} l_f \\ -\frac{b}{2}\cos\theta \\ r_{fw} - \frac{b}{2}\sin\theta - h \end{bmatrix}_3$$

Starting with equation 201 for the front left wheel.

$$\mathbf{v}^{G_{flw}} = \mathbf{v}^B + {}^B\mathbf{v}^{G_{flw}}, \; {}^B\mathbf{v}^{G_{flw}} = \frac{^1d}{dt}{}^B\mathbf{r}^{G_{flw}} = \frac{^3d}{dt}{}^B\mathbf{r}^{G_{flw}} + \boldsymbol{\omega}_b \times {}^B\mathbf{r}^{G_{flw}} \tag{235}$$

$$\frac{^3d}{dt}{}^B\mathbf{r}^{G_{flw}} = \begin{bmatrix} 0 \\ -\frac{b}{2}\dot{\theta}\sin\theta \\ \frac{b}{2}\dot{\theta}\cos\theta \end{bmatrix}_3 \tag{236}$$

In this case, $\frac{^3d}{dt}{}^B\mathbf{r}^{G_{flw}}$ is not zero because the configuration of the vehicle is changing as it leans. Combining this with equation 202 and again using the fact that $\frac{^3d}{dt}{}^P\mathbf{r}^B = 0$ we get:

$$\mathbf{v}^{G_{flw}} = \mathbf{v}^P + \boldsymbol{\omega}_b \times {}^P\mathbf{r}^B + \frac{^3d}{dt}{}^B\mathbf{r}^{G_{flw}} + \boldsymbol{\omega}_b \times {}^B\mathbf{r}^{G_{flw}} \tag{237}$$

Differentiating this expression:

$$\begin{aligned} \frac{^1d}{dt}\mathbf{v}^{G_{flw}} &= \mathbf{a}^{G_{flw}} = \frac{^1d}{dt}\left(\mathbf{v}^P + \boldsymbol{\omega}_b \times {}^P\mathbf{r}^B + \frac{^3d}{dt}{}^B\mathbf{r}^{G_{flw}} + \boldsymbol{\omega}_b \times {}^B\mathbf{r}^{G_{flw}}\right) \\ &= \frac{^1d}{dt}\mathbf{v}^P + \frac{^1d}{dt}\left(\boldsymbol{\omega}_b \times {}^P\mathbf{r}^B\right) + \frac{^1d}{dt}\left(\frac{^3d}{dt}{}^B\mathbf{r}^{G_{flw}}\right) + \frac{^1d}{dt}\left(\boldsymbol{\omega}_b \times {}^B\mathbf{r}^{G_{flw}}\right) \end{aligned} \tag{238}$$

Next, we need expressions for the last 2 terms on the right.

$$\frac{^1d}{dt}\left(\frac{^3d}{dt}{}^B\mathbf{r}^{G_{flw}}\right) = \frac{^3d}{dt}\left(\frac{^3d}{dt}{}^B\mathbf{r}^{G_{flw}}\right) + \boldsymbol{\omega}_b \times \frac{^3d}{dt}{}^B\mathbf{r}^{G_{flw}} \tag{239}$$

$$\frac{^3d}{dt}\left(\frac{^3d}{dt}{}^B\mathbf{r}^{G_{flw}}\right) = \frac{^3d^2}{dt^2}{}^B\mathbf{r}^{G_{flw}} = \begin{bmatrix} 0 \\ -\frac{b}{2}\left(\dot{\theta}^2\sin\theta + \ddot{\theta}\sin\theta\right) \\ \frac{b}{2}\left(-\dot{\theta}^2\sin\theta + \ddot{\theta}\cos\theta\right) \end{bmatrix}_3 \tag{240}$$

$$\boldsymbol{\omega}_b \times \frac{^3d}{dt}{}^B\mathbf{r}^{G_{flw}} = \begin{bmatrix} 0 \\ \frac{1}{2}\dot{\theta}^2 b\cos\theta \\ \frac{1}{2}\dot{\theta}^2 b\sin\theta \end{bmatrix}_3 = \begin{bmatrix} 0 \\ \frac{1}{2}\dot{\theta}^2 b \\ 0 \end{bmatrix}_4 \tag{241}$$

$$\frac{^1d}{dt}\left(\boldsymbol{\omega}_b \times {}^B\mathbf{r}^{G_{flw}}\right) = \frac{^3d}{dt}\left(\boldsymbol{\omega}_b \times {}^B\mathbf{r}^{G_{flw}}\right) + \boldsymbol{\omega}_b \times \left(\boldsymbol{\omega}_b \times {}^B\mathbf{r}^{G_{flw}}\right) \tag{242}$$

$$\frac{^3d}{dt}\left(\boldsymbol{\omega}_b \times {}^B\mathbf{r}^{G_{flw}}\right) = \boldsymbol{\omega}_b \times \frac{^3d}{dt}{}^B\mathbf{r}^{G_{flw}} + \left(\frac{^3d}{dt}\boldsymbol{\omega}_b\right) \times {}^B\mathbf{r}^{G_{flw}} \tag{243}$$

Listed explicitly, these terms are:

$$\frac{^1d}{dt}\left(\boldsymbol{\omega}_b \times {}^B\mathbf{r}^{G_{flw}}\right) = \boldsymbol{\omega}_b \times \frac{^3d}{dt}{}^B\mathbf{r}^{G_{flw}} + \left(\frac{^3d}{dt}\boldsymbol{\omega}_b\right) \times {}^B\mathbf{r}^{G_{flw}} + \boldsymbol{\omega}_b \times \left(\boldsymbol{\omega}_b \times {}^B\mathbf{r}^{G_{flw}}\right)$$

$$\begin{aligned}
\left(\frac{^3d}{dt}\boldsymbol{\omega}_b\right) \times {}^B\mathbf{r}^{G_{flw}} &= \begin{bmatrix} \dot{\theta}\left(h - r_{fw}\right)\cos\theta\dot{\psi} - \left(\frac{1}{2}b - \left(h - r_{fw}\right)\sin\theta\right)\ddot{\psi} \\ \left(\left(\cos\theta\right)\ddot{\psi} - \dot{\psi}\dot{\theta}\sin\theta\right) l_f - \ddot{\theta}\left(h - r_{fw} - \frac{1}{2}b\sin\theta\right) \\ -\frac{1}{2}\ddot{\theta}b\cos\theta + \left(\left(\sin\theta\right)\ddot{\psi} + \dot{\psi}\dot{\theta}\cos\theta\right) l_f \end{bmatrix}_3 \\
&= \begin{bmatrix} \dot{\psi}\dot{\theta}\left(h - r_{fw}\right)\cos\theta + \ddot{\psi}\left(h - r_{fw}\right)\sin\theta - \frac{1}{2}\ddot{\psi}b \\ \ddot{\theta}\left(r_{fw} - h\right)\cos\theta + l_f\ddot{\psi} \\ l_f\dot{\psi}\dot{\theta} - \ddot{\theta}\left(\frac{1}{2}b - \left(h - r_{fw}\right)\sin\theta\right) \end{bmatrix}_4
\end{aligned} \tag{244}$$

$$\begin{aligned}
\boldsymbol{\omega}_b \times \left(\boldsymbol{\omega}_b \times {}^B\mathbf{r}^{G_{flw}}\right) &= \begin{bmatrix} \xi_4\dot{\psi}\dot{\theta}\cos\theta - \dot{\psi}^2 l_f \\ \left(\dot{\psi}^2\xi_4\cos\theta + l_f\dot{\psi}\dot{\theta}\right)\sin\theta - \frac{1}{2}b\xi_3\cos\theta \\ -\xi_4\dot{\psi}^2\cos^2\theta - \dot{\theta}\dot{\psi}\left(\cos\theta\right) l_f + \xi_3\left(\xi_4 - \frac{1}{2}\left(\sin\theta\right)b\right) \end{bmatrix}_3 \\
&= \begin{bmatrix} \xi_4\dot{\psi}\dot{\theta}\cos\theta - \dot{\psi}^2 l_f \\ \left(\dot{\psi}^2 + \dot{\theta}^2\right)\left(h\sin\theta - r_{fw} - \frac{1}{2}b\right) \\ \left(-\dot{\theta}^2 r_{fw} + \dot{\theta}^2 h\right)\cos\theta - l_f\dot{\psi}\dot{\theta} \end{bmatrix}_4
\end{aligned} \tag{245}$$

$$\xi_3 = \dot{\psi}^2 + \dot{\theta}^2 \tag{246}$$

$$\xi_4 = h - r_{fw} \tag{247}$$

Equation 238 then becomes:

$$\begin{aligned}\mathbf{a}^{G_{flw}} &= \frac{^1d}{dt}\mathbf{v}^P + \frac{^1d}{dt}\left(\boldsymbol{\omega}_b \times {}^P\mathbf{r}^B\right) + \frac{^3d^2}{dt^2}{}^B\mathbf{r}^{G_{flw}} + 2\boldsymbol{\omega}_b \times \frac{^3d}{dt}{}^B\mathbf{r}^{G_{flw}} \\ &\quad + \left(\frac{^3d}{dt}\boldsymbol{\omega}_b\right) \times {}^B\mathbf{r}^{G_{flw}} + \boldsymbol{\omega}_b \times \left(\boldsymbol{\omega}_b \times {}^B\mathbf{r}^{G_{flw}}\right) \end{aligned} \tag{248}$$

Explicitly this is:

$$\mathbf{a}^{G_{flw}} = \begin{bmatrix} \dot{v} - \dot{\psi}\dot{y} - 2\dot{\psi}\dot{\theta}\left(\cos\theta\right)r_{fw} - \left(\sin\theta\right)\ddot{\psi}r_{fw} - \frac{1}{2}\ddot{\psi}b - \dot{\psi}^2 l_f \\ v\dot{\psi} + \ddot{y} + \left(\cos\theta\right)\ddot{\theta}r_{fw} + l_f\ddot{\psi} - \dot{\psi}^2 r_{fw}\sin\theta - \left(\sin\theta\right)\dot{\theta}^2 r_{fw} - \frac{1}{2}\dot{\psi}^2 b \\ -\left(\sin\theta\right)\ddot{\theta}r_{fw} - \left(\cos\theta\right)\dot{\theta}^2 r_{fw} \end{bmatrix}_4 \tag{249}$$

Using the same process for the front right wheel, we get:

$$\mathbf{a}^{G_{frw}} = \begin{bmatrix} \dot{v} - \dot{\psi}\dot{y} - 2\dot{\psi}\dot{\theta}\left(\cos\theta\right)r_{fw} - \left(\sin\theta\right)\ddot{\psi}r_{fw} + \frac{1}{2}\ddot{\psi}b - \dot{\psi}^2 l_f \\ v\dot{\psi} + \ddot{y} + \left(\cos\theta\right)\ddot{\theta}r_{fw} + l_f\ddot{\psi} - \dot{\psi}^2 r_{fw}\sin\theta - \left(\sin\theta\right)\dot{\theta}^2 r_{fw} + \frac{1}{2}\dot{\psi}^2 b \\ -\left(\sin\theta\right)\ddot{\theta}r_{fw} - \left(\cos\theta\right)\dot{\theta}^2 r_{fw} \end{bmatrix}_4 \tag{250}$$

C.2.1.1 Resultant Force.

$$\begin{aligned}\mathbf{F}_{fw} &= {}^{fw}\mathbf{P}^b + \mathbf{F}_{fw}^{ext} \\ &= {}^{fw}\mathbf{P}^b + \begin{bmatrix} 0 \\ F_f \\ N_{fw} - m_{fw}g \end{bmatrix}_4 \end{aligned} \tag{251a}$$

C.2.1.1 Resultant Force.

$$m_{flw}\mathbf{a}^{G_{flw}} = {}^{flw}\mathbf{P}^{b} + \mathbf{F}^{ext}_{flw} \tag{252a}$$

$$m_{frw}\mathbf{a}^{G_{frw}} = {}^{frw}\mathbf{P}^{b} + \mathbf{F}^{ext}_{frw} \tag{252b}$$

C.2.2 Moment Balance. Next, we need an expression for equation 200 for the front wheels. It is this expression that becomes too complicated to use without any simplifying assumptions. For completeness however, the steps are shown as to how this expression would be found. We start by finding $\boldsymbol{\omega}_{fw}$ in the body fixed coordinate system 6.

$$\boldsymbol{\omega}_{fw} = {}^{1}\boldsymbol{\omega}^{4} + {}^{4}\boldsymbol{\omega}^{3} + {}^{3}\boldsymbol{\omega}^{6} + \boldsymbol{\omega}^{spin}_{fw} = \boldsymbol{\omega}_{b} + {}^{3}\boldsymbol{\omega}^{6} + \boldsymbol{\omega}^{spin}_{fw} = {}^{1}\boldsymbol{\omega}^{6} + \boldsymbol{\omega}^{spin}_{fw} \tag{253}$$

$$\begin{aligned} {}^{1}\boldsymbol{\omega}^{6} &= \boldsymbol{\omega}_{b} + \begin{bmatrix} 0 \\ 0 \\ \dot{\delta} \end{bmatrix}_{6} \\ &= \begin{bmatrix} -\left(\cos\beta\cos\delta\right)\dot{\theta} - \left(\sin\delta\sin\theta\right)\dot{\psi} + \left(\sin\beta\cos\delta\cos\theta\right)\dot{\psi} \\ \left(\cos\beta\sin\delta\right)\dot{\theta} - \left(\cos\delta\sin\theta\right)\dot{\psi} - \left(\sin\beta\sin\delta\cos\theta\right)\dot{\psi} \\ \left(\sin\beta\right)\dot{\theta} + \left(\cos\beta\cos\theta\right)\dot{\psi} + \dot{\delta} \end{bmatrix}_{6} \end{aligned} \tag{254}$$

$$\boldsymbol{\omega}^{spin}_{fw} = \begin{bmatrix} 0 \\ \omega^{spin}_{fw} \\ 0 \end{bmatrix}_{6} \tag{255}$$

$$\boldsymbol{\omega}_{fw} = \begin{bmatrix} -\left(\cos\beta\cos\delta\right)\dot{\theta} - \left(\sin\delta\right)\dot{\psi}\sin\theta + \left(\sin\beta\cos\delta\right)\dot{\psi}\cos\theta \\ \omega_{fw}^{spin} + \left(\cos\beta\sin\delta\right)\dot{\theta} - \left(\cos\delta\right)\dot{\psi}\sin\theta - \left(\sin\beta\sin\delta\right)\dot{\psi}\cos\theta \\ \dot{\delta} + \left(\sin\beta\right)\dot{\theta} + \left(\cos\beta\right)\dot{\psi}\cos\theta \end{bmatrix}_6 \tag{256}$$

Notice that $\omega_{fw}^{spin} > 0$ when the vehicle has forward velocity. This is then used to find $\mathbf{H}_{flw}$ and $\mathbf{H}_{frw}$.

$$\begin{aligned} \mathbf{H}_{fw} &= \mathbf{I}_{fw}\boldsymbol{\omega}_{fw} \\ &= \begin{bmatrix} I_{fw}^{xx}\left(-\left(\cos\beta\cos\delta\right)\dot{\theta} - \left(\sin\delta\right)\dot{\psi}\sin\theta + \left(\sin\beta\cos\delta\right)\dot{\psi}\cos\theta\right) \\ I_{fw}^{yy}\left(\omega_{fw}^{spin} + \left(\cos\beta\sin\delta\right)\dot{\theta} - \left(\cos\delta\right)\dot{\psi}\sin\theta - \left(\sin\beta\sin\delta\right)\dot{\psi}\cos\theta\right) \\ I_{fw}^{zz}\left(\dot{\delta} + \left(\sin\beta\right)\dot{\theta} + \left(\cos\beta\right)\dot{\psi}\cos\theta\right) \end{bmatrix}_6 \end{aligned} \tag{257}$$

The axes of system 6 are principle axes so the products of inertia are 0. The next step is to find $\frac{^1d}{dt}\mathbf{H}_{fw}$. As we did with the vehicle body, we use the transport theorem.

$$\frac{^1d}{dt}\mathbf{H}_{fw} = \frac{^6d}{dt}\mathbf{H}_{fw} + {}^1\boldsymbol{\omega}^6 \times \mathbf{H}_{fw} \tag{258}$$

The cross product term involves the rotation of coordinate system 6. As we can see from the expression for $\mathbf{H}_{fw}$, the derivative and cross product terms in equation 258 will be quite complex. For the sake of completeness, and that alone, they are listed here.

$${}^1\boldsymbol{\omega}^6 \times \mathbf{H}_{fw} = \begin{bmatrix} \left(I_{fw}^{yy} - I_{fw}^{zz}\right)\breve{A}_7^x - I_{fw}^{yy}\breve{A}_6^x\omega_{fw}^{spin} \\ \left(I_{fw}^{xx} - I_{fw}^{zz}\right)\breve{A}^y \\ \left(I_{fw}^{xx} - I_{fw}^{yy}\right)\breve{A}_9^z + I_{fw}^{yy}\left(\breve{A}_7^z + \breve{A}_8^z\right)\omega_{fw}^{spin} \end{bmatrix}_6 \tag{259}$$

Where the coefficients for the x term are:

$$\breve{A}_1^x = \cos\delta\sin\theta\sin\beta + \left(1 - 2\cos^2\beta\right)\sin\delta\cos\theta \tag{260a}$$

$$\breve{A}_2^x = \cos\delta\sin\theta + \cos\theta\sin\beta\sin\delta \tag{260b}$$

$$\breve{A}_3^x = -\cos\beta\sin\delta \tag{260c}$$

$$\breve{A}_4^x = -\cos\beta\sin\beta\sin\delta \tag{260d}$$

$$\breve{A}_5^x = \left(\cos\theta\cos\delta\sin\theta + \cos^2\theta\sin\beta\sin\delta\right)\cos\beta \tag{260e}$$

$$\breve{A}_6^x = \dot{\delta} + \dot{\theta}\sin\beta + \dot{\psi}\cos\theta\cos\beta \tag{260f}$$

$$\breve{A}_7^x = \left(\breve{A}_1^x\dot{\psi}\dot{\theta} + \breve{A}_2^x\dot{\psi}\dot{\delta} + \breve{A}_3^x\dot{\theta}\dot{\delta} + \breve{A}_4^x\dot{\theta}^2 + \breve{A}_5^x\dot{\psi}^2\right) \tag{260g}$$

For the y term:

$$\begin{aligned}\breve{A}^y = &\left(\dot{\delta} + \dot{\theta}\sin\beta + \dot{\psi}\cos\theta\cos\beta\right) \\ &\cdot\left(\dot{\psi}\cos\theta\cos\delta\sin\beta - \dot{\psi}\sin\theta\sin\delta - \dot{\theta}\cos\beta\cos\delta\right)\end{aligned} \tag{261}$$

For the z term:

$$\breve{A}_1^z = \cos\beta\sin\theta - 2\cos\theta\cos\beta\cos\delta\sin\beta\sin\delta - 2\cos\beta\cos^2\delta\sin\theta \tag{262a}$$

$$\breve{A}_2^z = \cos^2\beta\cos\delta\sin\delta \tag{262b}$$

$$\breve{A}_3^z = -\cos\delta\sin\delta - \cos\theta\sin\theta\sin\beta \tag{262c}$$

$$\breve{A}_4^z = 2\cos^2\theta\cos\delta\sin\delta \tag{262d}$$

$$\breve{A}_5^z = 2\cos\theta\cos^2\delta\sin\theta\sin\beta \tag{262e}$$

$$\breve{A}_6^z = -\cos^2\theta\cos^2\beta\cos\delta\sin\delta \tag{262f}$$

$$\breve{A}_7^z = -\dot{\theta}\cos\beta\cos\delta \tag{262g}$$

$$\breve{A}_8^z = (\cos\theta\cos\delta\sin\beta - \sin\theta\sin\delta)\,\dot{\psi} \tag{262h}$$

$$\breve{A}_9^z = \left(\breve{A}_1^z\dot{\theta}\dot{\psi} + \breve{A}_2^z\dot{\theta}^2 + \left(\breve{A}_3^z + \breve{A}_4^z + \breve{A}_5^z + \breve{A}_6^z\right)\dot{\psi}^2\right) \tag{262i}$$

The derivative term is:

$$\frac{{}^6d}{dt}\mathbf{H}_{fw} = \begin{bmatrix} I_{fw}^{xx}\left(\breve{B}_1^x\ddot{\theta} + \breve{B}_2^x\ddot{\psi} + \breve{B}_3^x\dot{\theta}\dot{\psi} + \breve{B}_4^x\dot{\theta}\dot{\delta} + \breve{B}_5^x\dot{\psi}\dot{\delta}\right) \\ I_{fw}^{yy}\left(\dot{\omega}_{fw}^{spin} + \breve{B}_1^y\ddot{\theta} + \breve{B}_2^y\ddot{\psi} + \breve{B}_3^y\dot{\theta}\dot{\psi} + \breve{B}_4^y\dot{\theta}\dot{\delta} + \breve{B}_5^y\dot{\psi}\dot{\delta}\right) \\ I_{fw}^{zz}\left(\delta_{2d} + \ddot{\theta}\sin\beta + \ddot{\psi}\cos\theta\cos\beta - \dot{\psi}\dot{\theta}\sin\theta\cos\beta\right) \end{bmatrix}_6 \tag{263}$$

For the x term:

$$\breve{B}_1^x = -\cos\beta\cos\delta \tag{264a}$$

$$\breve{B}_2^x = \sin\beta\cos\delta\cos\theta - \sin\delta\sin\theta \tag{264b}$$

$$\breve{B}_3^x = -\sin\delta\cos\theta - \sin\beta\cos\delta\sin\theta \tag{264c}$$

$$\breve{B}_4^x = \cos\beta\sin\delta \tag{264d}$$

$$\breve{B}_5^x = -\sin\theta\cos\delta - \sin\beta\sin\delta\cos\theta \tag{264e}$$

For the y term:

$$\breve{B}_1^y = \breve{B}_4^x = \cos\beta\sin\delta \tag{265a}$$

$$\breve{B}_2^y = \breve{B}_5^x = -\sin\theta\cos\delta - \sin\beta\sin\delta\cos\theta \tag{265b}$$

$$\breve{B}_3^y = -\cos\theta\cos\delta + \sin\beta\sin\delta\sin\theta \tag{265c}$$

$$\breve{B}_4^y = -\breve{B}_1^x = \cos\beta\cos\delta \tag{265d}$$

$$\breve{B}_5^y = -\breve{B}_2^x = -\sin\beta\cos\delta\cos\theta + \sin\delta\sin\theta \tag{265e}$$

C.2.2.1 Simplified Moment Balance. This form of the moment balance for the front wheels is too cumbersome to be useful. There are 2 sources to the complexity. They are the front wheels being steered and that they are steered about an axis that is not parallel to the $\mathbf{k}_3$ axis. To make the problem tractable, the approximation is made that the front wheels have zero steering angle, $\delta \equiv 0$. The approximation is justified partly because the mass of the front wheels is only around 5% of the total mass of the vehicle in our case and because the equations would be too complex without it. When this simplification is made, coordinate system 6, the front wheels' principle coordinate system, becomes the same as system 3. The angular momentum then becomes:

$$\mathbf{H}_{fw} = \mathbf{I}_{fw}\boldsymbol{\omega}_{fw}$$

$$\begin{aligned}\boldsymbol{\omega}_{fw} &= {}^{1}\boldsymbol{\omega}^{6} + \boldsymbol{\omega}_{fw}^{spin} = \begin{bmatrix} -\dot{\theta} - (\sin\beta)\,\dot{\delta} \\ -(\sin\theta)\,\dot{\psi} \\ (\cos\theta)\,\dot{\psi} + (\cos\beta)\,\dot{\delta} \end{bmatrix}_3 + \begin{bmatrix} 0 \\ \omega_{fw}^{spin} \\ 0 \end{bmatrix}_3 \\ &= \begin{bmatrix} -\dot{\theta} - (\sin\beta)\,\dot{\delta} \\ \omega_{fw}^{spin} - (\sin\theta)\,\dot{\psi} \\ (\cos\theta)\,\dot{\psi} + (\cos\beta)\,\dot{\delta} \end{bmatrix}_3 \end{aligned} \tag{266}$$

$$\mathbf{H}_{fw} = \begin{bmatrix} I_{fw}^{xx}\left(-\dot{\theta} - (\sin\beta)\,\dot{\delta}\right) \\ I_{fw}^{yy}\left(\omega_{fw}^{spin} - (\sin\theta)\,\dot{\psi}\right) \\ I_{fw}^{zz}\left((\cos\theta)\,\dot{\psi} + (\cos\beta)\,\dot{\delta}\right) \end{bmatrix}_3 \tag{267}$$

Using this for equation 258 we get:

$$\frac{{}^{6}d}{dt}\mathbf{H}_{fw} = \begin{bmatrix} I_{fw}^{xx}\left(-\ddot{\theta} - (\sin\beta)\,\delta_{2d}\right) \\ I_{fw}^{yy}\left(\dot{\omega}_{fw}^{spin} - (\sin\theta)\,\ddot{\psi} - \dot{\psi}\dot{\theta}\,(\cos\theta)\right) \\ I_{fw}^{zz}\left((\cos\theta)\,\ddot{\psi} - \dot{\psi}\dot{\theta}\,(\sin\theta) + (\cos\beta)\,\ddot{\delta}\right) \end{bmatrix}_3 \tag{268}$$

The cross product term is:

$${}^{1}\boldsymbol{\omega}^{6} \times \mathbf{H}_{fw} = \begin{bmatrix} \breve{C}_1^{x}\left(I_{fw}^{yy} - I_{fw}^{zz}\right) - \omega_{fw}^{spin} I_{fw}^{yy} \breve{C}_2^{x} \\ \breve{C}^{y}\left(I_{fw}^{zz} - I_{fw}^{xx}\right) \\ \breve{C}_1^{z}\left(I_{fw}^{yy} - I_{fw}^{xx}\right) + \breve{C}_2^{z}\left(I_{fw}^{yy} - I_{fw}^{xx}\right) + \breve{C}_3^{z} I_{fw}^{yy} \end{bmatrix}_3 \tag{269}$$

For the x term:

$$\breve{C}_1^{x} = \dot{\psi}\,(\sin\theta)\left[(\cos\beta)\,\dot{\delta} + (\cos\theta)\,\dot{\psi}\right] \tag{270a}$$

$$\breve{C}_2^{x} = (\cos\theta)\,\dot{\psi} + (\cos\beta)\,\dot{\delta} \tag{270b}$$

For the y term:

$$\breve{C}^{y} = \dot{\theta}\dot{\psi}\left(\cos\theta\right) + \dot{\delta}^{2}\left(\cos\beta\sin\beta\right) + \dot{\theta}\dot{\delta}\left(\cos\beta\right) + \dot{\psi}\dot{\delta}\left(\cos\theta\sin\beta\right) \tag{271a}$$

For the z term:

$$\breve{C}_{1}^{z} = \dot{\psi}\dot{\delta}\left(\sin\theta\sin\beta\right) \tag{272a}$$

$$\breve{C}_{2}^{z} = \dot{\theta}\dot{\psi}\left(\sin\theta\right) \tag{272b}$$

$$\breve{C}_{3}^{z} = -\omega_{fw}^{spin}\left(\dot{\theta} + \left(\sin\beta\right)\dot{\delta}\right) \tag{272c}$$

C.2.2.2 Resultant Moment. The resultant moment is found about the center of gravity of each front wheel. This is due to the moments from the vehicle body on the front wheels and any moments due to external forces. The translational reactions from the vehicle body on the front wheels as well as gravity are assumed to act at the center of gravity of the front wheels and so have no affect on the resultant moment.

$$\mathbf{M}_{fw} = {}^{fw}\mathbf{M}^{b} + \mathbf{r}_{fw}^{\mathbf{F}} \times \overline{\mathbf{F}_{fw}^{ext}} + \frac{1}{2}\mathbf{M}_{\delta} \tag{273}$$

Where:

$$\overline{\mathbf{F}_{fw}^{ext}} = \mathbf{F}_{fw}^{ext} - \mathbf{F}_{fw}^{grav} = \begin{bmatrix} 0 \\ F_{f} \\ N_{fw} \end{bmatrix}_{4} \tag{274}$$

$$\mathbf{r}_{fw}^{\mathbf{F}} = \begin{bmatrix} 0 \\ 0 \\ -r_{fw} \end{bmatrix}_{3} = \begin{bmatrix} -\left(\sin\beta\cos\delta\right)r_{fw} \\ \left(\sin\beta\sin\delta\right)r_{fw} \\ -\left(\cos\beta\right)r_{fw} \end{bmatrix}_{6} \tag{275}$$

$$
\begin{aligned}
\mathbf{r}_{fw}^{\mathbf{F}} \times \overline{\mathbf{F}_{fw}^{ext}} &= \begin{bmatrix} (\cos\beta)\, r_{fw} F_f \cos\theta \cos\delta - (\cos\beta)\, r_{fw} N_{fw} \cos\delta \sin\theta \\ (\cos\beta)\, r_{fw} F_f \sin\delta \cos\theta + (\cos\beta)\, r_{fw} N_{fw} \sin\theta \sin\delta \\ -(\sin\beta)\, r_{fw} F_f \cos\theta + (\sin\beta)\, r_{fw} N_{fw} \sin\theta \end{bmatrix}_6 \\
&= \begin{bmatrix} -(\sin\theta)\, N_{fw} r_{fw} + (\cos\theta)\, F_f r_{fw} \left(\left(\cos^2\beta\right)\left(-2\sin^2\delta\right) + 1\right) \\ 2\left(\cos\delta \cos\theta \cos\beta \sin\delta\right) F_f r_{fw} \\ -2\left(\sin^2\delta\right) F_f r_{fw} \cos\theta \cos\beta \sin\beta \end{bmatrix}_3
\end{aligned} \tag{276}
$$

The cross product, $\mathbf{k}_6$, term matches M_{trail} for reference (33) when $r_{fw} \sin\beta = \gamma \cos\beta$.

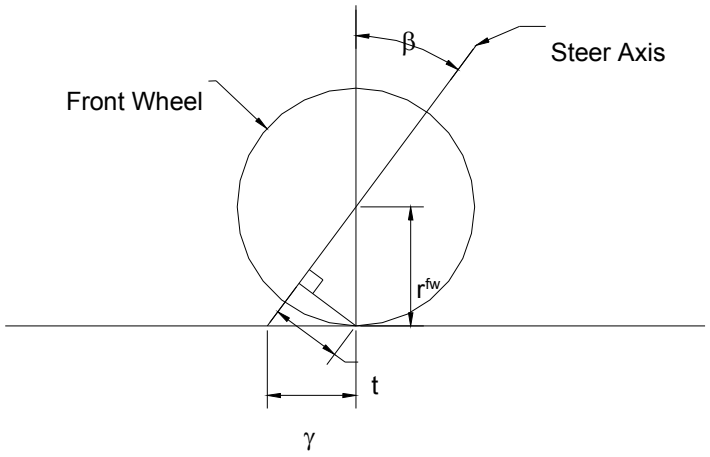

Figure C-1 Front wheel side view: trail schematic

The trail affects and model dynamics are discussed in more detail the following references (7), (12), (18:pp. 19), (23), (25), (28), (32), and (33).

C.2.2.3 Moment Balance Expression.

$$\frac{^1d}{dt}\mathbf{H}_{flw} = {}^{flw}\mathbf{M}^b + \mathbf{r}^{\mathbf{F}}_{flw} \times \overline{\mathbf{F}^{ext}_{flw}} + \frac{1}{2}\mathbf{M}_\delta \tag{277a}$$

$$\frac{^1d}{dt}\mathbf{H}_{frw} = {}^{frw}\mathbf{M}^b + \mathbf{r}^{\mathbf{F}}_{frw} \times \overline{\mathbf{F}^{ext}_{frw}} + \frac{1}{2}\mathbf{M}_\delta \tag{277b}$$

C.3 Rear Wheel

C.3.1 Translational Balance. We proceed as before. The relative position vector was given in equation 209c.

$${}^B\mathbf{r}^{G_{rw}} = \begin{bmatrix} -l_r \\ 0 \\ r_{rw} - h \end{bmatrix}_3 \tag{278}$$

$$\mathbf{v}^{G_{rw}} = \mathbf{v}^B + {}^B\mathbf{v}^{G_{rw}},\ {}^B\mathbf{v}^{G_{rw}} = \frac{^1d}{dt}{}^B\mathbf{r}^{G_{rw}} = \frac{^3d}{dt}{}^B\mathbf{r}^{G_{rw}} + \boldsymbol{\omega}_b \times {}^B\mathbf{r}^{G_{rw}} \tag{279}$$

Since, $\frac{^3d}{dt}{}^B\mathbf{r}^{G_{rw}} = \frac{^3d}{dt}{}^P\mathbf{r}^B = \mathbf{0}$ we get:

$$\mathbf{v}^{G_{rw}} = \mathbf{v}^P + \boldsymbol{\omega}_b \times {}^P\mathbf{r}^B + \boldsymbol{\omega}_b \times {}^B\mathbf{r}^{G_{rw}} \tag{280}$$

Where we used equation 202. Again, the next step is to differentiate this.

$$\frac{^1d}{dt}\mathbf{v}^{G_{rw}} = \mathbf{a}^{G_{rw}} = \frac{^1d}{dt}\mathbf{v}^P + \frac{^1d}{dt}\left(\boldsymbol{\omega}_b \times {}^P\mathbf{r}^B\right) + \frac{^1d}{dt}\left(\boldsymbol{\omega}_b \times {}^B\mathbf{r}^{G_{rw}}\right) \tag{281}$$

The last term is found as we did before. Explicitly, it is:

$$\frac{^1d}{dt}\left(\boldsymbol{\omega}_b \times {}^B\mathbf{r}^{G_{rw}}\right) = \begin{bmatrix} \dot{\psi}^2 l_r + \xi_5\left((\cos\theta)\, 2\dot{\psi}\dot{\theta} + (\sin\theta)\,\ddot{\psi}\right) \\ -\xi_5\left(\ddot{\theta} - (\cos\theta\sin\theta)\,\dot{\psi}^2\right) - (\cos\theta)\, l_r\ddot{\psi} \\ \xi_5\left(\dot{\theta}^2 + \left(\sin^2\theta\right)\dot{\psi}^2\right) - l_r(\sin\theta)\,\ddot{\psi} \end{bmatrix}_3 \tag{282}$$

$$= \begin{bmatrix} \dot{\psi}^2 l_r + \xi_5\left(2(\cos\theta)\,\dot{\psi}\dot{\theta} + (\sin\theta)\,\ddot{\psi}\right) \\ \xi_5\left(-\ddot{\theta}(\cos\theta) + (\sin\theta)\left(\dot{\psi}^2 + \dot{\theta}^2\right)\right) - l_r\ddot{\psi} \\ \xi_5\left(\ddot{\theta}\sin\theta + \dot{\theta}^2\cos\theta\right) \end{bmatrix}_4 \tag{283}$$

$$\xi_5 = h - r_{rw} \tag{284}$$

Combining equations 213, 220, and 282 we get the acceleration of the rear wheel.

$$\mathbf{a}^{G_{rw}} = \begin{bmatrix} \dot{v} - \dot{\psi}\dot{y} + \dot{\psi}^2 l_r - 2(\cos\theta)\,\dot{\psi}\dot{\theta}r_{rw} - (\sin\theta)\,\ddot{\psi}r_{rw} \\ \left(-\dot{\psi}^2 - \dot{\theta}^2\right) r_{rw}\sin\theta + v\dot{\psi} + \ddot{y} + \ddot{\theta}(\cos\theta)\, r_{rw} - l_r\ddot{\psi} \\ -(\cos\theta)\,\dot{\theta}^2 r_{rw} - (\sin\theta)\,\ddot{\theta}r_{rw} \end{bmatrix}_4 \tag{285}$$

C.3.1.1 Resultant Force.

$$\mathbf{F}_{rw} = {}^{rw}\mathbf{P}^b + \mathbf{F}_{rw}^{ext} = {}^{rw}\mathbf{P}^b + \begin{bmatrix} 0 \\ F_r \\ N_{rw} - m_{rw}g \end{bmatrix}_4 \tag{286}$$

C.3.1.2 Translational Balance Expression.

$$m_{rw}\mathbf{a}^{G_{rw}} = {}^{rw}\mathbf{P}^b + \mathbf{F}_{rw}^{ext} \tag{287}$$

C.3.2 Moment Balance. The moment balance for the rear wheel is significantly more simple than that of the front wheels.

$$\begin{aligned}\boldsymbol{\omega}_{fw} &= {}^1\boldsymbol{\omega}^4 + {}^4\boldsymbol{\omega}^3 + \boldsymbol{\omega}_{rw}^{spin} = \boldsymbol{\omega}_b + \boldsymbol{\omega}_{rw}^{spin} = \boldsymbol{\omega}_b + \begin{bmatrix} 0 \\ \omega_{rw}^{spin} \\ 0 \end{bmatrix}_3 \\ &= \begin{bmatrix} -\dot{\theta} \\ -\dot{\psi}\sin\theta \\ \dot{\psi}\cos\theta \end{bmatrix}_3 + \begin{bmatrix} 0 \\ \omega_{rw}^{spin} \\ 0 \end{bmatrix}_3 = \begin{bmatrix} -\dot{\theta} \\ -\dot{\psi}\sin\theta + \omega_{rw}^{spin} \\ \dot{\psi}\cos\theta \end{bmatrix}_3 \end{aligned} \tag{288}$$

The angular momentum $\mathbf{H}_{rw}$ is the product of the inertia tensor and the angular velocity in system 3. System 3 is the principle axis system so that the inertia tensor is again diagonal.

$$\mathbf{H}_{rw} = \mathbf{I}_{rw}\boldsymbol{\omega}_{rw} = \begin{bmatrix} -I_{rw}^{xx}\dot{\theta} \\ I_{rw}^{yy}\left(-\dot{\psi}\sin\theta + \omega_{rw}^{spin}\right) \\ I_{rw}^{zz}\dot{\psi}\cos\theta \end{bmatrix}_3 \tag{289}$$

Using the transport theorem for the time derivative of $\mathbf{H}_{rw}$:

$${}^1\frac{d}{dt}\mathbf{H}_{rw} = {}^3\frac{d}{dt}\mathbf{H}_{rw} + \boldsymbol{\omega}_b \times \mathbf{H}_{rw} \tag{290}$$

$${}^3\frac{d}{dt}\mathbf{H}_{rw} = \begin{bmatrix} -I_{rw}^{xx}\ddot{\theta} \\ I_{rw}^{yy}\left(-\dot{\psi}\dot{\theta}\cos\theta - \ddot{\psi}\sin\theta + \dot{\omega}_{rw}^{spin}\right) \\ I_{rw}^{zz}\left(-\dot{\psi}\dot{\theta}\sin\theta + \ddot{\psi}\cos\theta\right) \end{bmatrix}_3 \tag{291}$$

$$\boldsymbol{\omega}_b \times \mathbf{H}_{rw} = \begin{bmatrix} \left(-I_{rw}^{zz} + I_{rw}^{yy}\right)\left(\sin\theta\cos\theta\right)\dot{\psi}^2 - \dot{\psi}\left(\cos\theta\right)I_{rw}^{yy}\omega_{rw}^{spin} \\ \left(-I_{rw}^{xx} + I_{rw}^{zz}\right)\left(\cos\theta\right)\dot{\psi}\dot{\theta} \\ \left(I_{rw}^{yy} - I_{rw}^{xx}\right)\dot{\theta}\dot{\psi}\sin\theta - \dot{\theta}I_{rw}^{yy}\omega_{rw}^{spin} \end{bmatrix}_3 \tag{292}$$

Thus $\frac{^1d}{dt}\mathbf{H}_{rw}$ is:

$$\frac{^1d}{dt}\mathbf{H}_{rw} = \begin{bmatrix} -I_{rw}^{xx}\ddot{\theta} + \left(-I_{rw}^{zz} + I_{rw}^{yy}\right)\left(\sin\theta\cos\theta\right)\dot{\psi}^2 - \dot{\psi}\left(\cos\theta\right)I_{rw}^{yy}\omega_{rw}^{spin} \\ I_{rw}^{yy}\left(-\dot{\psi}\dot{\theta}\cos\theta - \ddot{\psi}\sin\theta + \dot{\omega}_{rw}^{spin}\right) + \left(-I_{rw}^{xx} + I_{rw}^{zz}\right)\left(\cos\theta\right)\dot{\psi}\dot{\theta} \\ I_{rw}^{zz}\left(-\dot{\psi}\dot{\theta}\sin\theta + \ddot{\psi}\cos\theta\right) + \left(I_{rw}^{yy} - I_{rw}^{xx}\right)\dot{\theta}\dot{\psi}\sin\theta - \dot{\theta}I_{rw}^{yy}\omega_{rw}^{spin} \end{bmatrix}_3 \tag{293}$$

C.3.2.1 Resultant Moment.

$$\mathbf{M}_{rw} = {}^{rw}\mathbf{M}^b + \mathbf{r}_{rw}^{\mathbf{F}} \times \overline{\mathbf{F}_{rw}^{ext}} \tag{294}$$

Where:

$$\overline{\mathbf{F}_{rw}^{ext}} = \mathbf{F}_{rw}^{ext} - \mathbf{F}_{rw}^{grav} = \begin{bmatrix} 0 \\ F_r \\ N_{rw} \end{bmatrix}_4 \tag{295}$$

$$\mathbf{r}_{rw}^{\mathbf{F}} = \begin{bmatrix} 0 \\ 0 \\ -r_{rw} \end{bmatrix}_3 \tag{296}$$

$$\mathbf{r}_{rw}^{\mathbf{F}} \times \overline{\mathbf{F}_{rw}^{ext}} = \begin{bmatrix} r_{rw}\left(\left(\cos\theta\right)F_r - \left(\sin\theta\right)N_{rw}\right) \\ 0 \\ 0 \end{bmatrix}_3$$

C.3.2.2 Moment Balance Expression.

$$\frac{^1d}{dt}\mathbf{H}_{rw} = {}^{rw}\mathbf{M}^b + \mathbf{r}^{\mathbf{F}}_{rw} \times \overline{\mathbf{F}^{ext}_{rw}} \tag{297}$$

C.4 Total Model

At this point, we have, 2 vector equations for each of the 4 bodies with the constraint equations:

$$^{fw}\mathbf{P}^b = -{}^b\mathbf{P}^{fw} \tag{298a}$$

$$^{rw}\mathbf{P}^b = -{}^b\mathbf{P}^{rw} \tag{298b}$$

$$^{fw}\mathbf{M}^b = -{}^b\mathbf{M}^{fw} \tag{298c}$$

$$^{rw}\mathbf{M}^b = -{}^b\mathbf{M}^{rw} \tag{298d}$$

We use these constraints to outline the procedure to derive the final equations of motion.

C.4.1 Translational Balance. Combining equations 225,252a,252b, and 287 we get the overall translational balance expression, equation 299.

$$m_b\mathbf{a}^{G_b} + m_{flw}\mathbf{a}^{G_{flw}} + m_{frw}\mathbf{a}^{G_{frw}} + m_{rw}\mathbf{a}^{G_{rw}} = \mathbf{F}^{ext}_b + \mathbf{F}^{ext}_{flw} + \mathbf{F}^{ext}_{frw} + \mathbf{F}^{ext}_{rw} \tag{299}$$

Explicitly, this simplifies to equation 300.

$$m\begin{bmatrix} \dot{v} - \dot{\psi}\dot{y} - h\ddot{\psi}\sin\theta - 2h\dot{\psi}\dot{\theta}\cos\theta \\ v\dot{\psi} + \ddot{y} - h\dot{\theta}^2\sin\theta + h\ddot{\theta}\cos\theta - h\dot{\psi}^2\sin\theta \\ -h\left(\ddot{\theta}\sin\theta + \dot{\theta}^2\cos\theta\right) \end{bmatrix}_4 = \begin{bmatrix} 0 \\ 2F_f + F_r \\ 2N_{fw} + N_{rw} - mg \end{bmatrix}_4 \tag{300}$$

C.4.2 Moment Balance. This is where our ability to be explicit ends. The literal expressions for the total moment balance without any more simplifications becomes too complex to

calculate or manipulate explicitly. With the following definitions, we combine equations 234, 277a, 277b, and 297 to get

$$\begin{aligned}
\frac{^1d}{dt}\mathbf{H} &= \frac{^1d}{dt}\mathbf{H}_b + 2\frac{^1d}{dt}\mathbf{H}_{fw} + \frac{^1d}{dt}\mathbf{H}_{rw} \\
&= {}^B\mathbf{r}^{G_{flw}} \times \overline{\mathbf{F}^{ext}_{flw}} + {}^B\mathbf{r}^{G_{frw}} \times \overline{\mathbf{F}^{ext}_{frw}} + {}^B\mathbf{r}^{G_{rw}} \times \overline{\mathbf{F}^{ext}_{rw}} \\
&\quad + {}^B\mathbf{r}^{G_{flw}} \times \mathbf{F}^{grav}_{flw} + {}^B\mathbf{r}^{G_{frw}} \times \mathbf{F}^{grav}_{frw} + {}^B\mathbf{r}^{G_{rw}} \times \mathbf{F}^{grav}_{rw} \\
&\quad + \mathbf{r}^{\mathbf{F}}_{fw} \times \overline{\mathbf{F}^{ext}_{flw}} + \mathbf{r}^{\mathbf{F}}_{fw} \times \overline{\mathbf{F}^{ext}_{frw}} + \mathbf{r}^{\mathbf{F}}_{rw} \times \overline{\mathbf{F}^{ext}_{rw}} \\
&\quad - {}^B\mathbf{r}^{G_{flw}} \times m_{fw}\mathbf{a}^{G_{flw}} - {}^B\mathbf{r}^{G_{frw}} \times m_{fw}\mathbf{a}^{G_{frw}} \\
&\quad - {}^B\mathbf{r}^{G_{rw}} \times m_{rw}\mathbf{a}^{G_{rw}}
\end{aligned} \tag{301}$$

$$\begin{aligned}
\frac{^1d}{dt}\mathbf{H} &= \left(\mathbf{r}^{\mathbf{F}}_{fw} + {}^B\mathbf{r}^{G_{flw}}\right) \times \overline{\mathbf{F}^{ext}_{flw}} + \left(\mathbf{r}^{\mathbf{F}}_{fw} + {}^B\mathbf{r}^{G_{frw}}\right) \times \overline{\mathbf{F}^{ext}_{frw}} \\
&\quad + \left(\mathbf{r}^{\mathbf{F}}_{rw} + {}^B\mathbf{r}^{G_{rw}}\right) \times \overline{\mathbf{F}^{ext}_{rw}} + {}^B\mathbf{r}^{G_{flw}} \times \mathbf{F}^{grav}_{flw} \\
&\quad + {}^B\mathbf{r}^{G_{frw}} \times \mathbf{F}^{grav}_{frw} + {}^B\mathbf{r}^{G_{rw}} \times \mathbf{F}^{grav}_{rw} \\
&\quad - {}^B\mathbf{r}^{G_{flw}} \times m_{fw}\mathbf{a}^{G_{flw}} - {}^B\mathbf{r}^{G_{frw}} \times m_{fw}\mathbf{a}^{G_{frw}} \\
&\quad - {}^B\mathbf{r}^{G_{rw}} \times m_{rw}\mathbf{a}^{G_{rw}}
\end{aligned} \tag{302}$$

The complication arises because of the front wheels' principle coordinate system 6. We simplify this expression by assuming that the mass of the wheels is negligible compared with the total mass of the vehicle. When this is done, the last line of equation 302 disappears and we get equation 303.

$$\begin{aligned}
\frac{^1d}{dt}\mathbf{H} &= \frac{^1d}{dt}\mathbf{H}_b + 2\frac{^1d}{dt}\mathbf{H}_{fw} + \frac{^1d}{dt}\mathbf{H}_{rw} \\
&= \left(\mathbf{r}^{\mathbf{F}}_{fw} + {}^B\mathbf{r}^{G_{flw}}\right) \times \overline{\mathbf{F}^{ext}_{flw}} + \left(\mathbf{r}^{\mathbf{F}}_{fw} + {}^B\mathbf{r}^{G_{frw}}\right) \times \overline{\mathbf{F}^{ext}_{frw}} \\
&\quad + \left(\mathbf{r}^{\mathbf{F}}_{rw} + {}^B\mathbf{r}^{G_{rw}}\right) \times \overline{\mathbf{F}^{ext}_{rw}} + {}^B\mathbf{r}^{G_b} \times \mathbf{F}^{grav}_{b} \\
&\quad + {}^B\mathbf{r}^{G_{flw}} \times \mathbf{F}^{grav}_{flw} + {}^B\mathbf{r}^{G_{frw}} \times \mathbf{F}^{grav}_{frw} + {}^B\mathbf{r}^{G_{rw}} \times \mathbf{F}^{grav}_{rw}
\end{aligned} \tag{303}$$

An explicit expression for the left side of equation 303, is found by converting the expression for $\frac{^1d}{dt}\mathbf{H}_{fw}$ which is listed in system 6, to the system in which $\frac{^1d}{dt}\mathbf{H}_b$ and $\frac{^1d}{dt}\mathbf{H}_{rw}$ are given, system 3. By doing this, we get equation 304.

$$\frac{^1d}{dt}\mathbf{H} = \begin{bmatrix} -I^{xx}\ddot{\theta} + \breve{D}_1^x \left(I^{yy} - I^{zz}\right) - \left(\cos\theta\right) I_b^{xz}\ddot{\psi} + \breve{D}_5^x \\ -\ddot{\psi}\left(\sin\theta\right) I^{yy} + \left(\cos\theta\right)\dot{\theta}\dot{\psi}\left(I^{zz} - I^{xx} - I^{yy}\right) + \breve{D}_4^y \\ \ddot{\psi}\left(\cos\theta\right) I^{zz} + \left(\sin\theta\right)\dot{\theta}\dot{\psi}\left(I^{yy} - I^{xx} - I^{zz}\right) + \breve{D}_5^z \end{bmatrix}_3 \tag{304}$$

With the following definitions.

$$\breve{D}_1^x = \dot{\psi}^2\left(\cos\theta\sin\theta\right) \tag{305a}$$

$$\breve{D}_2^x = \left(\cos\beta\right)\dot{\delta}\omega_{fw}^{spin} I_{fw}^{yy} + \left(\sin\beta\right)\delta_{2d} I_{fw}^{xx} \tag{305b}$$

$$\breve{D}_3^x = 2\dot{\psi}\dot{\delta}\left(\cos\beta\sin\theta\right)\left(I_{fw}^{yy} - I_{fw}^{zz}\right) \tag{305c}$$

$$\breve{D}_4^x = \left(\cos\theta\right)\dot{\psi}\left(2\omega_{fw}^{spin} I_{fw}^{yy} + \omega_{rw}^{spin} I_{rw}^{yy}\right) \tag{305d}$$

$$\breve{D}_5^x = -2\breve{D}_2^x + \breve{D}_3^x - \breve{D}_4^x \tag{305e}$$

$$\breve{D}_1^y = I_b^{xz}\left(\dot{\theta}^2 - \left(\cos^2\theta\right)\dot{\psi}^2\right) + 2\omega_{dfw}^s I_{fw}^{yy} + \omega_{drw}^s I_{rw}^{yy} \tag{306a}$$

$$\breve{D}_2^y = \dot{\delta}^2\left(\cos\beta\sin\beta\right)\left(I_{fw}^{zz} - I_{fw}^{xx}\right) \tag{306b}$$

$$\breve{D}_3^y = \left(\left(\cos\beta\right)\dot{\theta}\dot{\delta} + \left(\cos\theta\sin\beta\right)\dot{\psi}\dot{\delta}\right)\left(I_{fw}^{zz} - I_{fw}^{xx}\right) \tag{306c}$$

$$\breve{D}_4^y = \breve{D}_1^y + 2\breve{D}_2^y + 2\breve{D}_3^y \tag{306d}$$

$$\breve{D}_1^z = I_b^{xz}\left(\ddot{\theta} - (\cos\theta\sin\theta)\,\dot{\psi}^2\right) \tag{307a}$$

$$\breve{D}_2^z = (\cos\beta)\,\delta_{2d} I_{fw}^{\tilde{z}\tilde{z}} - (\sin\beta)\,\dot{\delta}\omega_{fw}^{spin} I_{fw}^{yy} \tag{307b}$$

$$\breve{D}_3^z = \dot{\psi}\dot{\delta}\,(\sin\theta\sin\beta)\left(I_{fw}^{yy} - I_{fw}^{xx}\right) \tag{307c}$$

$$\breve{D}_4^z = \dot{\theta}\left(2\omega_{fw}^{spin} I_{fw}^{yy} + \omega_{rw}^{spin} I_{rw}^{yy}\right) \tag{307d}$$

$$\breve{D}_5^z = \breve{D}_1^z + 2\breve{D}_2^z + 2\breve{D}_3^z - \breve{D}_4^z \tag{307e}$$

These last three terms are due to the spinning and steering of the front wheel. Because the wheels are significantly lighter than the body, we neglect these terms when using the dynamic model. The right side of equation 303 is listed explicitly as equations 308a and 308b.

$$\begin{aligned}
&\left(\mathbf{r}_{fw}^{\mathbf{F}} + {}^{B}\mathbf{r}^{G_{flw}}\right) \times \overline{\mathbf{F}_{flw}^{ext}} + \left(\mathbf{r}_{fw}^{\mathbf{F}} + {}^{B}\mathbf{r}^{G_{frw}}\right) \times \overline{\mathbf{F}_{frw}^{ext}} + \left(\mathbf{r}_{rw}^{\mathbf{F}} + {}^{B}\mathbf{r}^{G_{rw}}\right) \times \overline{\mathbf{F}_{rw}^{ext}} \\
&= \begin{bmatrix} h\,(\cos\theta)\,(2F_f + F_r) - h\,(\sin\theta)\,(2N_{fw} + N_{rw}) \\ (\sin\theta)\,(F_r l_r - 2F_f l_f) + (\cos\theta)\,(l_r N_{rw} - 2l_f N_{fw}) \\ (\sin\theta)\,(l_r N_{rw} - 2l_f N_{fw}) + (\cos\theta)\,(2F_f l_f - F_r l_r) \end{bmatrix}_3
\end{aligned} \tag{308a}$$

$${}^{B}\mathbf{r}^{G_b} \times \mathbf{F}_b^{grav} + {}^{B}\mathbf{r}^{G_{flw}} \times \mathbf{F}_{flw}^{grav} + {}^{B}\mathbf{r}^{G_{frw}} \times \mathbf{F}_{frw}^{grav} + {}^{B}\mathbf{r}^{G_{rw}} \times \mathbf{F}_{rw}^{grav} = \mathbf{0} \tag{308b}$$

The final explicit expression for the moment balance is found by combining equations 304, 308a, and 308b along with equations 305 through 307.

$$\begin{aligned}
&\begin{bmatrix}
-I^{xx}\ddot{\theta} + \breve{D}_1^x \left(I^{yy} - I^{zz}\right) - \left(\cos\theta\right) I_b^{xz}\ddot{\psi} + \breve{D}_5^x \\
-\ddot{\psi}\left(\sin\theta\right) I^{yy} + \left(\cos\theta\right)\dot{\theta}\dot{\psi}\left(I^{zz} - I^{xx} - I^{yy}\right) + \breve{D}_4^y \\
\ddot{\psi}\left(\cos\theta\right) I^{zz} + \left(\sin\theta\right)\dot{\theta}\dot{\psi}\left(I^{yy} - I^{xx} - I^{zz}\right) + \breve{D}_5^z
\end{bmatrix}_3 \\
= &\begin{bmatrix}
h\left(\cos\theta\right)\left(2F_f + F_r\right) - h\left(\sin\theta\right)\left(2N_{fw} + N_{rw}\right) \\
\left(\sin\theta\right)\left(F_r l_r - 2F_f l_f\right) + \left(\cos\theta\right)\left(l_r N_{rw} - 2l_f N_{fw}\right) \\
\left(\sin\theta\right)\left(l_r N_{rw} - 2l_f N_{fw}\right) + \left(\cos\theta\right)\left(2F_f l_f - F_r l_r\right)
\end{bmatrix}_3
\end{aligned} \tag{309}$$

Equations 300 and 309 describe the motion of the vehicle in terms of the state variables. The state equation describing the front wheel angle, δ, which is one degree of freedom, comes from the moment balance in the $\mathbf{k}_6$ direction of equation 258.

$$\begin{aligned}
&I_{fw}^{zz}\left(\delta_{2d} + \ddot{\theta}\sin\beta + \ddot{\psi}\cos\theta\cos\beta - \dot{\psi}\dot{\theta}\sin\theta\cos\beta\right) \\
&+\left(I_{fw}^{xx} - I_{fw}^{yy}\right)\left(\breve{A}_1^z\dot{\theta}\dot{\psi} + \breve{A}_2^z\dot{\theta}^2 + \left(\breve{A}_3^z + \breve{A}_4^z + \breve{A}_5^z + \breve{A}_6^z\right)\dot{\psi}^2\right) \\
&+I_{fw}^{yy}\left(\breve{A}_7^z + \breve{A}_8^z\right)\omega_{fw}^{spin} \\
= &-\left(\sin\beta\right) r_{fw} F_f \cos\theta + \left(\sin\beta\right) r_{fw} N_{fw}\sin\theta + \frac{1}{2}M_\delta
\end{aligned} \tag{310}$$

For our purposes, this equation is not important since there was too much friction in the motion of the front wheels to be able to use M_δ as a control input. Instead, we used the front wheel angle, δ, from the position control command of the steering motor amplifier to control δ directly.

C.4.3 Nonlinear Closed Form. We can now obtain a closed form, one that does not contain the normal forces, N_n, with some manipulations and simplifications. We start by finding the closed form for the vehicle's yaw motion by combining the scalar moment balance equations for the $\mathbf{j}_3$ and

$\mathbf{k}_3$ directions of equation 309 to obtain:

$$\begin{aligned} & \ddot{\psi}\left(\left(\cos\theta\right)I^{zz}+\left(\tan\theta\right)\left(\sin\theta\right)I^{yy}\right) \\ = \quad & \frac{\breve{D}_4^y}{\cos\theta}\sin\theta-\breve{D}_5^z+2\dot{\theta}\dot{\psi}\left(\sin\theta\right)\left(I^{zz}-I^{yy}\right) \\ & +\left(2F_f l_f-F_r l_r\right)\left(\left(\tan\theta\right)\left(\sin\theta\right)+\left(\cos\theta\right)\right) \end{aligned} \tag{311}$$

The closed form equation describing the vehicle's tilt motion is found by combining the scalar moment balance equation in the $\mathbf{i}_3$ direction of equation 309, with the scalar translational balance equation in the $\mathbf{k}_4$ direction of equation 300.

$$\begin{aligned} & \ddot{\theta}\left(-I^{xx}-h^2 m\sin^2\theta\right) \\ = \quad & h\left(\cos\theta\right)\left(2F_f+F_r\right)+h^2 m\left(\cos\theta\sin\theta\right)\dot{\theta}^2-mgh\sin\theta \\ & -\dot{\psi}^2\left(\cos\theta\sin\theta\right)\left(I^{yy}-I^{zz}\right)+\left(\cos\theta\right)I_b^{xz}\ddot{\psi}-\breve{D}_5^x \end{aligned} \tag{312}$$

$$\text{let } J=I^{xx}+h^2 m\sin^2\theta, \text{ then:} \tag{313}$$

$$\begin{aligned} \ddot{\theta} \quad = \quad & \frac{1}{J}\left(mgh\left(\sin\theta\right)-h^2 m\left(\cos\theta\sin\theta\right)\dot{\theta}^2\right) \\ & +\frac{1}{J}\dot{\psi}^2\left(\cos\theta\sin\theta\right)\left(I^{yy}-I^{zz}\right) \\ & -\frac{1}{J}\left(I_b^{xz}\ddot{\psi}\left(\cos\theta\right)+\breve{D}_5^x-h\left(2F_f+F_r\right)\left(\cos\theta\right)\right) \end{aligned} \tag{314}$$

Neglecting the product of inertia we get the nonlinear closed form equation of tilting motion.

$$\begin{aligned} \ddot{\theta} \quad = \quad & \frac{1}{J}\left(mgh\left(\sin\theta\right)-h^2 m\left(\cos\theta\sin\theta\right)\dot{\theta}^2\right) \\ & +\frac{1}{J}\left(\dot{\psi}^2\left(\cos\theta\sin\theta\right)\left(I^{yy}-I^{zz}\right)-h\left(2F_f+F_r\right)\left(\cos\theta\right)\right) \\ & +\frac{1}{J}\breve{D}_5^x \end{aligned} \tag{315}$$

The lateral translation equation is now found as:

$$\begin{aligned}
\ddot{y} &= -v\dot{\psi} - \frac{1}{J}gh^2 m\cos\theta\sin\theta \\
&\quad + h\dot{\theta}^2\left((\sin\theta) + \frac{1}{J}h^2 m\cos^2\theta\sin\theta\right) \\
&\quad + h\dot{\psi}^2\left(\sin\theta + \frac{1}{J}\left(\cos^2\theta\sin\theta\right)\left(I^{zz} - I^{yy}\right)\right) \\
&\quad + \left(2F_f + F_r\right)\left(\frac{1}{J}h^2\cos^2\theta + \frac{1}{m}\right) \\
&\quad - \frac{1}{J}h\breve{D}_5^x\cos\theta
\end{aligned} \tag{316}$$

C.5 Model Linearization

In order to make the control design and simulation process more tractable (we are not concerned with strict simulation accuracy), we linearize the above derived model. The equations are linearized about the nominal values of $\theta = \dot{\theta} = \dot{\psi} = \dot{y} = \dot{\delta} = 0$. When this is done, equations 300 and 309 respectively become:

$$\begin{bmatrix} m\dot{v} - mh\ddot{\psi}\theta \\ mv\dot{\psi} + m\ddot{y} + mh\ddot{\theta} \\ -mh\ddot{\theta}\theta \end{bmatrix}_4 = \begin{bmatrix} 0 \\ 2F_f + F_r \\ mg + 2N_{fw} + N_{rw} \end{bmatrix}_4 \tag{317}$$

$$\begin{aligned}
&\begin{bmatrix} -I^{xx}\ddot{\theta} - I_b^{xz}\ddot{\psi} + \breve{D}^x \\ -\ddot{\psi}\theta I^{yy} + \breve{D}^y \\ \ddot{\psi}I^{zz} + I_b^{xz}\ddot{\theta} + \breve{D}^z \end{bmatrix}_3 \\
= &\begin{bmatrix} h\left(2F_f + F_r\right) - h\theta\left(2N_{fw} + N_{rw}\right) \\ \theta\left(F_r l_r - 2F_f l_f\right) + \left(l_r N_{rw} - 2l_f N_{fw}\right) \\ \theta\left(l_r N_{rw} - 2l_f N_{fw}\right) + \left(2F_f l_f - F_r l_r\right) \end{bmatrix}_3
\end{aligned} \tag{318}$$

$$\breve{D}^x = -2\left(\cos\beta\right)\dot{\delta}\omega_{fw}^{spin}I_{fw}^{yy} - 2\left(\sin\beta\right)\delta_{2d}I_{fw}^{xx} - \dot{\psi}\left(2\omega_{fw}^{spin}I_{fw}^{yy} + \omega_{rw}^{spin}I_{rw}^{yy}\right) \tag{319a}$$

$$\breve{D}^y = 2\omega_{dfw}^{s}I_{fw}^{yy} + \omega_{drw}^{s}I_{rw}^{yy} \tag{319b}$$

$$\breve{D}^z = -2\left(\sin\beta\right)\dot{\delta}\omega_{fw}^{spin}I_{fw}^{yy} + 2\left(\cos\beta\right)\delta_{2d}I_{fw}^{zz} - \dot{\theta}\left(2\omega_{fw}^{spin}I_{fw}^{yy} + \omega_{rw}^{spin}I_{rw}^{yy}\right) \tag{319c}$$

This yields the scalar equations:

$$m\dot{v} = mh\ddot{\psi}\theta \tag{320a}$$

$$mv\dot{\psi} + m\ddot{y} + mh\ddot{\theta} = 2F_f + F_r \tag{320b}$$

$$m\left(g - h\ddot{\theta}\theta\right) = 2N_{fw} + N_{rw} \tag{320c}$$

$$-I^{xx}\ddot{\theta} - I_b^{xz}\ddot{\psi} + \breve{D}^x = h\left(2F_f + F_r\right) - h\theta\left(2N_{fw} + N_{rw}\right) \tag{320d}$$

$$-\ddot{\psi}\theta I^{yy} + \breve{D}^y = \theta\left(F_r l_r - 2F_f l_f\right) + \left(l_r N_{rw} - 2l_f N_{fw}\right) \tag{320e}$$

$$\ddot{\psi}I^{zz} + I_b^{xz}\ddot{\theta} + \breve{D}^z = \theta\left(l_r N_{rw} - 2l_f N_{fw}\right) + \left(2F_f l_f - F_r l_r\right) \tag{320f}$$

Combining equations 320c and 320d gives equation 321.

$$I^{xx}\ddot{\theta} + I_b^{xz}\ddot{\psi} - D^x = -2hF_f - hF_r + mgh\theta \tag{321}$$

Equations 320e and 320f combine.

$$\ddot{\psi}I^{zz} + I_b^{xz}\ddot{\theta} + \breve{D}^z = \theta\breve{D}^y + 2F_f l_f - F_r l_r \tag{322}$$

Using the approximation that the rotation of the wheels is related to the wheel radius and vehicle velocity with together with equation 320a, the term involving $\breve{D}^y$, is seen to be nonlinear in θ.

$$\ddot{\psi}I^{zz} + I_b^{xz}\ddot{\theta} + \breve{D}^z = 2F_f l_f - F_r l_r \tag{323}$$

If we have an expression for the tire forces F_f, and F_r, in terms of the state variables, we will be in a position to define a closed form linear model that we can use to design our controller. The tire forces were modeled linearly with tire slip angles. Figure 95 shows the important dimensions.

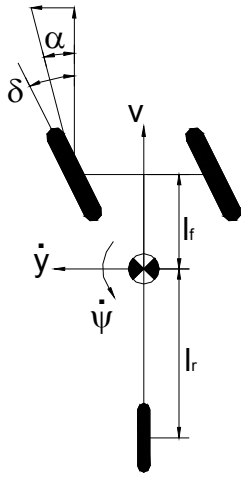

Figure C-2 Top view schematic of vehicle with relavent slip angle velocities

$$\tan\alpha = \frac{\dot{y} + l_f\dot{\psi}}{v} \tag{324}$$

Since for moderate velocities, α is small, we can make the approximation that $\tan\alpha \simeq \alpha$ so that the slip angle becomes:

$$\delta - \frac{\dot{y} + l_f\dot{\psi}}{v} \tag{325}$$

For the rear wheel this is:

$$-\frac{\dot{y} - l_r\dot{\psi}}{v} \tag{326}$$

A camber effect term was also included in the final expressions for the lateral tire forces.

$$F_f = C_f\left(\delta - \frac{\dot{y} + l_f\dot{\psi}}{v}\right) + \lambda_f\theta \tag{327}$$

$$F_r = C_r\left(-\frac{\dot{y} - l_r\dot{\psi}}{v}\right) + \lambda_r\theta \tag{328}$$

C_f and C_r were the proportionality gains from the slip angle and λ_f and λ_r are the proportionality gains from the lean angle. The final linear model is now found using equations 320b, 321, and 323 while neglecting the product of inertia and the gyroscopic influences of the tires.

$$\ddot{\psi} = \frac{1}{I^{zz}}\left(2F_f l_f - F_r l_r\right) \tag{329}$$

$$\ddot{\theta} = \frac{1}{I^{xx}}\left(mgh\theta - 2hF_f - hF_r\right) \tag{330}$$

$$\begin{aligned}\ddot{y} &= v\dot{\psi} - h\ddot{\theta} + \frac{1}{m}\left(2F_f + F_r\right) \\ &= v\dot{\psi} - gh^2 m\frac{\theta}{I^{xx}} + \left(2F_f + F_r\right)\left(\frac{1}{m} + \frac{h^2}{I^{xx}}\right)\end{aligned} \tag{331}$$

Using equations 327 and 328:

$$\begin{aligned}&\ddot{\psi} \\ &= \frac{C_r l_r - 2C_f l_f}{vI_z}\dot{y} - \frac{2C_f l_f^2 + C_r l_r^2}{vI_z}\dot{\psi} \\ &\quad + \frac{1}{I_z}\left(2l_f\lambda_f - l_r\lambda_r\right)\theta + 2\frac{l_f}{I_z}C_f\delta\end{aligned} \tag{332}$$

$$\begin{aligned}&\ddot{\theta} \\ &= h\frac{2C_f + C_r}{I^{xx}v}\dot{y} + h\frac{2l_f C_f - l_r C_r}{I^{xx}v}\dot{\psi} \\ &\quad + \left(\frac{mgh}{I^{xx}} - \frac{h}{I^{xx}}\left(2\lambda_f + \lambda_r\right)\right)\theta - 2\frac{h}{I^{xx}}C_f\delta\end{aligned} \tag{333}$$

Let $\alpha = 1 + \frac{mh^2}{I^{xx}}$ then:

$$\begin{aligned} & \ddot{y} \\ = & -\frac{1}{mv}\alpha\left(2C_f + C_r\right)\dot{y} - \left(v + \frac{\alpha}{mv}\left(2C_f l_f - C_r l_r\right)\right)\dot{\psi} \\ & + \left(\frac{\alpha}{m}\left(2\lambda_f + \lambda_r\right) - \frac{mh^2}{I^{xx}}g\right)\theta + 2\frac{\alpha}{m}C_f\delta \end{aligned} \tag{334}$$

For consistency with other work we have done and to make cross-referencing easier, these equations are re-ordered and listed in linear matrix form.

$$\begin{aligned} \mathbf{x} &= \begin{bmatrix} y & \dot{y} & \psi & \dot{\psi} & \theta & \dot{\theta} \end{bmatrix}^{\mathbf{T}} \\ \dot{\mathbf{x}} &= \mathbf{A}\mathbf{x} + \mathbf{B}\delta \end{aligned} \tag{335}$$

$$\mathbf{A} = \begin{bmatrix} 0 & 1 & 0 & 0 & 0 & 0 \\ 0 & -\frac{\alpha}{mv}\left(2C_f + C_r\right) & 0 & -\left(v + \frac{\alpha}{mv}\left(2C_f l_f - C_r l_r\right)\right) & \frac{\alpha}{m}\left(2\lambda_f + \lambda_r\right) - \frac{mh^2}{I^{xx}}g & 0 \\ 0 & 0 & 0 & 1 & 0 & 0 \\ 0 & \frac{C_r l_r - 2C_f l_f}{vI_z} & 0 & -\frac{2C_f l_f^2 + C_r l_r^2}{vI_z} & \frac{1}{I_z}\left(2l_f\lambda_f - l_r\lambda_r\right) & 0 \\ 0 & 0 & 0 & 0 & 0 & 1 \\ 0 & h\frac{2C_f + C_r}{I^{xx}v} & 0 & h\frac{2l_f C_f - l_r C_r}{I^{xx}v} & \frac{mgh}{I^{xx}} - \frac{h}{I^{xx}}\left(2\lambda_f + \lambda_r\right) & 0 \end{bmatrix} \tag{336}$$

$$\mathbf{B} = \begin{bmatrix} 0 & 2\frac{\alpha}{m}C_f & 0 & 2l_f\frac{C_f}{I_z} & 0 & -\frac{2}{I_x}hC_f \end{bmatrix}^{\mathbf{T}} \tag{337}$$

The output of this state space depends on whether or not you can assume the driver's intentions known or not. In our case, we are not concerned with lateral control or global vehicle position but only with tilting stabilization. In this case, the tilting is not dependent on the state variables y or ψ so we can re-write these equations as:

$$\mathbf{x} = \begin{bmatrix} \dot{y} & \dot{\psi} & \theta & \dot{\theta} \end{bmatrix}^{\mathbf{T}} \tag{338}$$

$$\mathbf{A} = \begin{bmatrix} -\frac{\alpha}{mv}\left(2C_f + C_r\right) & -\left(v + \frac{\alpha}{mv}\left(2C_f l_f - C_r l_r\right)\right) & \frac{\alpha}{m}\left(2\lambda_f + \lambda_r\right) - \frac{mh^2}{I^{xx}}g & 0 \\ \frac{C_r l_r - 2C_f l_f}{vI_z} & -\frac{2C_f l_f^2 + C_r l_r^2}{vI_z} & \frac{1}{I_z}\left(2l_f\lambda_f - l_r\lambda_r\right) & 0 \\ 0 & 0 & 0 & 1 \\ h\frac{2C_f + C_r}{I^{xx}v} & h\frac{2l_f C_f - l_r C_r}{I^{xx}v} & \frac{mgh}{I^{xx}} - \frac{h}{I^{xx}}\left(2\lambda_f + \lambda_r\right) & 0 \end{bmatrix} \tag{339}$$

$$\mathbf{B} = \begin{bmatrix} 2\frac{\alpha}{m}C_f & 2l_f\frac{C_f}{I_z} & 0 & -\frac{2}{I_x}hC_f \end{bmatrix}^{\mathbf{T}} \tag{340}$$

With the output equation:

$$\mathbf{y} = \mathbf{C}\mathbf{x} = \begin{bmatrix} 0 & 1 & 0 & 0 \\ 0 & 0 & 1 & 0 \\ 0 & 0 & 0 & 1 \end{bmatrix} \mathbf{x} \tag{341}$$

C.6 Error Coordinates

The last step is to derive a lateral mode error coordinate transformation similar to (8). The coordinate transformations we used were:

$$\ddot{e}_1 = \ddot{y} + v\dot{\psi} - v\dot{\psi}_{des} = \ddot{y} + v\dot{e}_2 \tag{342a}$$

$$\dot{e}_1 = \dot{y} + v\psi - v\psi_{des} = \dot{y} + ve_2 \tag{342b}$$

$$e_2 = \psi - \psi_{des} \tag{342c}$$

$$e_3 = \theta - \theta_{des} \tag{342d}$$

Where the subscripted *des* terms are the properties of the vehicle trajectory the driver is trying to follow. This trajectory can be parameterized by the maneuver curvature C_v, using the equations developed in the section 2.2. By combining these transformation equations with equations 320b, 321, and 323 and making the simplifying assumptions we used in the other models, we get the equations for the regulator model laterally tracking a maneuver with a curvature, C_v. These coordinates are

useful for analyzing the first two control systems we designed which relied heavily on the lateral control of the vehicle.

The assumptions are as such. The wheels are considered to have negligible mass and inertia compared with the vehicle. This allows for the approximation, $D^x \simeq \breve{D}^z \simeq 0$. Lastly, the axes of coordinate system 3 are considered principle. When this is done, the product of inertia for the vehicle body, I_b^{xz}, is zero. Using these assumptions, we get equation 323 to be:

$$\ddot{\psi} I^{zz} = 2F_f l_f - F_r l_r \tag{343}$$

In terms of error coordinates:

$$I^{zz}\ddot{e}_2 = 2F_f l_f - F_r l_r - I^{zz}\ddot{\psi}_{des} \tag{344}$$

The term $\ddot{\psi}_{des}$ is zero in a steady state turn but is certainly not zero in a transient maneuver. Next, equation 321, with the simplifying assumptions becomes:

$$I^{xx}\ddot{\theta} = -2hF_f - hF_r + mgh\theta \tag{345}$$

Again, with error coordinates:

$$I^{xx}\ddot{e}_3 = -2hF_f - hF_r + mgh\left(e_3 + \theta_{des}\right) - I^{xx}\ddot{\theta}_{des} \tag{346}$$

Lastly, we use equation 345 with equation 320b to get the lateral equation of motion.

$$m\ddot{e}_1 = \alpha F_r + 2\alpha F_f - mve_2 - mv\dot{\psi}_{des} - m^2\frac{h^2}{I^{xx}}ge_3 - m^2\frac{h^2}{I^{xx}}g\theta_{des} \tag{347}$$

Where we defined $\alpha = 1 + \frac{mh^2}{I^{xx}}$. Using equations 342a - 342d, equations 327 and 328 become:

$$F_f = C_f \left(\delta - \frac{(\dot{e}_1 - v e_2) + l_f \left(\dot{e}_2 + \dot{\psi}_{des} \right)}{v} \right) + \lambda_f \left(e_3 - \theta_{des} \right) \tag{348}$$

$$F_r = C_r \left(-\frac{(\dot{e}_1 - v e_2) - l_r \left(\dot{e}_2 + \dot{\psi}_{des} \right)}{v} \right) + \lambda_r \left(e_3 - \theta_{des} \right) \tag{349}$$

We can now use equations 348 and 349 in the equations 344, 346, and 347.

$$\begin{aligned} \ddot{e}_1 = & -\frac{\alpha}{mv} \left(2C_f + C_r \right) \dot{e}_1 + \frac{\alpha}{m} \left(2C_f + C_r \right) e_2 + \left(\frac{\alpha}{mv} \left(C_r l_r - 2C_f l_f \right) - v \right) \dot{e}_2 \\ & + \left(\frac{\alpha}{m} \left(2\lambda_f + \lambda_r \right) + g \left(1 - \alpha \right) \right) e_3 + \frac{2\alpha}{m} C_f \delta \\ & + \left(\frac{\alpha}{mv} \left(C_r l_r - 2C_f l_f \right) - v \right) \dot{\psi}_{des} - \left(\frac{\alpha}{m} \left(2\lambda_f + \lambda_r \right) - g \left(1 - \alpha \right) \right) \theta_{des} \end{aligned} \tag{350}$$

The yaw equation becomes:

$$\begin{aligned} \ddot{e}_2 = & \frac{1}{vI^{zz}} \left(C_r l_r - 2C_f l_f \right) \dot{e}_1 + \frac{1}{I^{zz}} \left(2C_f l_f - C_r l_r \right) e_2 - \frac{1}{vI^{zz}} \left(2C_f l_f^2 + C_r l_r^2 \right) \dot{e}_2 \\ & + \frac{1}{I^{zz}} \left(2 l_f \lambda_f - l_r \lambda_r \right) e_3 + 2C_f \frac{l_f}{I^{zz}} \delta - \frac{1}{vI^{zz}} \left(2C_f l_f^2 + C_r l_r^2 \right) \dot{\psi}_{des} \\ & - \ddot{\psi}_{des} + \frac{1}{I^{zz}} \left(l_r \lambda_r - 2 l_f \lambda_f \right) \theta_{des} \end{aligned} \tag{351}$$

Finally, the leaning equation becomes:

$$\begin{aligned} \ddot{e}_3 = & \frac{h}{vI^{xx}} \left(2C_f + C_r \right) \dot{e}_1 - \frac{h}{I^{xx}} \left(2C_f + C_r \right) e_2 + \frac{h}{vI^{xx}} \left(2C_f l_f - C_r l_r \right) \dot{e}_2 \\ & + \frac{h}{I^{xx}} \left(mg - 2\lambda_f - \lambda_r \right) e_3 - 2h \frac{C_f}{I^{xx}} \delta \\ & + \frac{h}{vI^{xx}} \left(2C_f l_f - C_r l_r \right) \dot{\psi}_{des} + \frac{h}{I^{xx}} \left(gm + 2\lambda_f + \lambda_r \right) \theta_{des} - \ddot{\theta}_{des} \end{aligned} \tag{352}$$

These transformations are valuable for designing an autonomous vehicle performing lateral as well as tilt control. With this transformation, the driver will be laterally controlling the vehicle if the error coordinates tend to zero, $e_1, e_2, e_3 \rightarrow 0$.

References

1. Hibbard, R. and Karnopp, D., "The Dynamics of Small, Relatively Tall and Narrow Tilting Ground Vehicles", ASME 1993, Advanced Automotive Technologies, DSC-Vol 52, 1993 pp. 397-417.

2. Hibbard, R. and Karnopp, D., (1993) "Methods of Controlling the Lean Angle of Tilting Vehicles", ASME 1993, Advanced Automotive Technologies, DSC-Vol 52, pp. 311-320.

3. So, S. G., Karnopp, D., (1997) "Active Dual Mode Tilt Control for Narrow Ground Vehicles", Vehicle System Dynamics, v. 27 1997, pp. 19-36.

4. Karnopp, D., Fang, C., (1992) "A Simple Model of Steering-Controlled Banking Vehicles", ASME 1992, Transportation Systems, DSC-Vol 44, pp. 15-28.

5. So, S.G. and Karnopp, D., "Switching Strategies for Narrow Ground Vehicles with Dual Mode Automatic Tilt Control", Int. J. of Vehicle Design v. 18 No. 5 (Special Issue), 1997, pp. 518 – 533.

6. Karnopp, D. Hibbard, R., (1992) "Optimum Roll Angle Behavior for Tilting Ground Vehicles", ASME 1992, Transportation Systems, DSC-Vol 44, pp. 29-37.

7. Cossalter, V., Doria, A., Lot, R., (1999) "Steady Turning of Two-Wheeled Vehicles", Vehicle System Dynamics, v. 31 1999, pp. 157-181.

8. Cossalter, V., Lio, M. D., Lot, R., Fabbri, L., "A General Method for the Evaluation of Vehicle Manoevrability with Special Emphasis on Motorcycles", Vehicle System Dynamics, 31 1999, pp. 113-135.

9. Cossalter, V. and Lot, R., (2002) "A Motorcycle Multi-Body Model for Real Time Simulations Based on the Natural Coordinates Approach", Vehicle System Dynamics, v. 37 No. 6 2002, pp. 423-447.

10. Lee, Allan Y., (1997) "Matching Vehicle Responses Using the Model-Following Control Method", SAE SP-1228 Research into Vehicle Dynamics and Simulation, pp. 57-69.

11. Lee, A. Y., "Emulating the Lateral Dynamics of a Range of Vehicles Using a Four-Wheel-Steering Vehicle", SAE 950304, 1995, pp. 11 – 22.

12. Nishimi, T., Aoki, A., and Katayama, T., "Analysis of Straight Running Stability of Motorcycles", 10th International Technical Conference on Experimental Safety Vehicles, July 1985, pp. 1080 – 1094.

13. Aoki, A., "Experimental Study on Motorcycle Steering Performance", SAE 790265, 1979, 16 pp.

14. Yuhara, N., Tajima, J., Sano, S., and Takimoto, S., "Steer-by-Wire-Oriented Steering System Design: Concept and Examination", Vehicle System Dynamics suppl. 33, 1999, pp. 692 – 703.

15. Bundorf, R. T. and Leffert, R. L., "The Cornering Compliance Concept for Description of Vehicle Directional Control Properties", SAE 760713, 1976, 14 pp.

16. Ryu, J. and Kim, H., "Virtual Environment for Developing Electronic Power Steering & Steer-by-Wire Systems", Proceedings of the 1999IEEE/RSJ International Conference on Intelligent Robots and Systems, 1999, pp. 1374 – 1379.

17. Weir, D. H. and McRuer, D. T., "A Theory for Driver Steering Control of Motor Vehicles", Highway Research Record No. 247, 1968, pp. 7 – 28.

18. Weir, D.H., and Zellner, J.W., "Lateral-Directional Motorcycle Dynamics and Rider Control", SAE 780304, 1978 25 pp., (also in SP-428, pp. 7 – 31).

19. Zellner, J. W. and Weir, D. H., "Development of Handling Test Procedures for Motorcycles", SAE 780313, 1978 (also in SP-428, pp. 91 – 100), 10 pp.

20. Weir, D. H. and Zellner, J. W., "Experimental Investigation of the Transient Behavior of Motorcycles", SAE 790266, 1976, 17 pp.

21. Post, J. W., Burke, R. J., Drexel, M. V., and Robertson, J. D., "An Adaptive Control Model for Lateral Path Following with Closed-Loop Handling Simulations", SAE 971061, 1997, pp. 217 – 231.

22. Rice, R. S., "Rider Skill Influences on Motorcycle Maneuvering", SAE Transactions, v. 87 section 2, 1978, pp.1419 – 1430.

23. Sharp, R.S., "The Stability and Control of Motorcycles", Journal of Mechanical Engineering Science v. 13 No. 5 1971, pp. 316 – 329.

24. Sharp, R. S., "The Dynamics of Single Track Vehicles", Vehicle System Dynamics 5, 1975-1976, pp. 67 – 77.

25. Sharp, R. S., "Stability, Control and Steering Responses of Motorcycles", Vehicle System Dynamics, v. 35 No. 4 – 5, 2001, pp. 291 – 318.

26. Sharp, R. S., "Research Note: The Influence of Frame Flexibility on the Lateral Stability of Motorcycles", J. Mechanical Engineering Science, v. 16 No. 2, 1974, pp. 117 – 120.

27. Sharp, R. S., "A Review of Motorcycle Steering Behavior and Straight Line Stability Characteristics", SAE 780303, 1978 (also in SP-428, pp. 1 – 6), 6 pp.

28. Sharp, R. S., "The Lateral Dynamics of Motorcycles and Bicycles", Vehicle System Dynamics, 14 1985, pp. 265 – 283.

29. McKibben, J. S., "Motorcycle Dynamics-Fact, Fiction and Folklore", SAE 780309, 1978 (also in SP-428, pp. 63 – 71), 9 pp.

30. Roe, G. E., Pickering, W. M., and Zinober, A., "The Oscillations of a Flexible Castor, and the Effect of Front Fork Flexibility on the Stability of Motorcycles", SAE 780307, 1978 (also in SP-428, pp. 41 – 52), 12 pp.

31. Kane, T. R., The Effect of Frame Flexibility on High Speed Weave of Motorcycles", SAE 780306, 1978 (also in SP-428, pp. 33 – 40), 8 pp.

32. Kane, T. R., "Fundamental Kinematical Relationships For Single-Track Vehicles", International Journal of Mechanical Science v. 17, 1975, pp. 499 – 504

33. Rajamani, R., Gohl J., Alexander L., and Starr P., "Dynamics of Narrow Tilting Vehicles", Mathematical and Computer Modelling of Dynamical Systems, Swets and Zeitlinger.

34. Baruh, Haim, Analytical Dynamics, McGraw-Hill 1999.

35. Shabana, Ahmed A., "Dynamics of Multibody Systems" 2nd ed., Cambridge University Press 1998.

36. Gillespie, Thomas D., "Fundamentals of Vehicle Dynamics", SAE 1992.

37. Ogata, Katsuhiko, "Modern Control Engineering" 3rd ed., Prentice Hall 1997.

38. Franklin, Gene F., Powell, J. David, and Workman, Michael, "Digital Control of Dynamic Systems" 3rd ed., Addison Wesley 1998.

39. Beauchamp, K. G., Signal Processing Using Analog and Digital Techniques, John Wiley and Sons 1973.

40. Tewari, Ashish, Modern Control Design with Matlab and Simulink, John Wiley and Sons 2002.

41. Fitzpatrick, Patrick M., Advanced Calculus: A course in Mathematical Analysis, PWS Publishing Co. 1996.

42. "Motorcycle Safety", NHTSA DOT HS 807 709, October1999.

43. Mercedes-Benz website, http://www.mercedes-benz.com/e/innovation/fmobil/f300_mobilitaet.htm, March 11, 2003.

44. Tilting Three-Wheelers reference website, http://www.maxmatic.com/ttw_index.htm, March 22, 2003.

45. Millennium Motorcycle's website, http://members.iinet.net.au/126jsulman/tracer/, March 22, 2003.